Energy & Environmental Science

Accepted Manuscript

ROYAL SOCIETY OF CHEMISTRY

www.rsc.org/ees

Cite this: DOI: 10.1039/c0xx00000x

www.rsc.org/xxxxxx

ARTICLE TYPE

Flexible graphene devices related to energy conversion and storage

Xiluan Wang, and Gaoquan Shi*

Received (in XXX, XXX) Xth XXXXXXXXX 20XX, Accepted Xth XXXXXXXXX 20XX
DOI: 10.1039/b000000x

Graphene is a unique and attractive energy material because of its atom-thick two-dimensional structure and excellent properties. Graphene sheets are also mechanically strong and flexible. Thus, graphene materials are expected to have wide and practical applications in bendable, foldable and/or stretchable devices related to energy conversion and storage. We present a review on the recent advancements in flexible graphene energy devices including photovoltaic devices, fuel cells, nanogenerators (NGs), supercapacitors (SCs) and batteries, and the devices related to energy conversion such as organic light-emission diodes (OLEDs), photodetectors and actuators. The strategies of synthesizing the flexible graphene materials will be summarized and the challenges facing the design and construction of the devices will be discussed.

1. Introduction

Flexible energy devices are devices that can convert or store energy upon repeated bending, folding and/or stretching without dramatic decreasing their performances.[1–4] These devices have attracted a great deal of attention because of their potential applications in wearable and portable electronics, such as roll-up displays, electronic papers, touch screens, active radio-frequency identification tags, wearable sensors and implantable medical devices.[1, 5–18] For the applications in repeatedly deformed state, each component of the device should be mechanically stable and flexible. Furthermore, the materials for energy applications usually should have high electrical and/or ionic conductivities, large specific surface areas and good chemical, photochemical and/or electrochemical stabilities.[2, 19, 20] To satisfy these requirements, graphene is a unique and attractive material because of its atom-thick two-dimensional structure, excellent electrical, mechanical, optical and electrochemical properties.[21–25] Actually, graphene, graphene derivatives and their composites have been explored for the applications in flexible photovoltaics,[2, 26] batteries,[1, 3] fuel cells[20, 27] and SCs,[5, 28] etc.

A photovoltaic device essentially consists of transparent electrodes, active layers of electron donor and accepter and/or electrolytes.[2] Upon illumination of light, the active layer generates excimers and then occurs charge separation at the p-n junctions formed by the electron acceptors and donors. To improve the charge separation and transportation, buffer layers for electrons and holes are usually applied. On the other hand, an energy storage device (e. g., battery or SC) essentially consists of current collectors, electrode materials, electrolytes and separators.[3,28] Graphene materials can be used as flexible transparent conductive electrode or electron acceptor for photovoltaics, and flexible current collectors, electrodes, active materials or conductive additives for energy storage devices.[2, 29–33] Comparing with metals or metal oxides that widely used in energy devices, graphene materials usually have lighter weight densities, better optical transparency and superior optical, chemical or electrochemical stabilities. Graphene materials also frequently have much larger specific surface areas, higher conductivities, flexibilities or optical transparencies than those of other carbon nanomaterials including activated carbons, carbon black and carbon nanotubes.[31, 34–36] Furthermore, large-area or a large amount graphene can be easily prepared by chemical vapour deposition (CVD)[37] or chemical oxidation-reduction of graphite.[38] These graphene materials can be assembled into macroscopic materials through chemical, electrochemical, fluid or template induced self-assembly.[39–41] These graphene assembles can be directly used as the electrodes or active materials for energy devices without using any conducting additives or binders.[42] These facts explain why graphene materials have received extensive attention in flexible energy devices at both fundamental and applied levels.

Recently, several excellent reviews about flexible energy devices such as solar cells,[33] lithium ion batteries (LIBs)[1] or SCs[5] have been published. However, a comprehensive review about graphene-based flexible energy devices has not yet appeared. This review article will summarize the synthesis of flexible graphene materials and their applications in flexible devices related to energy conversion and storage.

2. Flexible graphene materials

The inherent excellent mechanical and electronic properties of graphene make it an attractive material for the applications in flexible energy devices. Graphene is an atom-thick two-dimensional (2D) carbon sheet. The σ carbon-carbon bond is the strongest single bond in nature, endowing graphene with high Young's modulus and tensile strength.[43] The one-atom thick structure also makes graphene sheet easily deforms in the direction normal to its surface, providing it with good flexibility. Thus, graphene sheets, especially chemically modified graphenes

(CMGs, e.g., graphene oxide (GO) and reduced graphene oxide (rGO)) can also be assembled into various macroscopic flexible materials, such as fibres, thin films, and three-dimensional (3D) porous networks.[5] Furthermore, graphene sheets are frequently blended with polymers or inorganic nanoparticles to form composites to improve their flexibility and/or extend their functions.[44, 45]

2.1 Single and few-layer graphene sheets

A variety of methods have been developed to synthesize single or few-layer graphene sheets. Among them, mechanical exfoliation of graphite with scotch tape was first employed for this purpose and led to the discovery of graphene.[46] This method can produce high-quality graphene sheets with small sizes in low yield for fundamental researches; thus, it cannot be used to produce large-amount graphene for energy applications. Directly growing graphene *via* CVD is the most promising technique to produce large-area graphene sheets.[47–49] In general, a transition metal (e.g., copper, or nickel) film was first annealed in Ar/H_2 atmosphere at 900–1000 °C to remove its surface oxide and increase its grain sizes. Then, it was exposed to an H_2/CH_4 gas mixture to catalyze the the decomposition of CH_4 molecules into carbon atoms, forming a carbon-metal solid solution. Upon rapid cooling, the carbon atoms in the matrix of metal diffused onto metal surface to form mono- or few-layer graphene, depending on cooling rate.[47]

On the other hand, oxidative exfoliation of natural graphite to GO followed by the reduction of GO is one of the most efficient methods for low-cost and large-scale production of single-layer graphene.[50–52] The reduction of GO sheets to rGO can be carried out by using reducing chemical agents (e. g., hydrazine hydrate,[53–55] sodium borohydride,[56–58] active metals,[59, 60] vitamin C,[61] hydroiodic acid[62–64]), thermal,[65,66] photocatalytic,[67–69] and electrochemical treatments,[70] laser irradiation,[71] hydrothermal/solvothermal reactions,[72–74] etc. GO/rGO sheets are dispersible in aqueous or organic media, making them can be fabricated or assembled into flexible films, fibres, and 3D networks. They can also be directly deposited on flexible substrates to form flexible graphene materials.

rGO has structural defects and residual oxygenated groups; thus, its electrical property is much worse than that of pristine graphene. In order to address this issue, a mechanical exfoliation technique has been developed. Typically, graphite powder was sonicated in N-methylpyrrolidone (NMP) or water containing a surfactant (e.g. sodium dodecylbenzene sulfonate (SDBS)) to produce a graphene dispersion.[75] The exfoliated graphene nanosheets are nearly free of defects and oxygen-containing groups; thus they can be used to produce high-quality graphene materials for flexible devices.[76] However, up to date, this technique can only produce suspensions of few-layer graphene sheets with low concentrations (<0.01 mg mL^{-1}), limiting its practical applications.[77–79]

2.2 Flexible graphene films

2.2.1 CVD-graphene films on flexible substrates. To fabricate flexible devices, CVD-graphene sheets have to be transferred from the surfaces of catalytic metal films onto flexible target substrates.[80] Typical transfer process can be accomplished by using a polymer coating such as poly (methyl methacrylate) (PMMA) as a provisional rigid support. This polymeric support layer prevents the folding or tearing of graphene sheet during the process of etching catalytic metal substrates (Ni, Cu). PMMA was successively removed by acetone, leaving a graphene film on the surface of target substrate, such as poly(ethylene terephthalate) (PET).[81] High-quality, large-area graphene membranes are expected to be used as transparent conductive electrodes (TCEs) in bendable/stretchable energy devices. A typical few-layer graphene/PET film showed a sheet resistance of about 500 Ω sq^{-1} with a transmittance around 75% at 550 nm.[49] The optoelectronic property of the graphene/PET film remained virtually unperturbed upon several cycles of folding (180°) and decreased only by 7.9% after 100 bending cycles (0°→150°→0°).

The critical step of preparing flexible graphene electrode is to transfer graphene from the metal substrate to desired flexible substrate without degrading the quality of graphene. However, the widely used method described above suffers from PMMA residual on graphene surface. The removing of PMMA by solvent rinsing possibly causes the tearing of graphene sheet, introducing structural discontinuities such as cracks. To address this problem, a cost- and time-save roll-to-roll method was developed.[82, 83] In this case, the graphene film on a flexible copper foil was attached to a thermal release tape by applying a weak pressure (~0.2 MPa) between two rollers (Fig. 1a). After etching away the copper foil, graphene film on the tape can be transferred to the surfaces of any flexible substrates (Fig. 1b). This technique is scalable; a 30-inch multilayer graphene film has been successfully transferred to a roll of PET for the fabrication of touch-screen panels (Fig. 1c-e).

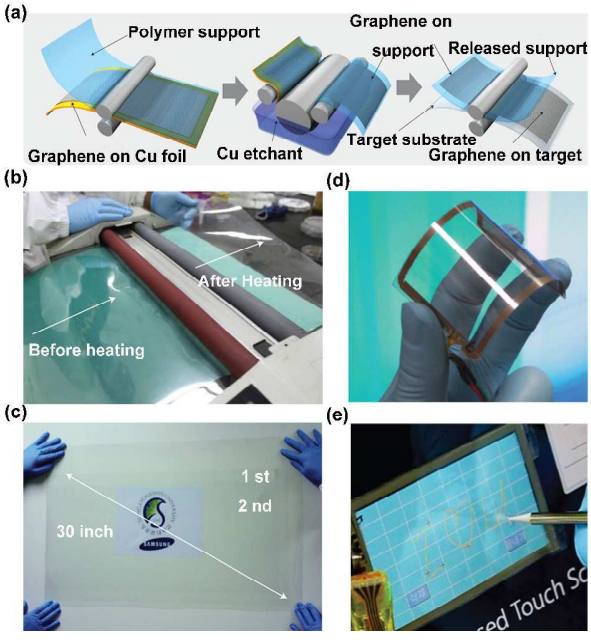

Fig. 1. (a) Schematic illustration of the roll-based production of graphene film grown on a copper foil. (b) Roll-to-roll transfer of graphene film from a thermal release tape to a PET film at 120 °C. (c) A transparent ultralarge-area graphene film transferred on a 35-inch PET sheet. (d) An assembled graphene/PET touch panel showing outstanding flexibility. (e) A graphene-based touch-screen panel connected to a computer with control software. Reproduced with permission from ref. 83.

A unique "clean-lifting transfer" method without using any support has been used to transfer graphene films.[84] This method is based on the electrostatic interaction between graphene sheet and target substrate. First, charges were accumulated at the surface of target substrate, then the CVD-graphene on a Cu foil was electrostatically attracted to its surface. Pressing the substrate can create uniformly distributed attachment sites between both surfaces. Successively, Cu foil was etched away using an iron nitrate solution, followed by rinsing with de-ionized water to remove any residues. This technique has been successfully applied for transferring large-area single layer graphene film onto flexible PET.

2.2.2 GO/rGO films on flexible substrates. Flexible graphene thin films can also be prepared by the deposition of multilayer GO/rGO sheets onto various substrates.[85] Spin coating is the most convenient method to produce uniform thin films on a flexible substrate.[24] Typically, an excess amount of GO solution was dropped on a flexible substrate which was then rotated at a high speed to spread the fluid over its entire surface by a centrifugal force. The GO films prepared by spin coating are usually highly continuous, and their thicknesses can be easily controlled by modulating spin speeds and GO concentrations.[86] Similar to spin coating, spray coating is a painting technique; the coating material is air sprayed onto the surface of a flexible substrate. This technique is fast, scalable and facile to operate. However, in many cases, the thickness varied largely across the film caused by the fast dynamics of deposition and the flexible nature of GO sheets. Moreover, it is very difficult to avoid partial aggregation and crumpling or wrinkling of GO/rGO sheets during the spin or spray coating process.

Dip coating is another popular technique used for preparing flexible thin films. It involves three steps, i.e., immersing a flexible substrate into a tank containing the coating material, removing the substrate from the tank, and drying of the coating material.[85, 87] During the process of dipping, part of graphene sheets were inevitably scrolled or folded, leading to decrease the transparency of graphene film. To avoid the folding of graphene sheets, layer-by-layer (LbL) sequential assembly of positively and negatively charged rGO sheets was developed based on dip coating.[88, 89] This approach relies on the electrostatic attraction between the oppositely charged rGO sheets, and enables the preparation of multilayer rGO films with tunable thicknesses, electrical resistances and transmittances by modulating the number of bilayers.[90] For example, poly(diallyldimethylammonium chloride) (PDDA)-modified positively-charged rGO was combined with negatively-charged rGO to construct flexible thin films.[91] This rGO-based thin film on PET substrate showed a good conductivity retention after multiple cycles (30 cycles) of bending to a large angle of 180°.

Electrophoretic deposition technique is an efficient approach to decrease the aggregation of GO sheets for forming uniform films. In this case, GO sheets in their suspension migrated under the influence of a constant electrical field to deposit onto a conductive electrode.[92] This technique has the advantages of high deposition rate, good thickness controllability and simplicity of scaling up. Nevertheless, it is limited to electrically conductive substrates, such as indium tin oxide (ITO) sheets. The obtained multilayered rGO films on ITO have to be transferred to other flexible substrates for keeping their flexibility.

2.2.3 Free-standing graphene papers. Free-standing paper-like GO films can be prepared by vacuum filtration.[52] GO sheets are hydrophilic because of their oxygenated functional groups; thus water molecules can readily intercalate into GO interlayer galleries. The layered GO paper consists of tightly packed interlocking sheets with an intersheet spacing around 8.3 Å. By modulating the amount of GO sheets in their dispersion, the thickness of GO paper can be facilely controlled. The GO films thinner than 5 μm are semitransparent and thicker papers are fully opaque. GO papers are mechanically strong with Young's moduli ranging from 23–42 GPa,[52, 93, 94] comparable to that of concrete,[95] and tensile strengths ranging from 15–193 MPa,[52, 93, 94, 96] comparable to that of cast iron. Further modification of the functional groups on GO sheets could improve the mechanical properties of GO papers to some extent. For example, the treatment of GO papers with 1 wt% of divalent cations (Mg^{2+} or Ca^{2+}) to crosslink the edge-bonded carboxylic acid groups of adjacent GO sheets can improve their Young's modulus by 10–40% and tensile strength by 10–80%.[85]

GO paper is inherently electronically insulating, limiting its energy applications. In addition, the presence of oxygenated functional groups makes GO thermally unstable. A GO paper can be converted into a conductive rGO paper by the treatment with an aqueous hydrazine solution at 90 °C for 1 h. This rGO paper is mechanically strong, showing a Young's modulus ~3.0 GPa and a tensile strength ~13.2 MPa.[93] However, its electrical conductivity is relative low (about 200 S cm^{-1}).[53] rGO papers prepared by self-assembling rGO sheets showed greatly improved properties including high Young's moduli (~ 20.5 GPa) and tensile strengths (~ 150 MPa), and good electrical conductivities (~7,200 S m^{-1}). Dispersing rGO sheets to prevent their aggregation is the most critical issue to obtain high-quality flexible rGO films. This is mainly due to that the contact resistances between rGO sheets would drastically decrease the conductivities of rGO films. For this purpose, some stabilizers have been used to stabilize the dispersions of rGO sheets. The typical stabilizers include poly-(sodium 4-styrenesulfonate) (PSS),[97] poly(ethylene oxide)-b-poly(propylene oxide)-b-poly(ethylene oxide) (PEO-PPO-PEO),[98] isocyanates,[99] quaternary amines,[100] diazonium salts,[101] sodium cholate,[102] ionic liquids,[103] and single-stranded DNA.[104] Nevertheless, the blending of stabilizers negatively affects the conductivities and mechanical flexibility of rGO papers. Moreover, the electrical properties of rGO papers are also decreased by graphene defects and residual oxygen-containing groups.[105,106] Thermal annealing can partly address these issues. For example, a flexible rGO paper treated by annealing at 500 °C has a more ordered microstructure and showed an electrical conductivity as high as 35,000 S m^{-1}.

2.3 Flexible graphene fibres

In virtue of their intrinsic 2D structure, graphene sheets have been assembled into 2D flexible materials such as papers, and conductive transparent membranes. Inspired by carbon fibres and carbon nanotube (CNT) yarns, the fabrication and applications of graphene-based 1D fibres have attracted intensive attentions.[5]

Graphene fibres (GFs) possess the common characteristics of fibres, especially the mechanical flexibility for textiles. Furthermore, they are light, ease of functionalization and/or have good electrical conductivity. Unfortunately, directly assembling 2D microscopic graphene sheets into macroscopic fibres is a challenge because of the poor dispersibility and the irregular sizes/shapes of graphene sheets. Thus, most graphene fibres were prepared from their GO precursors.[107–111]

GO fibres have been prepared by wet-spinning the liquid-crystalline GO dispersion. In this case, liquid crystalline GO dispersion was continuously injected into a coagulation bath to form fibres with tunable diameters (50–100 μm) and several meters long fibres can be obtained within 10 min (Fig. 2a and b).[112] After chemical reduction, GO fibres were converted into rGO fibres with good mechanical properties (~ 140 MPa at an ultimate elongation of 5.8%) and high conductivity (~ 2.5×10^4 S m^{-1}). Notably, these GFs are flexible; can be fastened into tight knots without any breakage, or integrated into conductive patterned textiles with other threads (Fig. 2c-f).

Hydrothermally reducing a GO suspension sealed in a long and thin tube can also produce conductive rGO fibres.[41] By using a glass pipeline of 0.4 mm inner diameter, 1 mL GO suspension (8 mg mL^{-1}) can generate longer than 6 m rGO fibre (ca. 35 μm in diameter) with a density less than 1/7 that of conventional carbon fibre. The as-obtained GFs exhibited a tensile strength up to 180 MPa and an elongation at break of 3–6%, comparable to those of CNT fibres.[113, 114] The strong and flexible GFs are wearable and shapeable and can be woven into engineered structures. Hollow graphene fibres can also be prepared by template guided assembling rGO sheets in a tube *via* a similar hydrothermal process.[115] One removable metal wire (e.g., Cu) was placed in a glass pipeline and the hydrothermally reduced GO sheets were assembled around the wire to form a compact skin. Successively, the Cu wire was removed by etching to release a hollow rGO fibre. The as-prepared hollow GFs are mechanically stable and flexible, can be shaped to a specific geometry with required structure.

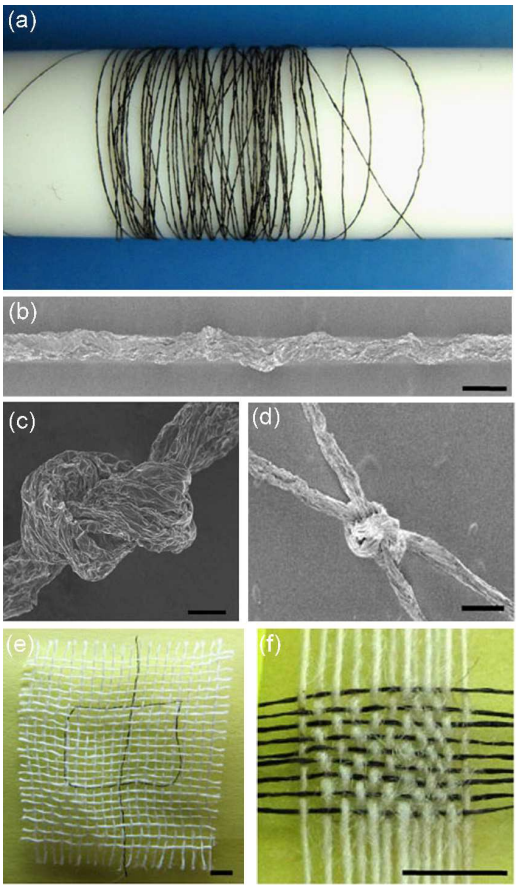

Fig. 2. (a) Four-metre-long GO fibre wound on a Teflon drum (diameter, 2 cm). SEM image of the fibre (b), and its typical tighten knots (c and d). (e) A Chinese character ("中", Zhong) pattern knitted in the cotton network (white) using two graphene fibres (black). (f) A mat of graphene fibres (horizontal) woven together with cotton threads (vertical). Scale bars, 50 μm (b–d) and 2 mm (e , f). Reprinted with permission from ref. 112.

2.4 Graphene-based flexible 3D porous architectures

For the applications in energy devices, graphene sheets are frequently constructed into 3D porous architectures to provide conductive frameworks for electron transfer or loading other functional materials, and accessible surface areas for the adsorption/desorption of ions.[116] The 3D graphene frameworks have unique properties including high porosity, huge specific surface area, light weight, and excellent electrical conductivity.[117] Typical 3D graphene materials include hydrogels,[22, 63, 72] aerogels,[118, 119] foams,[19, 120, 121] sponges[122, 123] etc., however, only several of them were reported for flexible devices.

Graphene-based flexible 3D porous architectures were usually prepared via self-assembly of graphene sheets.[117, 124] A GO sheet can be considered as a 2D amphiphilic conjugated polyelectrolyte with a hydrophobic basal plane and hydrophilic oxygenated groups. Thus, the self-assembly behavior of GO sheets in aqueous media is mainly controlled by the balance between the inter-planar Van der Waals force and electronic repulsion of GO sheets. Moreover, in many cases, dipole and hydrogen bonding interactions are also the driving forces of self-assembly. Hydrothermal reduction of GO dispersion with a concentration higher than about 1 mg mL^{-1} can produce a mechanically strong, electrically conductive and thermally stable rGO hydrogel.[72] This hydrogel can be converted to an aerogel by freeze or supercritical drying. However, these hydrogels or aerogels are usually brittle, cannot be stretched or compressed.[119, 125, 126] By carefully controlling both the amount of oxygen-containing groups of GO sheets and freezing conditions, a cork-like graphene macroporous structure was obtained.[127] This graphene monolith exhibited a good elasticity; it can sustain its structural integrity under a load 50,000 times its own weight and can rapidly recover from a compression strain <80 %. This pioneering work opened a door to obtain self-standing graphene flexible materials with 3D porous microstructures. Nevertheless, this process is time-consuming for large scale production. We have employed a rapid template method to fabricate macroporous graphene monoliths from an aqueous emulsion of GO containing hexane droplets.[128] In this case, GO sheets were reduced by hydrothermal treatment and assembled around hexane droplets to form a 3D network (Fig. 3a). Then the hydrogel was immersed in 80 °C water for 1 h to evaporate hexane and fill water into the graphene pores.

Successively, the rGO hydrogel was freeze dried and followed by annealing in moisture to form a flexible aerogel (Fig. 3b). The density and conductivity of these rGO aerogels can be modulated by the concentrations of feeding GO dispersions. They are light (6.73–12.32 mg cm^{-3}), conductive (0.48–1.76 S m^{-1}), and have excellent elasticity. The aerogel prepared from 5 mg mL^{-1} GO can recover to its initial shape upon repeatedly compression up to 30 % strain for 300 cycles (Fig. 3c).

rGO foams can be prepared by chemical reduction of GO papers with hydrazine vapor at an elevated temperature (e.g. 90 °C for 1 h).[120] GO papers obtained by filtration have a layered structure. The reduction of a GO paper releases gaseous species such as H_2O and CO_2 and will result in forming pores in rGO matrix.[53, 129, 130] The microstructure of this rGO film is just like that of a "leavened bread", having open pores and continuous cross-links. The as-obtained rGO foams are conductive and flexible. They showed a tensile strength of about 3.2 MPa and a Young's modulus of 7 MPa.

A "breath-figure" method has been developed to self-assemble chemically functionalized rGO sheets into large-area flexible porous films.[131–133] For example, polystyrene-grafted GO sheets were dispersed in benzene, and then cast onto a flexible PET substrate and exposed to a stream of humid air.[134] Endothermic evaporation of the volatile benzene resulted in the spontaneous condensation and close packing of aqueous droplets. Subsequent drying and pyrolysis resulted in forming a 3D macroporous film of polymer-grafted rGO on the substrate. This film is mechanically robust and flexible.

Recently, laser-scribed graphene (LSG) attracted special attentions for flexible energy devices.[135–137] This graphene material was prepared by the irradiation of a GO film on PET substrate with an infrared laser inside a commercial LightScribe CD/DVD drive, reducing GO to LSG with porous network. The conductivity after 1,000 bending cycles (curvature radius = 5 mm).

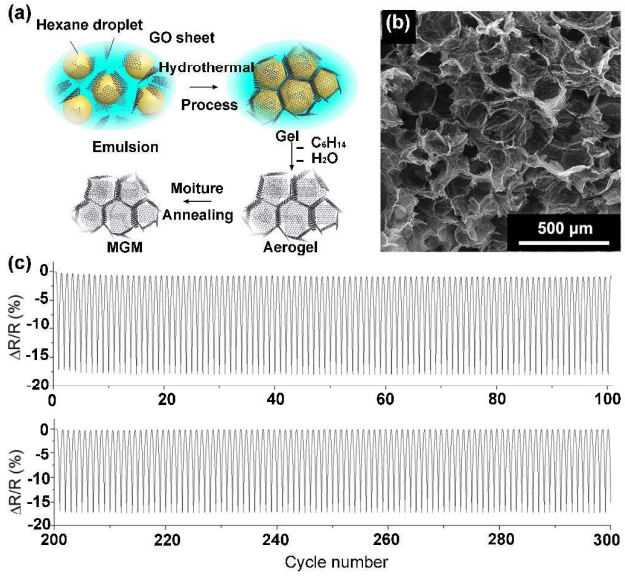

Fig. 3. (a) Schematic illustration of the preparation of a macroporous graphene monolith (MGMs). (b) Cross-sectional SEM image of a MGM. (c) Resistance response of a MGM prepared from 5 mg mL^{-1} GO to compression recorded during 300 cycles. Reprinted with permission from ref. 128.

LSG film showed a high conductivity (1,738 S m^{-1}) and excellent mechanical flexibility, exhibiting only ~1 % change in its The simple direct fabrication of LSG on flexible substrate simplifies the development of lightweight devices, such as flexible capaticors,[137] gas sensors,[135] and actuators.[136]

2.5 Flexible graphene composites

2.5.1 Composites with carbon nanotubes. An rGO/CNT composite paper was prepared by casting the mixed dispersion of GO and functionalized CNTs followed by thermal reduction.[138] This hybrid paper was mechanically stable and it can recover to its original shape by releasing from its twisted or bent state. The electrical resistivity of this paper (3×10^{-4} Ω cm) was measured to be about one order of magnitude lower than that of an rGO paper (4.26×10^{-3} Ω cm).

For the applications as flexible transparent conducting electrodes, CVD-graphene is a better choice than rGO sheets as the starting material for preparing graphene/CNT composites. A transparent flexible graphene/CNT membrane was fabricated by covering a CVD-graphene sheet onto the surface of a large-area CNT thin film.[139] This as-prepared vein-membrane-like hybrid film showed an elastic feature at strains smaller than ~2% and a plastic feature at strains from ~2 to 30% before breaking. Besides, this ultra-thin film (sub-nanometer thick graphene on tens nanometer thick CNT) is transparent (52.5 % at 600 nm) and has a low sheet resistance (573 Ω sq^{-1}). A transparent conductive thin film called "rebar graphene" was prepared by simply annealing dodecyl-functionalized single walled carbon nanotubes (SWCNTs) on a Cu foil without introducing extraneous carbon source.[140] The SWCNTs were partially unzipped to form a seamless 2D conjoined graphene/SWCNT hybrid. Thus CNTs act as reinforcing bars (rebar), toughening graphene through both regional π-π stacking and covalent bonding. The "rebar graphene" membranes can float on water and then be transferred onto flexible substrates. These membranes showed a low sheet resistance (~600 Ω sq^{-1}) and high transmittance (95.8 % at 550 nm). Furthermore, after transferring onto a PET substrate, this "rebar graphene" membrane is an ideal material for flexible transparent electrode, and can be repeatedly bent to large angles without mechanical failures.

3D macroporous architectures of CNTs or graphene have been extensively studied.[141–144] Actually, CNTs and graphene sheets are theoretically considered as the best building blocks to construct ultralight yet elastic and conductive aerogels.[145–148] A graphene coated CNT aerogel showed super elasticity and complete fatigue resistance to large cyclic strains (1×10^6 cycles), whereas its weight density (ρ) was increased from 8.8 to 14.0 mg cm^{-3}.[149] Furthermore, an ultra-flyweight CNT/graphene hybrid aerogel with a ρ of ~ 0.16 mg cm^{-3} was reported, and this value is even smaller than that of air under ambient condition (ρ=1.2 mg cm^{-3}).[150] The procedures of preparing the ultralight CNT/graphene composites are briefly described as follows. The mixed aqueous dispersion of CNTs and giant GO sheets (average size ~ 18.5 μm) was poured into a mould followed by freeze-drying for 2 days. After reducing with hydrazine vapour at 90 °C for 24 h, the mixture was vacuum-dried at 160°C for 24 h to yield

the CNT/graphene aerogel. This super elastic hybrid aerogel can keep its original thickness, macroscopic shape and porous 3D microscopic structure after a fatigue test of 1,000 cycles. Another straightforward approach to prepare CNT/graphene foam is growing a CNTs forest or array on graphene 3D framework.[151, 152] CVD-graphene was firstly deposited in a Ni foam to form a 3D porous structure, then the CNT forest was grown on graphene. Finally, Ni foam was removed to release a CNT/graphene foam. The good connection between graphene and CNT provide the composite foam with a robust and flexible mechanical property.

2.5.2 Composites with polymers. Graphene materials are frequently blended with polymers to form functional composites. The polymer component can improve the processability and/or flexibility of graphene materials, and also possibly provide them with new functions such as pesodocapacitances or electrocatalytic activities.[27, 153–155] Our group reported strong flexible composite films of GO or rGO with PVA or chitosan.[156, 157] These films were prepared by vacuum filtrating the mixed solutions of both components and showed layered microstructures because of directional fluid induced parallel orientation of graphene sheets. These composite papers can be bent into large angles or be shaped into various desired structures. Similarly, we also prepared rGO/polyaninilne nanowire composite films by vacuum filtration and used as flexible electrodes of electrochemical capacitors.[158] A more convenient method was drop casting graphene/polymer composite solution on a rigid substrate and then peeled off the film into a free-standing state after drying. We have prepared rGO/poly(vinyl pyrrolidone) flexible films on supported graphite foils in this way and applied them in flexible SCs as electrodes.[159]

On the other hand, the blending of large amounts of polymers will greatly decrease the conductivity, moduli and tensile strengths of graphene films. Recently, we developed a gel-film transformation (GFT) method to prepare paper-like films of GO and silk fibroin (SF). In this case, the composite films were formed by facile solution casting of soft GO/SF composite hydrogel, and the film containing 85 wt% showed mechanical strength surpasses that of natural nacre.[160] This GFT technique has been extended to prepare rGO films containing trace amounts (<8%, by weight; wt%) of poly(acrylic acid-co-(4-acrylamidophenyl)boronic acid) ($PAPB_{0.2}$, the subscript refers to the molar ratio of carboxylate groups amidated with 3-aminophenylboronic acid，Fig. 4a-d).[161] The film with 4 wt% $PAPB_{0.2}$ exhibited an electrical conductivity of 337 ± 12 S cm^{-1}, a tensile strength of 381.78 ± 11.83 MPa, and a toughness of 7.50 ± 0.40 MJ m^{-3} (Fig. 4e-f). Particularly, it delivers a high gravimetric specific strength (208 N m g^{-1}) comparable to those of widely used metals or alloys such as stainless steel, Al, Mg and Ti alloys (Fig. 4g).

Graphene/polymer composites can also be synthesized by *In-situ* growth of polymers in graphene matrices. This technique is effective to form composites with uniform distributions of both components.[162, 163] For example, graphene composites with conducting polymers such as polyaniline (PANI) and polypyrrole are usually prepared by *in-situ* polymerization.[164–167] Particularly, a flexible graphene/PANI composite film was obtained by *in-situ* growing PANI on a graphene film, and it can be folded into a 3D structure.[168] Upon folding to a large angle of 180° and further compressed to 50% of its original length, this composite film can

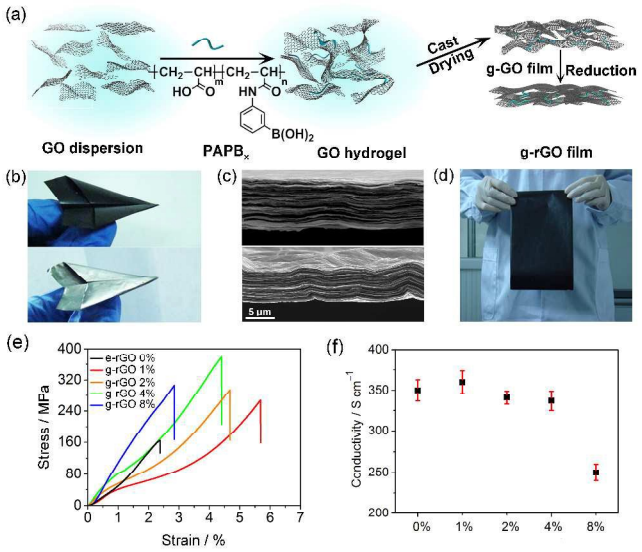

Fig. 4. (a) Schematic illustration of the preparation of GO and rGO films by GFT method; they are nominated as g-GO and g-rGO, respectively. (b) Photographs of g-GO (top) and g-rGO (bottom) films, showing their flexibility. (c) SEM images of the fractured cross sections of g-GO (top) and g-rGO (bottom) films, exhibiting their laminated structures. (d) Photograph of a large-area g-GO film. (e) Typical stress–strain curves of the rGO films prepared by GFT method, or reducing the GO film prepared by evaporation of GO dispersion (e-rGO). The percentages are the polymer weight contents relative to GO. (f) Electrical conductivities of e-rGO and g-rGO films with the compositions as indicated. Reprinted with permission from ref. 161.

keep its physical integrity. Furthermore, its thermoelectric properties were improved as a result of the formation of an electrically connected between adjacent folded layers. Except conducting polymers, an electroactive polymer, polyselenophene (PSe), has also been introduced to GO by *in-situ* polymerization to form a composite and its GO component was successively reduced into rGO.[169] The resulting rGO/PSe nanohybrid electrode could be folded or repeatedly bent without introducing any structural defects.

Highly ordered ultrathin graphene/polymer composite membranes (several to hundreds of nanometers in thicknesses) showing high elasticity and robustness can be fabricated using LbL assembly.[170–173] For example, negatively charged GO layers were incorporated into positively charged polyelectrolyte multilayers.[174] The polyelectrolyte multilayer was formed by alternatively spin-coating positively charged poly(allylamine hydrochloride) (PAH) layer and negatively charged poly(sodium 4-styrene sulfonate) (PSS) layer. In order to deposit negatively charged GO layers, the polyelectrolyte multilayer was terminated with positively charged PAH layer. The elastic modulus of the polymer film (thickness = 50 nm) was increased by about one order of magnitude from 1.5 to about 20 GPa for the composite with 8.0 vol % GO. These tough composite films can be freely suspended over a copper substrate with a 150 μm aperture and sustain large mechanical deformations. A similar strategy has been used to prepare multilayer hybrid film of poly (*p*-phenylene vinylene) (PPV)/rGO composite membrane on a PET substrate.[175] These LbL assembly strategies effectively prohibited the

aggregation of graphene sheets, and improved the transparencies and decreased the thicknesses of the composite films.

The flexibility of a graphene/polymer composite can be improved by optimizing the interfacial interaction between its components. An example is the formation of efficient crosslinking between hyperbranched polyurethane (NHPU) chains with the aliphatic hydroxyl groups decorated to GO sheets.[176] The resulting GO/NHPU composite exhibited a 98% shape recovery and 93% shape retention as it was used as a shape memory material.

2.5.3 Composites with inorganic nanoparticles. Flexible composites of graphene and inorganic nanoparticles have also been extensively studied. These flexible composites are widely employed in portable and wearable devices, such as solar cells,[45] OLEDs,[177] fuel cells,[178] SCs,[179] LIBs,[180] sensors.[181] A variety of inorganic nanostructures have been blended with graphene and their derivatives, including metals: Pt,[182] Pd,[183] Ag,[184] Si,[180] Cu;[178] oxides: RuO_2,[185] MnO_2,[186] V_2O_5,[187] Mn_3O_4,[188] Co_3O_4,[189] SnO_2,[190] TiO_2,[191] NiO,[192] Fe_3O_4,[193] ZnO[194] and $BaTiO_3$;[195] compounds: InN[196] and CdS;[197] CdSe,[198] bimetallic hybrids: Al-TiO_2,[199] Fe_2O_3-SnO_2,[200] Au-Pt[201] and Cu-Ag.[202] The methods used to synthesize this type of composites can be simply classified as *ex-situ* and *in-situ* hybridizations. In the following section, we give several examples of preparing flexible graphene/metal or oxide composites.

Ex-situ hybridization usually involves using the mixed solutions of graphene sheets and pre-synthesized nanoparticles as the starting materials. LbL deposition has been widely used for *ex-situ* fabricating layered thin films on flexible substrates.[203, 204] Following this approach, a Au nanoparticle/graphene composite film has been successfully fabricated. First, Au nanoparticle monolayers were prepared by dipping[203] or electrophoretic deposition.[204] Then the Au monolayers and rGO sheets alternately deposited on the PET substrate to form multi-layered films. Interestingly, 2D array of Au nanoparticles at oil-water interfaces could be transferred onto flexible GO paper by dip coating, forming a monolayer of densely packed gold nanoparticles on GO paper.[205] Similar approach has also been used to assemble Au@Pt core-shell nanoparticles on flexible rGO paper.[201] A graphene/WS_2 composite film can be fabricated by transferring a CVD graphene film onto a polymer substrate and then depositing a WS_2 layer on the surface of graphene.[206] This procedure was repeated for 4 times to achieve a flexible and robust composite film. Similarly, graphene/Ag nanowire composite films on flexible PET substrates were also prepared.[207] These films were fabricated by depositing Ag nanowires on the surface of CVD-grown graphene films or transferring graphene films onto Ag nanowire networks. All of these composite films showed good mechanical flexibility and stretchability.

Although *ex-situ* hybridization is able to pre-select nanostructures with desired functionalities; however it sometimes suffers from the low loadings and non-uniform coverages of the nanostructures on graphene surfaces. In contrast, *in-situ* hybridization can form uniform surface coverage of nanocrystals by controlling the nucleation sites on graphene surfaces. Chemical reduction is the most popular strategy for the synthesis of metal nanostructures. Precursors of noble metals, such as $HAuCl_4$, $AgNO_3$, K_2PtCl_4 and H_2PtCl_6, can be simply *in-situ* reduced by reducing agents such as amines, $NaBH_4$, and ascorbic acid.[208] For example, a mixed aqueous solution of GO, ascorbic acid and metal precursors such as $Ag(COOCH_3)$ or $HAuCl_4$, or $HPtCl_4$ was ultrasonicated and heated at 90 °C for 45 min.[209] Then a stable suspension of metal particle/rGO dispersion filtered with a porous membrane to form flexible metal (Ag, Au and Pt)/rGO composite papers. Another chemical method for *in-situ* synthesis of inorganic nanocrystals is hydrothermal reduction.[210] The hydrothermal process can produce nanostructures with higher crystallinity compared with chemical reduction without post-synthetic annealing or calcination. GO can be reduced to rGO during the hydrothermal process. An example is a flexible N-doped graphene/SnO_2 composite paper was obtained by hydrothermal treatment of the mixed solution of $SnCl_4 \cdot 5H_2O$ and GO at 180 °C for 24 h and followed by vacuum filtrating of the reaction solution.[190] In addition, direct electrochemical deposition of inorganic crystals on graphene-based flexible substrates is an attractive approach without the requirement for post-synthetic transfer of the composite solution and filtration. This technique has been used to load MnO_2 nanoparticles on a flexible 3D CVD-grown graphene network.[211] The 3D MnO_2/graphene hybrid network was bendable and foldable, little change (less than 1%) in electrical resistance was observed after bending for 500 cycles to different angles ranging from 0° to 180°.

3. Flexible devices related to energy conversion

Flexible graphene materials and their composites, including 1D fibres, 2D films and 3D networks, have wide applications in flexible, portable, and wearable energy devices.[212-215] For example, transparent and electrical conductive graphene thin films can replace the traditional rigid electrodes in optoelectronics such as organic photovoltaics (OPVs),[33, 212] dye-sensitized solar cells (DSSCs),[182, 216] organic light-emitting diodes (OLEDs)[217, 218] and photodetectors.[219, 220] Graphene catalysts are expected to be applied in fuel cells.[19] Graphene based actuators[221, 222] and nanogenarators (NGs)[25, 223] have light weights, good flexibility and promising performances. The devices described above are related to energy conversion, and their recent advancements and challenges will be discussed in the following section.

3.1 Optoelectronic devices

Flexible optoelectronic devices are expected to be widely used in our daily lives, such as bendable, foldable and/or stretchable displays, OPV cells and touch panels.[33] The key component of these devices is flexible electrodes that can be stretched and/or bent without compromising their conductivities and transparencies. Indium-tin-oxide (ITO) electrodes have conventionally been used as transparent conductive electrodes (TCEs).[224] They exhibit a transparency of >90% in ultraviolet-visible light region and a sheet resistance of 10–30 Ω sq^{-1}. However, ITO electrodes have drawbacks of brittleness and high cost, making it unsuitable for flexible devices.[225]Among various materials for replacing ITO, graphene has emerged as a good candidate, because it possesses most of the features required for the electrode materials of flexible optoelectronics.[2,226] Monolayer graphene is transparent with a transmittance exceeding 97%, and it also has a high carrier concentration with mobility in the order of 10^6 with remarkable

Table 1 Graphene materials and their flexible optoelectronic devices

Graphene material	Synthesis method	Device	Performance			Flexibility	Ref.
			ρ [a] (Ω sq^{-1})	T [b] (%)	PCE [c] (%)		
rGO film	spin-coating annealing	OPV	3,200	65	0.78	1,000 cycles bending (r [d] = 5 mm)	234
LrGO film	spin-coating laser-irradiation	OPV	700	44	1.10	bending angles up to 135°	24
graphene film	CVD growth transferring	OPV	230	72	1.18	bending angles up to 138°	49
graphene film	CVD growth inkjet printing	OPV	12	73	2.90	500 bending cycles (r [d] = 4 mm)	45
graphene/PEDOT :PSS/Au film	CVD growth transferring	OPV	158±30	90	3.20	1,000 cycles bending (r [d] = 1.5 mm)	227
graphene/PEDOT :PSS film	CVD growth LbL	OPV	36.6	85	4.33	bendable	48
graphene/PEDOT film	CVD growth in-situ polymerisation	DSSC			6.26	bending number of 10 (r [d] = 4.7 mm)	243

Graphene material	Synthesis method	Device	ρ [a] (Ω sq^{-1})	T [b] (%)	CE [e] (cd A^{-1})	LE [f] (lm W^{-1})	Flexibility	Ref.
graphene/PEDOT :PSS/perfluorinated ionomer film	CVD growth spin-coating	OLED	30		F [g] 30.2 P [h] 98.1	F [g] 37.2 P [h] 102.7	1,000 cycles bending (r [d] = 7.5 mm)	249
graphene/CNT fim	CVD growth LbL	OLED	76	89.13	P [h] 14.7	P [h] 9.2	bending angles up to 90° for hundreds cycles	250
graphene film	CVD growth transferring	OLED	750	96.6	P [h] 11.44	P [h] 2.24	r [d] = 0 – 0.72 cm	251
graphene film	CVD growth LbL	OLED	40-60	80	P [h] >250	P [h] >160	bending at r [d] = 0.5 cm	252

Graphene material	Synthesis method	Device	Responsivity (A W^{-1})	Flexibility	Ref.
doped graphene film	CVD growth transferring	photodetector	120 (>780 nm)	bending number >20 angles: 30, 60, 70 and 80°	219
CdSe NB/graphene film	CVD growth transferring	photodetector	8.7 (633 nm)	bendable	260
graphene/PbS QD film	CVD growth transferring	photodetector	10^7 (895 nm)	1,000 cycles bending (r [d] = 7 mm)	263
rGO film	drop-casting thermal	photodetector	~0.7 (895 nm)	1,000 cycles bending (r [d] = 7 mm)	264

[a] ρ-Resistance. [b] T-Transmittance at 550 nm. [c] PCE- Power conversion efficiency. [d] r-Curvature radius. [e] CE -Current efficiency. [f] LE -Luminous efficiency [g] F-Fluorescent. [h] P-Phosphorescent.

flexibility (elastic modulus ≈ 1 TPa).[2] Graphene TCEs have been applied in a variety of flexible optoelectronic devices, such as OPVs, OLEDs and photodetectors (Table 1).[24, 227, 228]

3.1.1 Organic photovoltaics. OPVs are solar cells that can produce electricity by converting sunlight power using conjugated polymer-based p-n junctions or heterojunctions. They are usually cheap, lightweight, and possibly to be flexible. To date, graphene materials have been utilized as the transparent electrodes, electron acceptors or hole transport layers of OPVs.[2, 229–232] Whereas, in flexible OPVs, graphene materials are mostly used as TCEs.

Recently, rGO films have been explored as the transparent bottom electrodes in OPV devices.[233] These graphene TCEs were fabricated by coating GO films on rigid substrates (e.g., glass, Si/SiO_2), followed by the reduction with hydrazine vapor or annealing. Because flexible polymeric substrates (e.g., PET)

cannot stand high temperatures (< 140 °C), this technique is unsuitable for preparing flexible TCEs. However, rGO films can be transferred to PET substrates to make the electrodes flexible.[234] Actually, a 16 nm-thick rGO film with a transmittance of 65% was used to fabricate a flexible OPV device, and this device can sustain a thousand cycles of bending (curvature radius = 5 mm) at a tensile strain ~2.9%. Unfortunately, the obtained devices exhibited a low power efficiency (PCE) of 0.78 % because of the large sheet resistance of rGO TCE (3.2 kΩ sq^{-1}). The PCE of a flexible OPV was greatly improved to 1.27% by replacing rGO film with an rGO/CNT composite film following a similar fabrication procedure.[225]

A laser reduction technique was used to convert spin-coated GO film on PET to a flexible TCE (Fig. 5a and b).[24] A 20 nm-thick laser reduced GO (LrGO) film showed a sheet resistance of 700 Ω sq^{-1} and a transmittance of 44%. The flexible OPV with this LrGO TCE exhibited a high PCE of 1.1%, an order of magnitude higher than that of the counterpart with a chemically reduced GO electrode. This OPV can be bent to angles up to 135° without decreasing its performance. In comparison, the devices with ITO/PET TCEs fabricated can partly keep their functions as the bending angles ≤ 45°, and they failed completely at a bending angle of 65°.

As described above, the PCEs (<2%) of the OPVs with rGO electrodes are usually lower than those of the devices with ITO electrodes (5~10%). This is mainly due to the low conductivities of graphene electrodes. High-quality, large-area graphene films with relatively low sheet resistances and high optical transparencies can be obtained via CVD approach. A flexible OPV with CVD-graphene based bottom TCE (thickness: 1–3 nm, sheet resistance: 230 Ω sq^{-1}) showed a maximum PCE of 1.18%. These flexible devices can be worked at bending angles up to 138°.[49] Whereas, the ITO-based device fabricated under the same conditions (PCE:1.27%) displayed cracks and irreversible failure as bent to 60°.

Introducing metal grid (e.g., Au, Ag, Ti, Cu, Ni, Al) into CVD-graphene/PET electrode can further reduce its sheet resistance.[45, 236] For example, the composite film of inkjet printed Ag grid and CVD-graphene exhibited a sheet resistance of 12 Ω sq^{-1} and 73% transparency at 550 nm.[45] This thin film was used to fabricate a flexible OPV with a high PCE of 2.9%. More importantly, this thin film showed no increase in its resistance even after 500 bending cycles (curvature radius = 4 mm). In comparison, the resistance of ITO/PET film increased rapidly to exceed 1 KΩ after only a few bending cycles, and reached to around 30 KΩ after several hundred bending cycles.

In order to improve the conductance of graphene films, blending conducting polymers such as poly(3,4-ethylenedioxythiophene)/poly(styrenesulfonate) (PEDOT:PSS) was another choice. Because PEDOT:PSS has a higher surface work function (energy to remove electron from surface) than that of graphene, electrons would transfer from graphene to PEDOT component. Thus graphene film will be doped with holes and the sheet resistance of the graphene film was decreased for more than 75%.[48] These composite films were applied in flexible OPV devices. A bendable device with an electrode consisting of three layered graphene on PET showed a high PCE of 4.33%, and this value is among the highest efficiencies attained for OPVs with CVD-graphene electrodes.

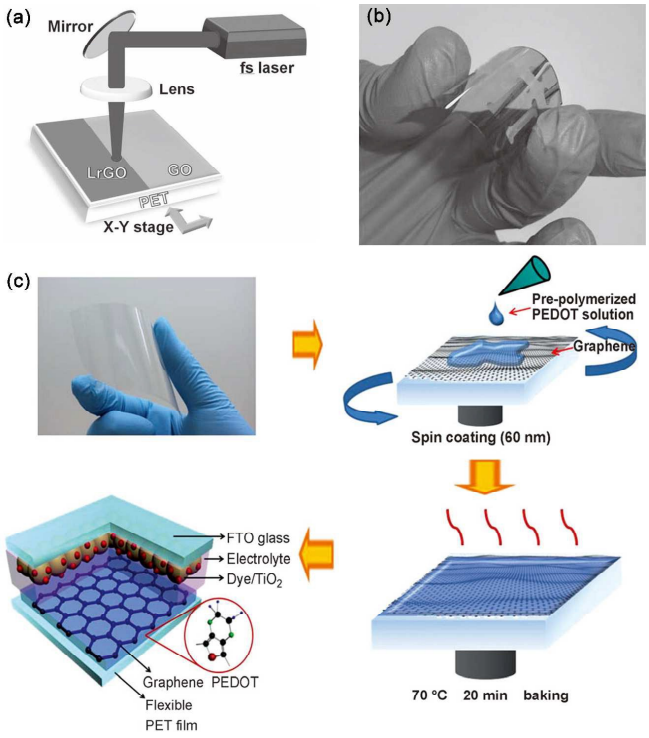

Fig. 5. (a) Schematic illustration of the experimental technique used for the reduction of GO films on PET substrates. (b) Picture of a flexible PET/rGO/PEDOT:PSS/P3HT:PCBM/Al photovoltaic device. (c) Photograph of a graphene-coated PET substrate, and schematic diagram of the fabrication steps involved in preparing a DSSC with a graphene/PEDOT counter electrode on a PET substrate. Reprinted with permission from ref. 24, 243.

Semitransparent OPVs are useful for some special applications, such as tinted thin films coated on electronics and OLEDs.[237, 238] Graphene is a candidate material for the top electrodes of these devices. This is mainly due to that a large-area graphene film can be easily transferred to a flexible substrate. For example, a hybrid CVD-graphene film was used as the transparent top electrode in a flexible OPV on polyimide (PI) substrate.[227] This composite film was prepared by coating a layer of PEDOT:PSS and Au nanoparticles on CVD-graphene film. The PEDOT:PSS and Au nanoparticles are p-type dopants of graphene because they can withdraw electrons from graphene. Thus the sheet resistance of four-layer graphene was decreased from 220 Ω sq^{-1} (undoped) to 68 Ω sq^{-1} (doped). The transmittance of doped graphene film was measured to be about 90%, comparable to that of ITO electrode. The double-layer graphene based flexible OPV device showed a maximum PCE of 3.2%, and it decreased for only about 8% after 1,000 times bending (curvature radius = 1.5 mm).

3.1.2 Dye-sensitized solar cells. DSSCs have attracted significant interests because of their low costs and relatively high PCEs.[239] A typical DSSC device consists of a dye-modified TiO_2 photoanode, Pt counter electrode, and iodide electrolyte. The photoexcitation of the molecular dye under light induces electron transfer to the photoelectrode. The collected electrons in the photoelectrode are transported through an external circuit to the

counter electrode. The development of next-generation flexible DSSCs is focused on replacing platinum for commercial use. Owing to its high conductivity and flexibility, graphene offers an attractive option of flexible and conductive counter electrodes for DSSCs.[239, 240] In 2008, we used pyrene butylate functionalized graphene as the counter electrode of DSSC and showed a low PCE around 2%.[241] Then, we improved the performance of the electrode by blending graphene with PEDOT:PSS and spun coated on ITO substrate, and the DSSC device showed a PCE (4.5 %) comparable to that of the counterpart with Pt counter electrode (6.3%).[242] Followed this method, Lee *et al.* spun coated graphene/PEDOT film on a plastic substrate to fabricate a flexible DSSC (Fig. 5c),[243] showing a PCE of 6.26%. In comparison, the efficiencies of the DSSCs with Pt/ITO and pure PEDOT counter electrodes are 6.68% and 5.62 %. The low costs and easy processing of graphene counter electrodes make them have practical importance in the development of new flexible DSSCs. More importantly, these graphene electrodes kept their functions after a symmetric bending for 10 cycles (bending radius = 0.47 mm).

3.1.3 Organic light-emitting diodes. OLEDs can convert electrical energy to light, having applications in panel displays and solid-state lighting with high luminous efficiency and flexibility.[244] The simplest OLED has an organic emissive layer sandwiched between two electrodes.[245] Electrons and holes are injected into the emissive layer from cathode and anode, respectively. The energy released by electron-hole quenching can excite the fluorescence molecules of emissive layer to emit light. This mechanism is opposite to that of OPVs. Thus, like OPVs, the performances of OLEDs also strongly depend on the properties of their TCEs. Graphene materials offer an excellent option as TCEs of OLEDs.[246] Solution processed graphene[247] and CVD-graphene[248] multilayer films have been explored for this purpose. However, the OLEDs with these TCEs exhibited a current efficiencies (CEs) of only around 1 cd A^{-1}, much lower than those of the devices with ITO electrodes. This is mainly due to their relatively lower work functions (~ 4.4 eV) and higher sheet resistances (> 300 Ω sq^{-1}) compared with those of ITO (4.7 – 4.9 eV and 10 Ω sq^{-1}). The low work function of graphene causes inefficient charge injection from graphene electrode into the organic layer. The low conductivity of pristine graphene films also limits the luminous efficiencies (LEs) of the devices. To overcome these issues, high-quality CVD-graphene films were doped with HNO_3 or $AuCl_3$ to decrease their sheet resistances to ~ 30 Ω sq^{-1} and spun coated with conducting polymers (PEDOT:PSS and perfluorinated ionomer) to increase their work function to ~5.95 eV.[249] This high work function enables holes to be efficiently injected into the organic layer from graphene, thus improves the efficiency of light emission. A fluorescent OLED with HNO_3 or $AuCl_3$ doped four-layer graphene exhibited a high CE of 30.2 cd A^{-1} (LE ~ 37.2 lm W^{-1}), and a phosphorescent counterpart showed a CE as high as 98.1 cd A^{-1} (LE~102.7 lm W^{-1}) (Fig. 6a-b). These efficiencies are significantly higher than those of the similar optimized devices with ITO anodes (24.1 lm W^{-1} for fluorescent OLEDs, and 85.6 lm W^{-1} for phosphorescent OLEDs). The devices based on graphene electrodes demonstrated excellent bending stability and maintained their performances even after 1,000 repeated bending (curvature radius = 7.5 mm). In comparison, the devices with ITO electrode completely failed their function after only 800 times of bending. This is a pioneering work on flexible OLEDs based on graphene anodes with performances surpassed those with ITO anodes. For commercial application, this technique has some drawbacks: HNO_3 doping is unstable and the performance of doped graphene TCE decays with time. On the other hand, $AuCl_3$ doping causes large surface roughness of graphene electrode, increasing the risk of short circuit the OLED devices.

To improve the chemical stability of graphene TCEs, graphene films supported on SWCNT arrays were fabricated as anodes in OLEDs.[250] After introducing CNT arrays, the graphene films showed a low sheet resistance of 76 Ω sq^{-1} and a high transmittance of 89%. The performances of the OLEDs with graphene-on-CNT hybrid electrodes were tested to be comparable to those of the devices with ITO electrodes. Most importantly, the graphene-on-CNT hybrid electrodes can be transferred onto plastic substrates to construct highly flexible devices. It can emit uniform green light at bending angles up to 90° and even can sustain hundreds of bending cycles. However, in this case, PMMA residual resulted from graphene transfer process may lead the structural discontinuity of graphene film and decrease its performance. A clean graphene can be transferred onto a flexible substrate by inserting an organic small molecular buffer layer (2-(diphenylphosphory) spirofluorene (SPPO1)) between PMMA and graphene. The generation of PMMA residue on graphene was avoided due to the superior solubility of SPPO1 in solvent (e.g., acetone).[251] As-prepared OLED devices based on clean graphene films exhibited better performances than those of their counterparts fabricated from the films transferred via a conventional process. Moreover, the flexibility of these OLEDs is much better than that of the devices with ITO electrodes. The sheet resistance of graphene electrode increased by 1.2 times as its curvature increased from 0 to 0.72 cm^{-1}, while that of ITO electrode increased by 10.4 times under the same condition.

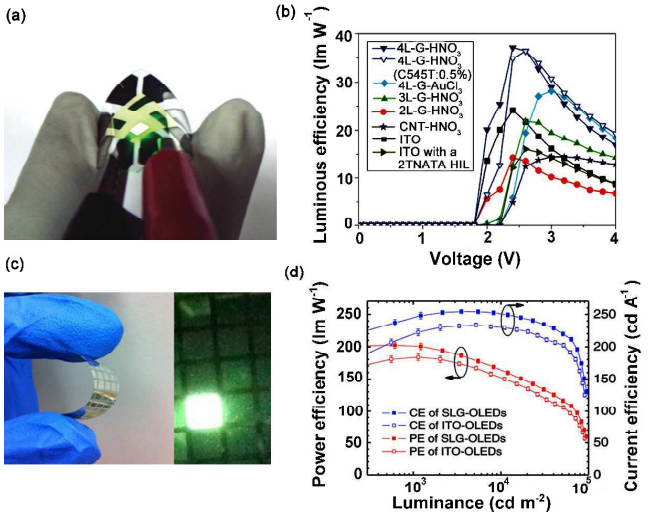

Fig. 6. (a) Digital image of light emission from a flexible fluorescent green OLED with a four-layered graphene anode doped with HNO_3. (b) Current efficiencies of OLED devices using various graphene layers (doped with HNO_3 or $AuCl_3$) or ITO as anode. (c) Pictures of flexible OLEDs on plastic substrate with SLG electrode. (d) PE and CE of green OLEDs on sinle layer

graphene (SLG) and ITO with enhanced coupling structure. Reprinted with permission from ref. 249, 252.

Graphene TCEs suffer the drawbacks of significant light absorption (2.3–3% for each monolayer) as they used in OLEDs. To minimize this negative effect, monolayer graphene film was used to fabricate a flexible OLED with an efficiency sufficiently high for general lighting.[252] Single-layer graphene was grown by CVD and transferred onto a plastic substrate. By soaking the graphene sample in 1 mg mL^{-1} triethyloxonium hexachloroantimonate/ dichloroethene solution, a charge transfer complex was produced. Successively, the graphene complex was spun coated with a thin layer of PEDOT:PSS and a thermally deposited MoO_3 layer. This two-step modification reduced the sheet resistance of monolayer graphene to 40–60 Ω sq^{-1} and increased its work function to 6.7 eV, outperformed those of ITO deposited on plastic substrate. Thus, the performance of a green OLED was improved by its high efficient hole injection from modified graphene layer to light-emitting layer (Fig. 6c). The flexible devices showed PE >160 lm W^{-1}, and LE >250 cd A^{-1}, respectively (Fig. 6d). The PE of white OLEDs reached 80 lm W^{-1} at 3000 cd m^{-2}, comparable to those of the most efficient lighting technologies. Furthermore, the device exhibited the same performance before and after bending to a radius of 0.5 cm, implying its promising application in portable electronics.

3.1.4 Photodetectors. Photodetectors can convert light into electrical signals, and they have applications in imaging, optical communications, and future intra-chip optical interconnects.[253–255] Upon the excitation of light, the electrons and holes generated by the incident photons move in opposite directions, yielding a photocurrent correlated with light intensity. Recently, flexible and transparent photodetectors built on lightweight and bendable plastic substrates have received increasing attention compared with conventional rigid photodetectors. This is mainly due to the potential applications in flexible phones, curved digital cameras and foldable displays.

Graphene has a strong and broadband light adsorption, covering ultraviolet light to terahertz.[256] Together with its extremely high carrier mobility, graphene films are expected to have practical applications in ultrafast broadband photodetectors with good flexibility.[257, 258] IBM group reported the first graphene-based photodetectors with operation wavelengths ranging from 300 nm to 6 μm.[259] Ultrafast graphene photodetector was confirmed to be able to work at high frequencies up to 40 GHz.[258] However, the weak light adsorption (~2.3% per layer) and short photocarrier lifetime of graphene cause the photoresponsivity of device to be low (5×10^{-4} mA W^{-1}). Moreover, the gapless nature of graphene usually results in strong dark current and low photosensitivity.

Recently, an N-type dopant (2-(2-methoxyphenyl)-1,3-dimethyl-2,3-dihydro-1*H*-benzoimidazole (o-MeO-DMBI)) was incorporated to CVD-graphene to produce a fully transparent and flexible IR photodetector (Fig. 7a).[219] The doped graphene induced large number of electron-hole pairs, and increased the responsivity of photodetector up to 120 A W^{-1} at the wavelengths >780 nm. This graphene photodetector also showed good reproducibility and stability when repeatedly bent back and forth numerous times (>20) to different angles: 33, 60, 70 and 80° (Fig. 7b). However, the photosensitivity (photocurrent vs. dark current ~ 5.0%) of the device is still relatively low because of the

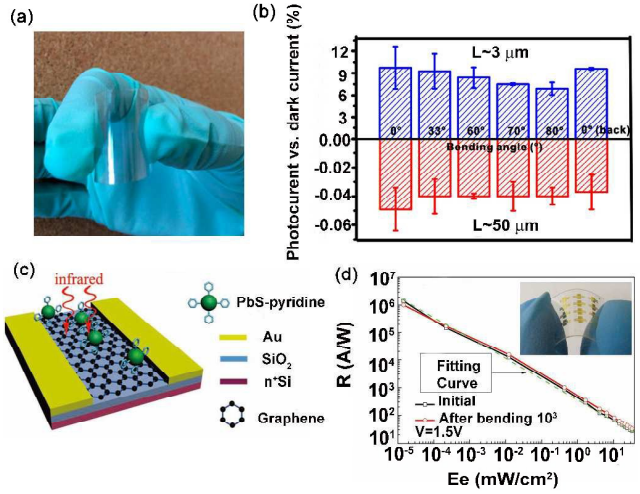

Fig. 7. (a) Photos showing the transparency and flexibility of graphene photodetector built on PET substrates. (b) Photoresponses of the metal-based photodetectors (top, channel length ~3 μm; bottom, channel length ~50 μm) on PET substrate at different bending angles. (c) Schematic diagram of a graphene transistor modified with PbS QDs under light illumination. (d) Responsivity of the photoconductor as functions of light irradiation characterized before and after a bending test. Reprinted with permission from ref. 219, 263.

zero bandgap of graphene.

Incorporating semiconductor materials can modulate the bandgaps of graphene materials to improve the performances of graphene based photodetectors,[260, 261] For example, CdSe nanobelt/graphene composite was coated on a PET substrate to fabricate high-performance photodetectors.[260] The CdSe semiconducting nanobelts has a bandgap of 1.74 eV; thus this component can suppress the dark current caused by graphene. Besides, these nanobelts have excellent flexibility; thus they are promising for the applications in flexible devices. The flexible photodetector with this transparent composite showed an ultrahigh photosensitivity (photocurrent vs. dark current ~ 1.2×10^5 %) upon a 633-nm light illumination.

Quantum dot (QD)-based photodetectors usually exhibit strong photocurrent responses (10^3 AW^{-1}); thus QDs have also been blended with graphene materials to further increase the light absorptions of photodetectors.[262] Strong and tunable light absorption in the QD layer can transfer electrons to graphene, thereby enhancing the photoresponse. For example, an infrared photodetector based on the composite of PbS QDs and single layer CVD-graphene (Fig. 7c) exhibited an ultrahigh responsivity of ~ 10^7 A W^{-1}, even after bending (curvature radius = 7 mm) for 1,000 times (Fig. 7d).[263]

Except CVD-graphene, rGO has also been used to fabricate flexible photodetectors. Drop casted GO films were annealed at 150 °C for different time to control their contents of oxygenated defects. The few-layer rGO films were transferred onto plastic substrates to fabricate flexible infrared photoconductors with responses in the range of 0.01 to 0.7 A W^{-1}.[264] These values among the highest for the photodetectors based on graphene or

graphene composites. More importantly, the flexible infrared photoconductor devices showed no obvious degradation of photoresponse even after 1,000 bending cycles (curvature radius = 7 mm). The solution-processable approach opens up a high throughput technology for graphene based flexible photodetectors.

Challenges: Thanks to its unique atom-thick two-dimensional electronic structure, superior transparency and high flexibility of graphene sheets, graphene based thin films are promising for the construction of flexible optoelectronic devices.[33, 265] Actually, graphene based touch panels have been successfully integrated into mobile phones which have already been selling in the market. The flexibility, neutral colour, and ambient stability of graphene-TCEs are unique and surpass those of ITO-TCEs. However, several challenges are still remained. (1) Unsatisfactory electrical conductivity and transparency: This is currently the major issue for the commercial use of graphene-TCEs in optoelectronics. Extensive effects have been devoted to improving the properties of graphene-TCEs, including the synthesis of high-quality graphene,[249] post-treatment of graphene,[247] hybrid with conducting polymers,[242, 243, 266] nanocrystals[45] or CNTs.[235, 250] Nevertheless, the performances of most graphene-TCEs are still not comparable to that of ITO. (2) The surface work functions and wettability of graphene thin films: In order to minimize the energy barrier at the electrode, the work function of a graphene thin film should be tuned by interfacial modification. Graphene thin film also needs to change its hydrophobic property to improve their solution processability. Therefore, it is highly desirable to develop effective interfacial modification methods for functionalizing graphene electrodes. (3) Transferring graphene materials to flexible substrates: Most of graphene thin films cannot be directly deposited on flexible plastic substrates. This is mainly due to CVD-graphene can only be grown on catalytic metal substrates, and the plastic substrate cannot resist the high-temperatures required for annealing rGO films.[267] Thus, the process of transferring graphene onto a flexible substrate is necessary and two strategies have already been developed. (i) Attaching graphene to the target substrate directly with chemical glues coated on the surfaces of target substrates; (ii) introducing new supporting layers for the easy removal of graphene sheets. However, there still has some obstacles. For example. The transfer of graphene film by strategy (i) needs chemical glues for special target substrates. Strategy (ii) requires to remove the supporting layer through a complicate process. For conventional ITO substrates, the post-cleaning treatment in organic solvent upon ultrasonication is efficient. Unfortunately, the graphene film is too thin and fragile to stand any harsh cleaning processes. The disadvantages existing in conventional graphene transferring techniques seriously impede the development of high performance optoelectronics. (4) Instability of doping: This is a bottleneck for the commercialization of graphene-based transparent electrodes. Because pristine graphene has a low charge concentration, chemicals must be used to increase the conductivity of graphene films. Unfortunately, commonly used dopants such as HNO_3 or $AuCl_3$ were found to be volatile, resulting in a rapid decreasing of doping level of graphene upon exposure to air.[232] New dopants are urgently needed for achieving a stable and efficient doping.[219, 268] (5) Large scale and low cost production: Although CVD method shows great potential to fabricate high quality transparent and conductive graphene materials, the cost of production is always the problem. Solution processing of GO/rGO dispersions provides an opportunity to solve the problem. However, the practical applications of CMG-based devices are still limited, largely because of the difficulties associated with controlling the defects of CMG sheets.

Although the performances of graphene based optoelectronic devices are mostly worse than those of the counterparts with ITO electrodes, it is believed that the excellent flexibility should render graphene a promising material for flexible optoelectronics. A few graphene materials showed performances superior to that of ITO in optoelectronic devices, reflecting their bright future.

3.2 Fuel cells

Fuel cells can efficiently generate clean, reliable electrical powers from chemical fuels. Flexible fuel cells have a wide range of portable applications from bendable battery to intelligent vehicles. Typically, the electricity is generated via an electrochemical oxidation of fuel (e.g., hydrogen, methanol) with oxygen or another oxidizing agent. At the anode and cathode of a cell, fuel and oxygen take place oxidizing and reducing reactions, respectively. An electrolyte is required to transfer protons and electrons resulted from the redox reaction. Electrons are drawn from the anode to the cathode through an external circuit, producing direct current electricity. In order to initiate and accelerate the electrochemical reactions, an appropriate catalyst is required.

Flexible graphene materials can act as catalytic supports for fuel cells because of its large specific surface area, chemical stability, high electrical conductivity, and electrochemical catalytic activity.[269–271] The light-weight graphene materials also provides new opportunity of portable fuel cells. Flexible graphene paper with electrodeposited Cu nanocubes was directly used as the anodes of hydrazine fuel cells.[178] A graphene coated carbon fibre (CF) paper can also be used as a flexible support of catalyst in anode.[272] After electrodepositing porous Pd nanocatalysts on the rGO/CF paper, the hybrid catalyst exhibited high catalytic activity and stability toward ethanol oxidation. Graphene materials were also used in flexible fuel cells as catalyst supports of cathodes. For example, a nitrogen doped rGO/CNT/Co_3O_4 paper was fabricated for oxygen reduction reaction (ORR).[273] Apart from the role of catalyst support, the incorporation of nitrogen atoms into graphene can provide catalytic sites for ORR. CNTs were sandwiched between graphene nanosheets to prevent the restacking of graphene sheets and improve the electrical conductivity of cathode. The flexible catalyst paper showed better durability and tolerance to methanol poisoning effects than that of commercial Pt/C catalyst.

More recently, graphene materials have also been explored for flexible microbial fuel cells, bacteria within the microbial fuel cell naturally decompose the organic wastes in water to generate electricity.[19, 274] For example, Hussain *et al.* reported a micrometer-sized microbial fuel cell comprised of a graphene anode, an air cathode, and a rubber substrate for flexibility.[274] As-fabricated microbial fuel cell was able to generate 1 nW of power from microliters of liquid. Another example is a rGO/nickel foam (NF) anode material used to fabricate microbial fuel cells (Fig. 8a

– e).[19] The rGO/NF anode was prepared by refluxing a NF in an aqueous GO solution at 120 °C in an autoclave, followed by annealing at 400 °C. This rGO–NF anode provided not only a large surface area for microbial colonization and electron mediators, but also a uniform macro-porous scaffold for effective mass diffusion of the culture medium. The 3D flexible microbial fuel cell produced a power density of 661 W m^{-3}, and this value is one of the highest for microbial fuel cells. This cell is highly bendable, foldable and scalable.

Challenges: Flexible liquid fuel cells are expected to have potential applications in hybrid vehicles and portable electric devices. However, the development of these cells is hindered by lacking appropriate flexible catalyst supports and packaging materials. In order to practically achieve the portable fuel cells used in vehicles and electronics, the designs of electrodes need to be innovated greatly. Furthermore, the safe and continuous feeding of liquid fuels into the cells is a big challenge. Fuel cells with large and stable energy outputs are also urgently required for practical applications. To satisfy this requirement, efficient catalysts with large accessible surface areas, good stability and strong activities are waiting to be developed.

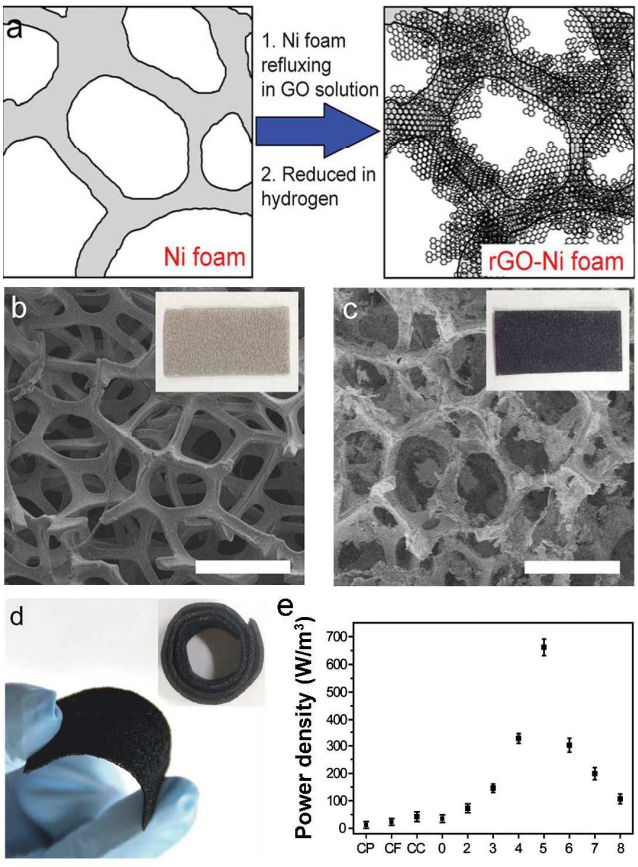

Fig. 8. (a) A schematic diagram illustrates the preparation of rGO–Ni anode. (b and c) SEM images and digital pictures (insets) of plain NF and rGO–NF. Scale bars are 200 µm. (d) Digital picture of a curved rGO–NF. Inset: rGO–NF rolled up into a cylindrical shape. (e) Maximum volumetric power densities collected for MFC devices with rGO–X–Ni electrodes as anodes. Reprinted with permission from ref. 19.

3.3 Actuators

Actuator is a mechanical device for moving or manipulating a system; it can convert external energy to mechanical energy. Actuators have been adopted in various flexible devices, including medical devices,[275] switches,[276] microrobotics,[277] artificial muscle,[278, 279] shape memory materials,[28, 280] etc. Traditional actuation materials such as memory alloys and piezoelectric ceramics have restricts in flexible devices. In recent years, several groups have developed graphene-based flexible actuators that responsive to electrical,[281, 282] electrochemical,[193, 283] acoustic,[284, 285] humid,[286] pH,[287] thermal,[288] and optical[289, 290] stimuli.

Carefully control the folding and unfolding of crumpled graphene films is a facile way to design a flexible actuator. For example, a graphene-polymer laminate was fabricated by transferring graphene thin film onto a stretched elastomer film (pre-strain 200–400%).[291] Upon relaxing the elastomer, a graphene layer with wrinkles and delaminated buckles was formed (Fig. 9). The flexibility restored in crumpled graphene enables to fabricate an artificial-muscle actuator. After stretched the elastomer film to a pre-strain of 450%, two thin graphene films were transferred on its top and bottom surfaces. Then the elastomer film was relaxed to a strain of 300%. Successively, a direct-current voltage was applied between graphene films, the elastomer developed an electric field to generate an electrostatic stress. This stress deformed the laminate by reducing its thickness and increasing its area for over 100%. Once the voltage was withdrawn, the graphene-elastomer laminate restored its unstrained state. The transmittance of the laminate varied between 40 and 60% during actuation, yielding an artificial muscle with tunable transparency. By controlling the microscopic morphology of graphene, this flexible graphene-based actuator can make visible nanoscale movement.

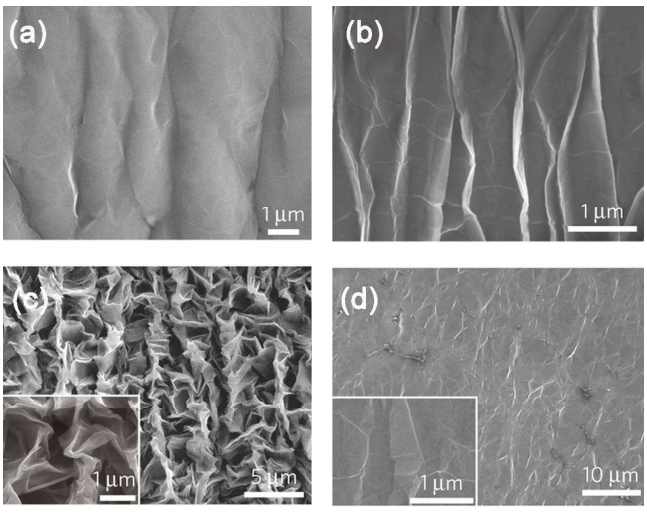

Fig. 9. (a–d) SEM images of patterns developed on the graphene sheet: first wrinkles form (a), then delaminated buckles as the substrate is uniaxially relaxed, (b) followed by crumples as the substrate is biaxially relaxed, (c) which unfold as the substrate is biaxially stretched back (d). Reprinted with permission from ref. 291.

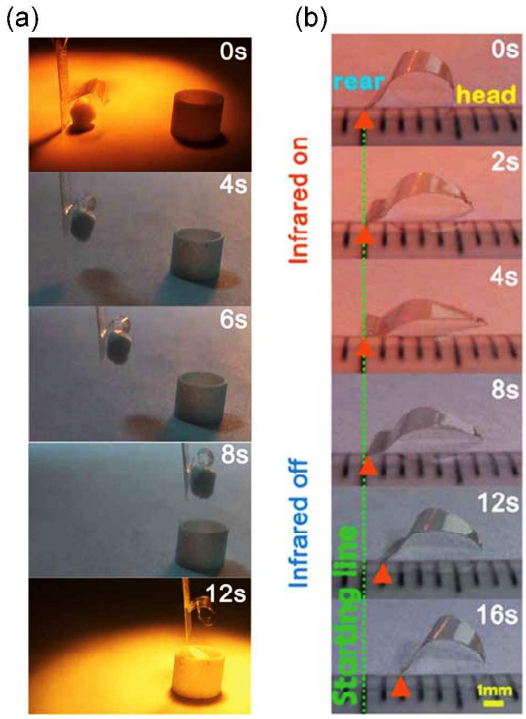

Fig. 10. (a) The photographs show the microrobot picking, lifting, moving, and placing the object to a nearby container by turning on and off the infrared light. (b) Time course of the typical walking worm due to the on–off switching modulation of the friction modes. Reprinted with permission from ref. 289.

Ionic polymer/metal composites are a representative class of materials for electrochemically stimulated actuators. In a typical device, an ion-exchange polymer membrane was sandwiched between two noble metal electrodes. During the actuation process, ion migration upon the driving of applied electric field caused the swelling of cathode side, and the contracting of anode side; thus the actuator bends. However, the traditional ionic polymer/metal composite based actuators are usually unstable because of the cracking of metallic electrodes. An ionic polymer-graphene actuator with asymmetrically graphene paper electrodes is developed to solve this durability problem.[136] The asymmetrical graphene paper has a smooth outer surface without apparent cracks during a long-term test. One side of the rGO paper was further reduced by laser-scribe to form a rough inner surface, making the actuator has an unsymmetrical structure. The performance of the actuator was stable even after 2,000 cycles of bending with a radius of 10 mm, which is superior to those of traditional ionic polymer. We also designed flexible polypyrrole (PPy)/sulfonated graphene (SG)/rGO tri-layer films as an asymmetric actuator.[292] PPy and rGO were acted as actuation and conductive inert layers. The SG layer was used to enhance the interfacial interactions. The flexible graphene based actuator exhibited stable actuating performance for over for over 1,000 actuation cycles, and the lifetime of the actuator was tested to be about 5,000 cycles. The bending angle of the actuator is larger than 360° and its movement rate was higher than 150° s^{-1}.

Photo-induced actuation technology offers many advantages over traditional electrically driven actuators, such as remote energy transfer, better scalability, low electromagnetic noise, easy construction, and the capability of working in harsh environment. The excellent optical properties of graphene thin films make them have great potentials in fabricating optical actuators.[293–295] For example, a graphene/chitosan solution was coated on a polyethylene (PE) film, forming a homogeneous brown and nearly transparent strip.[289] The transparency of the film ensures the interaction of photons. Graphene efficiently harvested infrared (IR) light, which converted to thermal energy. In this actuator, the difference of thermal expansion of polymers provided the driving force for actuation as shown in Fig. 10a. The on–off switching of IR light led to the switching of the motion states for the head and rear edge of the strip under the periodically external stimulation, exhibiting a worm-like motion (Fig. 10b). Moreover, the graphene-based transparent actuator is flexible even under rapid stimuli. Upon the excitation of a 10 mW cm^{-2} infrared light at a frequency of 1 Hz, this actuator could be repeated for movement for at least 1,000 times, with only about 15% fading in recovery rate.

Challenges: Graphene materials showed great potential applications in flexible actuators simulated by temperature,[286, 288] pH,[287] voice,[284] etc. However, compared with other fields of graphene researches, the studies of graphene-based flexible actuators are still insufficient. The actuation mechanisms need to be investigated more clearly for the design of new actuators with practical importance. Furthermore, the performances of most graphene-based actuators ate still unsatisfactory; their actuation strains, energy conversion efficiencies and lifetime are required to be improved. With the progress in material optimization and novel device design, graphene-based flexible actuators are expected to have a wide range of applications, including artificial muscles, robots, micro-electromechanical systems, etc.

3.4 Nanogenerators

Nanogenerators (NGs) have been developed on the basis of piezoelectric or pyroelectric effects of nanomaterials to effectively harvest energy.[296, 297] These materials can convert mechanical or thermal energy into electrical energy for portable electronic devices that require small powers. For this purpose, piezoelectric semiconductors such as ZnO, CdS, and GaN have been intensively studied and demonstrated in prototype devices.[197, 298, 299] However, these inorganic nanomaterials usually have short lifetime upon repeated deformation. Besides, the opaque property of traditional piezoelectric materials is an obstacle for the application in touch screens and wearable skins. The atomically layered structure of two-dimensional graphene sheets with high mechanical elasticity and high transparency make them promise for preparing flexible and/or rollable transparent piezoelectric power generators.[300–302]

PVDF–graphene composite films were prepared by casting PVDF/GO solution and successively treated by thermal reduction.[303] The dielectric constant of the composite prepared from the blend containing 0.1 wt% GO is much higher than that of PVDF. The PVDF/rGO-based NG generated a maximum power

of 36 nW. In order to further improve the performance of this NG,

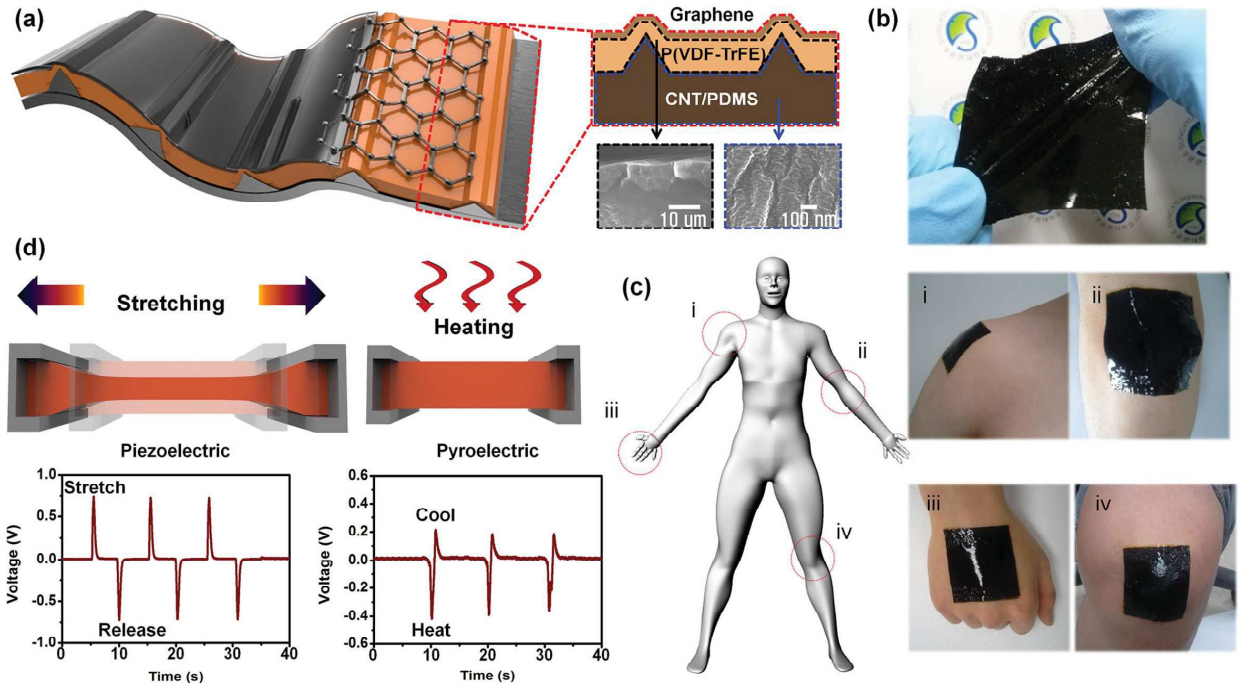

Fig. 11. (a) Schematic illustration of the device. (b) Photo image of the HSNG. (c) Photo images of the HSNG at various locations on human body, showing good compatibility of the device with various parts of body, and (d) piezoelectric output voltage from the HSNG under stretch-release condition, and pyroelectric output voltage under a thermal gradient (heat and cool). Reprinted with permission from ref. 305.

CVD-grown graphene films were transferred onto the both surfaces of a poly(vinylidene fluoride trifluoroethylene) [P(VDF-TrFE)] layer.[304] This NG is flexible for energy harvesting; rollable, stretchable, foldable, and twistable. When the NG was exposed to sound waves, piezoelectric voltages were generated because of sound pressures. These voltages drive carriers from the graphene electrodes to the external circuits to form measurable currents. The output power of the stretchable NG was 30 times higher than that of a normal graphene NG on a poly(ethylene naphthalate) (PEN) substrate under the same input sound pressure.

Most of the flexible NGs are designed for harvesting mechanical energy, however, a few of them are able to harvest thermal energy. Recently, Kim, *et al*.[305] fabricated a highly stretchable NG collecting both of mechanical and thermal energies because of the high electrical and thermal conductivities of graphene. A micro-line patterned Si wafer was used to deposit the composite film of polydimethylsiloxane (PDMS) and CNTs. Then, this composite film was peeled off into a free-standing state and spin-coated with a layer of P(VDF-TrFE). Successively, a CVD-grown graphene was deposited onto the P(VDF-TrFE)-CNT/PDMS layer (Fig. 11a). The NG based on this multilayer composite film is highly stretchable (Fig. 11b) and compatible with different parts of human body (Fig. 11c), making it suitable for the applications in robotics, and wearable or biomedical devices. The graphene layer generated the pyroelectric output signals driven by a temperature gradient, and it can also collect the piezoelectric output induced by stretching/releasing (Fig. 11d). Importantly, this NG is stable as it was stretched for 30%, making it promising for the applications in wearable electronics and artificial skins. In addition to PVDF, some other piezoelectric materials such as semiconductor ZnO[306, 307] and PZT materials[308] were also show great potentials for the applications in graphene based flexible NGs.

Recently, a new type of power-generating devices that can convert mechanical energy into triboelectricity have also been explored.[223] Flexible triboelectric NGs based on monolayer and few-layer CVD-grown graphene have been fabricated, and their output voltages and output current densities were measured under mechanical strains. Initially, the device is electrically neutral and no charge is generated on the surfaces of PET and graphene. When a vertical compressive force was applied to the top surface of the device, the surface of PET layer rubbed that of graphene layer. Thus, triboelectric charges with opposite signs were generated because of the electron injection from graphene to PET induced by the thermal energy caused by rubbing contact. The monolayer graphene flexible device exhibited a high output voltage and output current density of 5 V and 500 nA cm^{-2}, respectively. This graphene NG showed highly flexibility, stretchability, and adjustability of graphene because of its crumpled substrate.

Challenges: Graphene-based NGs provide an important route to develop durable energy sources for various flexible, stretchable and wearable electronics. However, these devices are mainly based on the composites with traditional piezoelectric materials, some of them are fragile and unstable. The fabrication processes of these NGs are still too complicate to be scaled up into industrial levels. Thus, a facile and cheap technique that can produce flexible graphene materials for constructing NG devices

are urgently required. For practical portable and flexible applications, the output powers and voltages of the NGs need to be greatly increased and their long-term mechanical and electrical stability requires to be improved. New strategies toward the design and package of graphene based NGs are also important in the aspects of science and technology.

4. Flexible graphene devices for energy storage

The production, storage, and consumption of sustainable energies are big challenges facing to human beings. For this purpose, a great deal of efforts have been devoted to increasing the efficiencies of energy storage.[31, 309, 310] Graphene and its composites have superior electrical and mechanical properties, large SSAs, good chemical stability and broad electrochemical windows.[311] Therefore, they have great potentials for the applications in the devices of energy storage such as SCs and LIBs.[1, 31, 213] Furthermore, the excellent flexibility of graphene materials possibly can provide the devices with good performances under deformed conditions.[215] In the following section, we will summarize the advancements and discuss the challenges of graphene devices for energy storage (Table 2).

4.1 Supercapacitors

Nowadays, energy storage devices are creating new services and products to revolutionize our daily life.[5, 312] Among various flexible energy storage technologies, SCs (also called electrochemical capacitors or ultracapacitors) have been considered as one of the most promising candidates because of their high specific power density (>10,000 W kg^{-1}), fast charge-discharge processes (within a second) and long cycling life (>10^5). SCs can be classified into double layer SCs and pseudocapacitors. SCs store charges at the interfaces of electrodes and electrolyte to form electrical double layers. Alternatively, the pseudocapacitors store energies by reversible redox reactions at the surfaces of their electrode materials. Flexible SCs usually require to integrate thin-film electrode materials on flexible substrates, exhibiting not only excellent electrochemical performances, but also high mechanical integrity upon bending, folding and/or even rolling.

Typically, a flexible SC consists a bendable plastic package, positive/negative electrodes (symmetric or asymmetric),[313, 314] electrolyte (liquid or solid),[22, 315, 316] and a separator (the bottom of Fig. 12). In comparison with the conventional SCs (the top of Fig. 12), flexible SCs have been simplified by removing independent current collectors, conductive additives and binders for connecting electroactive powder materials. Graphene-based fibres, free-standing films and 3D porous architectures have been explored for the applications in flexible SCs as electrode materials. Graphene component provide flexible electrode materials with highly conductive scaffolds for charge transfer and large specific surface area for the access of electrolyte or immobilizing other functional material. The high mechanical properties of graphene materials also facilitate to the flexibility and stability of SCs.

4.1.1 Substrate supported graphene electrodes. Graphene flexible electrodes can be prepared by depositing graphene materials on flexible substrates such as papers, sponges, and textiles. This is a simple and cheap process that can be easily scaled up into industrial levels. Yan *et al.*[299] fabricated graphene electrodes simply by brush-coating GO inks on cotton cloth and further treated by annealing. The flexible SC with these electrodes showed a specific capacitance of 81.7 F g^{-1} (calculated from CV curve at 10 mV s^{-1} in 6 M KOH aqueous electrolyte). Similarly, graphene/cellulose paper composites has been prepared by filtering the suspension of rGO sheets into the pores of filter papers.[318] The flexible SC based on these electrodes exhibited a specific capacitance of 120 F g^{-1} (calculated from CV curve at 1 mV s^{-1} in 1 M H_2SO_4 aqueous electrolyte) with a > 99% capacitance retention for over 5000 cycles. In addition, the membrane inherited the superior mechanical flexibility of filter paper, and its resistivity showed only 6% increase after bending to a radius of curvature of 4 mm for 1000 times.

The incorporation of CNTs in rGO can partly prevent the restacking of graphene sheets; thus increases the SSA of electrode material. A rGO/CNT composite was coated on the surface of a carbon cloth (CC) by electrophoretic deposition.[319] The specific capacitance of the SC with rGO/CNT/CC electrodes was 151.0 F g^{-1} (calculated from charge–discharge curve at 1 A g^{-1} in 1 M H_2SO_4 aqueous electrolyte), which was 2.5 times higher than that of the rGO/carbon cloth electrode (58.8 F g^{-1}). The performances of the SC before and after the bending (around 120°) were measured to be nearly identical, indicating the flexibility of this device. Transition-metal oxides such as RuO_2, NiO, and MnO_2,[192, 320, 321] have been studied extensively as electrode materials for SCs because of their large pseudocapacitances. However, the low conductivities of these materials limit their practical applications. Therefore, graphene/metal oxide composites have been widely explored for flexible SCs. The typical composites electrodes include rGO/RuO_2 films on PET (Fig. 13a and b)[322] and rGO/MnO_2 films on carbon fibre paper (Fig. 13c and d).[323] The SCs kept the flexibility of graphene materials and exhibited improved specific capacitances attributed to redox reactions.

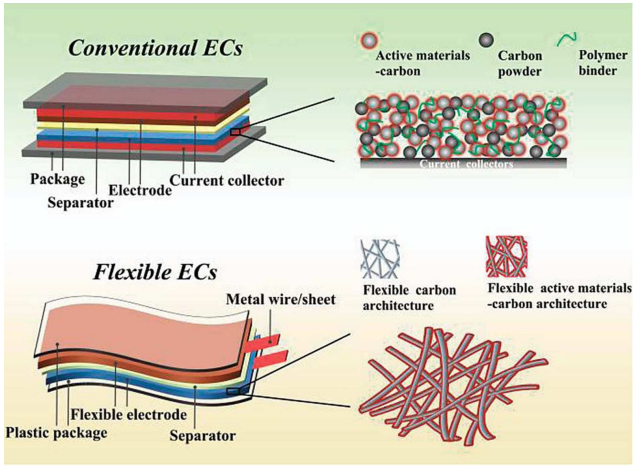

Fig. 12. Schematic illustrations of (a) the typical components of conventional SCs and (b) carbon-based flexible SCs. Reprinted with permission from ref. 5.

Table 2 Graphene materials and their flexible SCs

Graphene material	Synthesis method	Performance			Flexibility	Ref.
		C[a]	P[b]	E[c]		
rGO film	brush-coating annealing	81.7 F g^{-1}	1.5 kW kg^{-1}	7.13 W h kg^{-1}	bendable	317
rGO/cellulose paper	thermal expansion filtration	120 F g^{-1}	60 μW cm^{-2}	15 μW h cm^{-2}	1,000 cycles bending r = 4 mm	318
rGO/CNT	electrophoretic deposition	151.0 F g^{-1}	5.8 W kg^{-1}	14.5 W h kg^{-1}	bending angle:120°	319
rGO/Nafion/ RuO_2	casting	160 F g^{-1}			1,000 cycles bending (r = 2.2 mm)	322
MnO2–rGO/CFP	spray-coating	393 F g^{-1}			bendable	323
rGO fibre	wet-spinning annealing	409 F g^{-1}	25 kW kg^{-1}	14 W h kg^{-1}	Can be woven	329
rGO fibre	Spinning laser irradiation	1.2 mF cm^{-2}	3.6-9×10^{-2} W cm^{-2}	2–5.4 × 10^{-4} W h cm^{-2}	160 bending cycles	326
GF/3D graphene network fibre	electrochemical deposition	1.7 mF cm^{-2}	10^{-4} W cm^{-2}	1.7 × 10^{-7} W h cm^{-2}	500 cycles bending (r = 2 mm)	111
polymer-wrapped rGO fibre	wet-spinning	269 mFcm^{-2}	0.02 mWcm^{-2}	5.91 μW h cm^{-2}	1,000 cycles bending bending angles 180 °	331
rGO paper	hard templating vacuum filtration	92.7 F g^{-1}			bendable	332
MnO_2/graphene paper	hard templating vacuum filtration	389 F g^{-1}	25 kW kg^{-1}	44 W h kg^{-1}	bendable	333
rGO paper	water templating vacuum filtration	215.0 F g^{-1}	776.8 kW kg^{-1}	150.9 W h kg^{-1}	bendable	334
rGO foam paper	leaven strategy vacuum filtration	110 F g^{-1}			twisted or bent	120
CNF/rGO paper	CNF spacer vacuum filtration	207 F g^{-1}			bending angle 180°	336
CNF/rGO paper	LbL assembly	1.73 mF cm^{-2}			bendable	337
rGO/CNT paper	vacuum filtration	265 F g^{-1}			bendable	339
rGO/PANI nanofibre paper	vacuum filtration	210 F g^{-1}			bent or be shaped	158
rGO/MnO_2 paper	template free	243 F g^{-1}	3.8 mW cm^{-2}	11.5 μW h cm^{-2}		343
graphene/CNFs/ MnO_2 network	CVD growth microwave heating	946 F g^{-1}		53.4 W h kg^{-1}	100 cycles bending from 0° to 180°	351
rGO and graphene film	CVD growth LbL assembly	394 μF cm^{-2}				354
rGO film	Electrophoretic photolithography	285 F g^{-1}	324 W cm^{-3}	31.9 mW h cm^{-3}	bending distance 2.2 – 1 cm	355
MnO_2/rGO film	vacuum filtration	267 F g^{-1}	2520 W kg^{-1}	17 W h kg^{-1}		356
rGO/GO film	drop-cast laser-scribe	2.35 F cm^{-3}	200 W cm^{-3}		1,000 cycles bending (r = 7 mm) and 1,000 cycles twisted (angle = 90°)	137

[a] C-Specific Capacitance. [b] P-Power density. [c] E-Energy density.

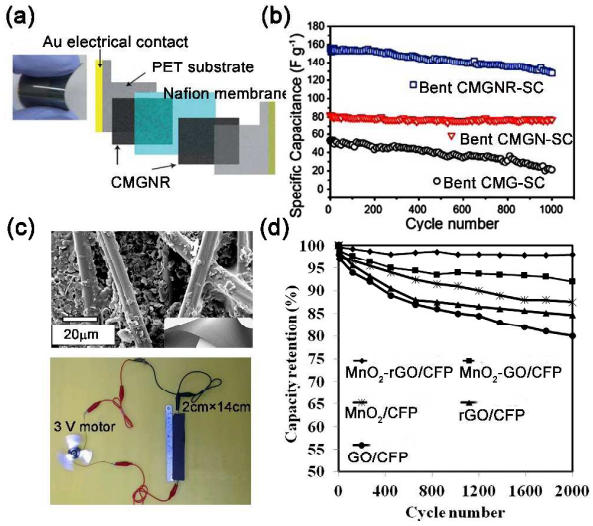

Fig. 13. (a) Photograph of a flexible CMG-SC and a schematic diagram of a SC device. (b) CVs of CMG-SC at the bent and relaxed states with scan rate of 100 mV/s. (c) Top: low magnification SEM image of MnO_2–rGO coated on CFP. Down: A 2 × 14 cm all-solid-state prototype of MnO_2–rGO/CFP SC supplying electricity to 3 V spinning motor. (d) Capacity retention of as-prepared electrodes over 2,000 cycles of galvanostatic charge–discharge tests. Reprinted with permission from ref. 322 and 323.

4.1.2 Fabric graphene electrodes. The recent developments of portable electronics demand high integration level of different components. For this purpose, fibre based devices are highly expected. GFs are usually strong, light, bendable, and chemically or electrochemically inert under ambient conditions. Thus, GFs can be woven into wearable textiles as electrodes.[107, 319, 324–329] GFs can be prepared by wet-spinning or via a hydrothermal reduction GO solutions and they showed high flexibility. These GF electrodes were further assembled into a yarn SC, showing a high specific capacitance of 409 F g^{-1} (calculated from charge–discharge curve at 1 A g^{-1} in 1 M H_2SO_4 aqueous electrolyte).[329]

Integrating the major components of SC into one block is a developing trend for portable devices. A flexible single fibre SC has been fabricated through regional reduction of spun GO fibre by laser irradiation. The rGO-GO-rGO triple layers combined major components of SC into one fibre; rGO layers were used as the electrodes and the current collectors, GO layers were used as a solid electrolyte and separator.[326] As-prepared fibrous SC inherited the mechanical flexibility of fibres, and also exhibited a high areal specific capacitance of 1.2 mF cm^{-2} at a current density of 80 mA cm^{-2} in the case of using 1-butyl-3-mthylimidazolium tetrafluoroborate ionic liquid as the electrolyte. The capacitance of this fibre SC showed only a slight fading after bending for over 160 cycles. Thus, it can be woven into the textile for wearable electronics and beyond.

Porous structure can increase the SSA of electrode, thus can improve the performance of SC.[111] A GF with a unique core-sheath hierarchical structure has been fabricated by electrochemical deposition of rGO sheets around the a rGO fibre formed by hydrothermal reduction of GO dispersion. In this fibre, rGO sheath has a 3D porous structure. An all-solid-state fibrous SC based on these fabric electrodes showed a good elasticity like a spring, highly compressable and stretchable. It showed a gravimetric capacitance of 25–40 F g^{-1} (calculated from charge–discharge curve at current densities of 0.1–4 A g^{-1} in 1 M $LiClO_4$ aqueous solution), and these values are close to the electric double layer capacitances of activated carbon textiles (25–70 F g^{-1}).[330] Moreover, this fibre SC in bending (radius of ~ 2 mm) state showed a capacitance comparable to that in straight state during 500 cycles of bending and relaxing. These ultraelastic all-graphene fibres can also be woven into a textile for various wearable electronics in large scale.

The GFs discussed above have a naked surfaces; thus the GF-based SCs are easy to be short-circuited as the electrodes contacted to each other during the process of deformation. Although post-coating a layer of PVA electrolyte can partly reduce the probability of short circuit, the coating process is complicate and time-consuming. Kou *et al.* prepared polymer-wrapped graphene core-sheath fibres, which can be directly used as safe electrodes for SCs (Fig. 14a-d).[331] In a typical wet-spinning process, the aqueous GO solution from the inner channel and the sodium carboxymethyl cellulose aqueous solution from the outer channel were injected into the coagulating bath. As a result, the polymer wrapped GO fibres were shaped rapidly and further reduced to polymer wrapped GF. The yarn SC based on this polymer wrapped GF with liquid (or solid) electrolyte showed an ultra-high areal capacitance of 269 (177) mF cm^{-2} (calculated from charge–discharge curve at 0.1 mA cm^{-2}) and a high energy density of 5.91 (3.84) mW h cm^{-2} (Fig. 14e and f). Upon bending to different angles (e.g., 45°, 90° and 180°), the changes in capacitance are negligible, reflecting that the inner structures of fibre SCs maintained well even at a large bending angle. Furthermore, the capacitance of this fibre SC dropped for only 2% after bending 200 times. Polymer wrapped GFs were also woven into cloth to form a bendable SC (Fig. 14g–i), promising the applications in garment devices and intelligent microsensors. This work developed a safe and scalable approach to fabricate flexible yarn SCs.

4.1.3 Paper-like graphene electrodes. Graphene papers have shown a great potential as flexible electrodes because of their facile fabrication process, low cost, large-scale production, and superior flexibility. However, the graphene papers prepared by filtration usually have low SSAs caused by the irreversible agglomeration and restacking of graphene sheets driven by π-π stacking. This will inevitably results in slowing the diffusion of the electrolyte ions, and limiting the electrochemical performances of SCs. In order to address this issue, pores or spacers have been adopted into graphene paper to increase their SSAs and promote the transport efficiencies of the electrolyte ions.

A microporous graphene film was fabricated by using a hard template strategy.[332] GO precursor and PMMA microspheres were orderly assembled by vacuum filtration, followed by pyrolysis to reduce GO into rGO as well as to remove the template. This microporous rGO paper showed a much higher specific capacitance compared with that of a compact counterpart. Huh *et al.*[333] employed the same technique to fabricate macroporous graphene films by using polystyrene (PS) colloidal particles as the template. The porous graphene paper with a large

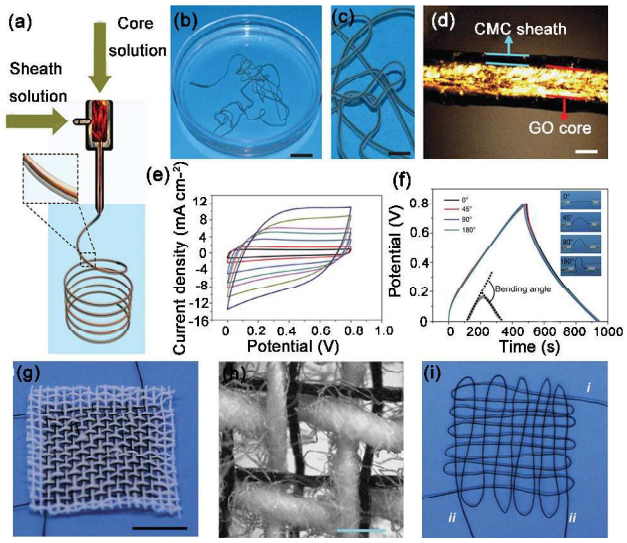

Fig. 14. (a) Schematic illustration showing the coaxial spinning process. (b) A single intact wet GO@CMC fibre and its magnified image (c). (d) Polarized-light optical microscopy image of wet GO@CMC fibre indicating the core-sheath structure and the well-aligned GO sheets in the core part. (e) CV curves of RGO + CNT@CMC, scan rates increased from 10 to 20, 50, 80, 100, 150 and 200 mV s^{-1}. (f) GCD curves of two-ply, all-solid-state, freestanding YSCs bended with different angles at the current density of 0.1 mA cm^{-2}, and the insets are the digital photos of YSCs with different bending angles. (g) Two intact coaxial fibres woven with cotton fibres. (h) Optical macroscopic image of a. (i) Cloth woven by two individual coaxial fibres. Scale bars, 1 cm (b, g) 100 μm (c) and 200 μm (h). Reprinted with permission from ref. 331.

SSA facilitates the ionic transport within the electrode and increased the capacitances of SCs. Water has also been used an effective "spacer" to prevent the restacking of graphene sheets.[334] A graphene paper solvated with water gave a specific capacitance of up to 215.0 F g^{-1} (calculated from CV curve at 0.01 V s^{-1} in 1.0 M aqueous H_2SO_4 electrolyte). Autoclaved leavening and steaming of GO layered papers can produce lightweight and electrically conductive rGO foam-like papers.[120] In this process, thermal steaming of GO papers with hydrazine was the key step to form rGO foams with open pores. The specific capacitance of the SC with these rGO foam electrodes was measured to be about 110 F g^{-1} (calculated from charge–discharge curve at a current of 0.5 A g^{-1} in 1 M H_2SO_4 aqueous electrolyte), and this value is much larger than the SC with the electrodes of compact rGO papers (17 F g^{-1}). Furthermore, the flexible rGO foams coated onto PET sheets acted as both current collectors and the SC can be twisted or bent without decreasing its performance.

To prevent the restacking of rGO sheets, carbon black (CB),[35] cellulose nanofibre (CNF),[336, 337] and CNTs[338, 339] were also intercalated into graphene papers as spacers. For example, cellulose nanofibres were blended into CNF/rGO hybrid aerogel by supercritical CO_2 drying.[336] The SC based on this three-component composite paper has a specific capacitance as high as 207 F g^{-1} (calculated from CV curve at 5 mV s^{-1} in H_2SO_4–PVA gel electrolyte), and its performance was nearly unchanged upon bending to 180°. Furthermore, a transparent rGO/CNF composite paper was prepared by LbL depositing GO sheets and CNFs, and further treated by reduction.[337] The SC based on these composite electrodes also showed good flexibility, without decreasing its performance upon bending. Other examples are free-standing rGO/CNT composite films prepared by in-situ thermal[338] or chemical reducing GO/CNT precursors.[339] In these electrodes, CNTs served not only as the spacers and the conducting bridges, but also reinforcement fillers to improve their flexibility and electrochemical properties.

Electroactive materials are commonly used for increasing the capacitances and energy densities of graphene paper-based flexible SCs. Polyaniline (PANI),[158, 340, 341] polypyrrole (PPy),[155] transition metal oxides or hydroxides (RuO,[185] MnO_2,[186] V_2O_5,[187] Mn_3O_4,[188] Co_3O_4[189]) have been explored for this purpose. We fabricated PANI nanofibre/rGO composite papers by vacuum filtration.[158] A SC device based on this conductive flexible paper showed a high specific capacitance (210 F g^{-1} at 0.3 A g^{-1} in 1 M H_2SO_4 aqueous electrolyte) and good flexibility. Hollow PPy spheres have also been sandwiched between graphene layers to form a sandwich to form a porous composite.[342] This graphene/PPy nanoarchitecture delivered an excitingly high specific capacitance of 504.5 F g^{-1} (calculated from charge–discharge curve at 5 A g^{-1} in 2 M H_2SO_4 aqueous electrolyte), about 5 times that (93.1 F g^{-1}) of pure rGO paper even after charging/discharging for 10,000 cycles. Among the pseudocapacitive oxides of transition metals, MnO_2 has been paid the most intensive attention because of its low cost, environmental friendliness and high theoretical specific capacitance (1370 F g^{-1}).[186, 333, 187, 343, 344] Lee *et al.* reported the fabrication of flexible rGO/MnO_2 paper electrode by vacuum filtration.[343] The specific capacitance of this electrode was measured to be as high as 897 mF cm^{-2} (243 F g^{-1}) (calculated from charge–discharge curve at 50 mA g^{-1} in 1 M Na_2SO_4 aqueous electrolyte), which is among the highest values of other flexible carbon-based and MnO_2/carbon-based electrodes.[21, 121, 179, 312, 344–346] Moreover, these graphene paper electrodes exhibited remarkable flexibility, making they are able to be bent into any desired angles. The performance of this device kept unchanged as it was bent to a radius of 1.2 cm.

4.1.4 Graphene electrodes with 3D porous architectures. Recently, to further improve the performance of flexible SCs, a great deal of attention has been paid to graphene-based 3D porous architectures such as hydrogels, aerogels, foams and sponges.[117, 118, 122, 137, 347–350] These 3D macrostructures, consisting of micro-, meso- and even macropores, can provide the electrodes with high SSAs, light weights, and fast ion/electron transports. However, most of these materials are too fragile to be used in bendable and stretchable SCs. He *et al.*[351] fabricated a freestanding, lightweight, flexible and mechanically robust 3D graphene materials. In this case, CNTs arrays were deposited on 3D graphene networks by CVD method, then, MnO_2 nanosheets decorated on their surface (Fig. 15a and b). Simultaneously, the interconnected porous 3D structure of graphene/CNT/MnO_2 provided uninterrupted accessible surfaces for forming electrical double layers and transporting both electrons and electrolyte ions to minimize electron accumulation and ion-diffusing resistances. Thus, the SC with these electrodes showed a high specific capacitance of 946 F g^{-1} (calculated from CV curve at a scan rate

of 2 mV s^{-1} in 1 M Na_2SO_4 aqueous electrolyte) (Fig. 15c). This flexible SC provided a maximum energy density of 53.4 W h kg^{-1}, which can drive a digital clock for 42 min. Inspiringly, its performance showed little changes (less than 1%) under bending from 0° to 180° or for to 90 ° for 100 bending/releasing cycles (Fig. 15b).

4.1.5 Planar SCs (microcapacitors). Conventional micro-fabrication techniques have proven to be cumbersome in building cost-effective micro-devices, thus limiting their practical applications. Recently, considerable efforts have been made for flexible micro-SCs for the emerging electronic devices.[352, 353] Planar SCs are regarded as a novel type of micro-SCs, requiring to integrate electrode material, electrolyte, and current collector onto the same plane. The planar configuration designs offer planar channels for electrolyte ions, facilitating fast ion transport in the 2D electrodes. Furthermore, the planar configuration would not affect the ion transport when the SCs are folded or rolled. Yoo *et al.*[354] reported the first "in-plane" ultrathin SCs comprised of pristine graphene and multilayer rGO. Specifically, the pristine CVD-graphene and rGO films were alternatively deposited onto a flexible copper foil by LbL deposition. The large conductive planar sheet of graphene was then separated into two electrodes with a physically created micrometer-sized gap by cutting with a pair of scissors. Polymer gel electrolyte served as both an ionic electrolyte and a separator. Such planar SC devices are compact,

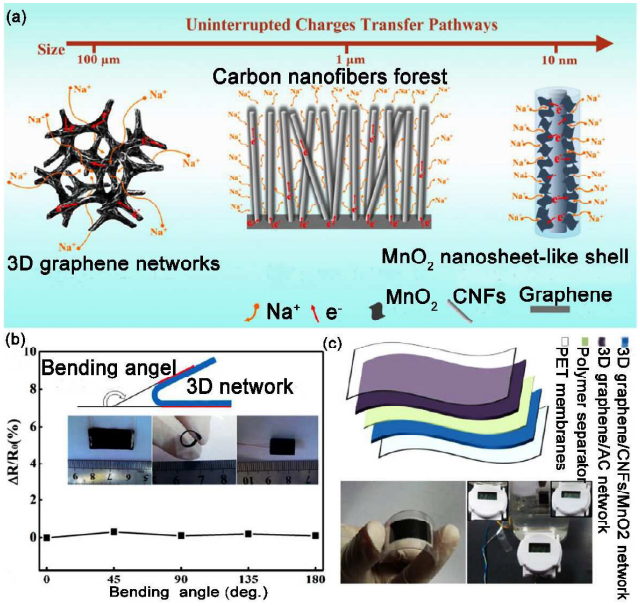

Fig. 15. (a) Schematic illustration of a 3D micro/nanointerconnected structure as flexible SC electrode. (b) Electrical resistance for 3D graphene/CNF networks at the different bending angles. The inset shows the digital photographs of the 3D graphene/CNF networks with different bending shapes. (c) CVs of a 3D graphene/CNFs/MnO_2 composite electrode with a fixed areal mass density of 0.1 mg cm^{-2} at different scan rates. (d) Schematic structure of the flexible SC consisting of a polymer separator, two PET membranes, and two asymmetric graphene-based electrodes. The left bottom digital photograph shows the flexibility of the device during bending operations. The right bottom digital photograph shows a digital clock driven by the flexible SC. Reprinted with permission from ref. 351.

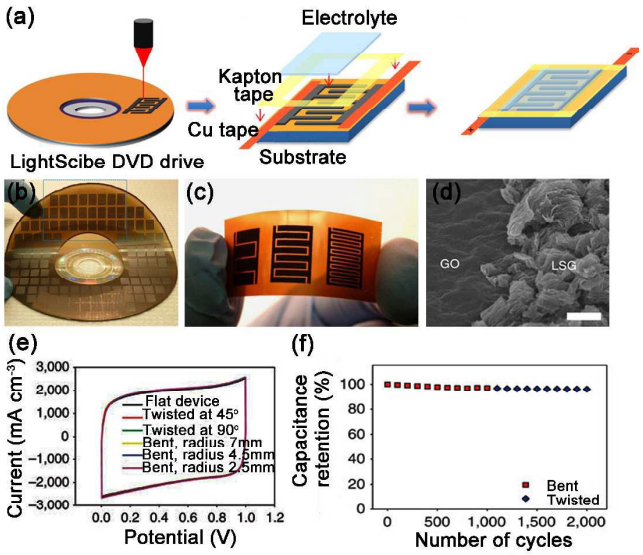

Fig. 16. (a) Schematic diagram showing the fabrication process for an LSG micro-SC. (b) This technique has the potential for the direct writing of micro-devices with high areal density. More than 100 micro-devices can be produced on a single run. The micro-devices are completely flexible and can be produced on virtually any substrate. (c) A digital photograph of the laser-scribed micro-devices with 4, 8 and 16 interdigitated electrodes. (d) A tilted-view (45°) SEM image shows the direct reduction and expansion of the GO film after exposure to the laser beam. Scale bar, 10 μm. (e) Bending/twisting the device has almost no effect on its performance, as can be seen from these CVs collected under different bending and twisting conditions at 1,000 mV s^{-1}. Photograph of the micro-devices. Reprinted with permission from ref. 137.

ultrathin, flexible, and optically transparent. The ultrathin architecture of graphene edges enabled the formation of a thinnest of device, consisting of 1 – 2 graphene layers, to achieve a specific capacitance up to 80 μF cm^{-2} (calculated from charge–discharge curve at 281 nA cm^{-2}). Furthermore, a much higher specific capacitance (394 μF cm^{-2}) was obtained by using multilayered graphene electrodes. This planar SC established a pioneering example of designing chip-scale energy devices with portable and flexible applications. Furthermore, an all-solid-state planar SC based on micro-patterned ultrathin rGO electrodes was developed.[355] A SC with a length of 2.2 cm did not show a significant change in its capacitance after bending to a state with a two-end distance of 1.0 cm.

Ultrathin 2D nanomaterials represented a promising platform to realize highly flexible planar energy storage devices as the power suppliers for stretchable/flexible electronic devices. A high-performance planar SCs based on the hybrid nanostructures of 2D ultrathin MnO_2/graphene was reported by Peng and co-workers.[356] The planar structures based on the MnO_2 nanosheets integrated on graphene sheets not only introduced more electrochemically active species, but also brought additional interfaces at the hybridized interlayer areas. The MnO_2/graphene film was deposited on a PET substrate and it was scrapped with narrow gaps to form separated electrodes. This planar SCs showed performance superior to that of graphene-only device, exhibiting a high specific capacitances of 267 F g^{-1} (calculated from charge–discharge curve at 0.2 A g^{-1} in PVA/H_3PO_4

electrolyte), and a capacitance retention of 92% after charging/discharging for 7000 cycles. Moreover, the high malleability of this planar SCs provided it with excellent flexibility and robust cyclability, yielding capacitance retention over 90% after 1,000 times of folding/unfolding.

A scalable fabrication of planar SCs over large areas was achieved by direct laser writing GO films using a LightScribe DVD burner (Fig. 16a).[137, 267] The conductive rGO electrodes were separated by insulating GO lines on PET substrate. After introducing electrolyte and encapsulated with Kapton tape, a plane of multisite of SCs was obtained. This technique can produce over than 100 micro-SCs on a single disc within 30 min (Fig. 16b).[137] Remarkably, miniaturizing devices to the microscale resulted in enhancing the charge-storage capacity and improving the rate capability of these SCs. This is mainly due to the microscale structure minimized the distances of ion diffusion from electrolyte to the electrode materials. Furthermore, the more the electrodes per unit area, the more the power and energy that can be delivered by these micro-devices. These micro-SCs demonstrated a power density of ~200 W cm^{-3}, which is among the highest values achieved for any SC. This device showed a capacitance retention of 97% after bending to a radius of 7 mm for 1,000 cycles, followed by another 1,000 cycles of twisting it for 90° (Fig. 16e-f). This single-step fabrication technique avoids the consuming and labor-intensive process of conventional microfabrication. Furthermore, these microcapacitors can be directly integrated on-chip, facilitating them to extract energies from solar, mechanical and thermal sources.

Challenges: Recent advancements in flexible SCs have inspired the exploration of new graphene electrode materials with superior electrochemical performances and excellent mechanical strengths and good flexibility. Several strategies have been developed to improve the performances of SCs: (1) reducing the thicknesses of electrode materials to attain high gravimetric capacitance; (2) increasing the accessible SSAs of electrodes to provide more reaction sites, and accumulate more charges in electrical double layers; (3) optimizing the microchannels for the facile diffusion of ions. However, the optimization of the whole configuration of a SC including its electrodes, electrolyte, and current collectors is also important. Various methods have been developed on decreasing the thicknesses of SCs to improve their flexibility and specific capacitances; however, the problem of short circuits in the devices without separators cannot be absolutely avoided. Moreover, to effectively keep the performance of a flexible SC at serious deformations still remains as a big challenge.

4.2 Lithium batteries

Flexible lithium batteries (LIBs) are attractive power sources of foldable or wearable electronic devices because of their high energy and power densities, and long-term stability.[1, 4] They are expected to have practical applications in roll-up displays, touch screens, conformable active radio-frequency identification tags, wearable sensors and implantable medical devices.[1] High-performance LIBs should have small sizes, lightweight and long cycling lives. Therefore, the active electrode materials should have high energy densities and the amounts of non-active additives in the whole cells should be minimized. Thus, flexible electrodes are usually made from various functional organic and/or inorganic materials immobilized on flexible conductive membrane substrates without conductive additives and binders. Flexible polymer solid membranes are commonly used as both separators and electrolytes. Packing materials for flexible LIBs are usually thin polymer films. The selection, assembly and suitable layout of electrode materials, separator and packages are central issues in developing high-performance flexible LIBs. Although a great deal of effort has been devoted to developing flexible LIBs, this field still remains in its early stage, and a suitable selection and integration of component materials has not yet to be demonstrated. To make flexible LIBs, flexible electrodes are needed to be able to deliver a capacity beyond a certain level to operate conventional portable devices, and can be reversibly deformed without decreasing its performance. Major technical barriers of changing conventional LIBs into flexible counterparts are summarized as follows. (1) Intrinsically powdery properties of electrode materials; (2) poor contacts between constituent materials; (3) low loading amounts of electrode materials; and (4) electrolyte leakage. To address these issues, graphene materials are a promising option and we summarize the progress on graphene based flexible LIBs in this section (Table 3).

4.2.1 Anodes. Graphene papers fabricated by vacuum filtration of rGO aqueous dispersions were the most widely used graphene flexible electrode materials.[52, 357] Wallace's group firstly used these materials as anodes of flexible LIBs,[358] and they delivered a reversible capacity of approximately 240 mAh g^{-1}.[309, 358] A lightweight non-annealed graphene anode was prepared by hydrazine reduction of a GO paper.[359] Although the cycling stability of rGO electrode was improved, its capacity and rate capability were still unsatisfactory. rGO sheets tended to agglomerate during the process of reducing and drying GO paper because of π-stacking interaction. The stacking of rGO sheets greatly reduced the accessible surface area of electrode to electrolyte. To address this problem, CNTs were introduced into graphene sheets to prevent rGO restacking, allowing more effective contact between electrolyte and graphene in the interior of the graphene anode, increasing the conductivity of rGO paper and simultaneously store Li atoms.[360]

Holey graphene sheets have been synthesized by the treatment of GO sheets with nitric acid under sonication.[361] The pores improved the access of electrolyte to the interior of graphene anode and thus enhanced the kinetics of electrochemical reactions. Koratkat *et al.* also reported a laser-reduced graphene paper as a high-rate anode for LIBs.[362] These techniques induced micro-pores, cracks, and inter-sheet voids in graphene paper. As a result, lithium ions can be easily diffused into graphene anode from electrolyte, enhancing lithium intercalation kinetics even at ultrafast charge/discharge rates, showing a maximum capacity of 370 mA h g^{-1}. Liu *et al.* prepared a folded graphene paper with interconnected porous network by mechanically pressing a graphene aerogel.[363] The first charge and discharge capacities of this graphene paper were measured to be as high as 1091 and 864 mA h g^{-1}. After 100 charging/discharging cycles, a reversible capacity of 568 mA h g^{-1} was maintained. Yin *et al.*

assembled graphene sheets into honeycomb structures through a

Table 3 Graphene materials and their flexible LIBs

Flexible material	Synthesis method	Capacity	Flexibility	Ref.
rGO paper	vacuum filtration	214 mAh· g^{-1} at 10 mA g^{-1}	bendable	359
rGO/CNT paper	vacuum filtration and annealing	375 mAh g^{-}1 at 100 mA g^{-1}	bendable	360
rGO paper	nitric acid under sonication and vacuum filtration	400 mAh g^{-1} at 50 mA g^{-1}	bendable	361
rGO paper	vacuum filtration and laser reduction	370 mAh g^{-1} at 1.86 A g^{-1}	bendable	362
rGO paper	freeze-drying and pressing	864 mA h g^{-1}1 at 100 mA g^{-1}	bendable	363
rGO/DODA film on PET	coating and breath figure	1600 mAh g^{-1} at 50 mA g^{-1}	bendable	364
graphene on Cu foil	CVD growth	0.06 mA h cm^{-2} at 100 mA cm^{-2}	bendable radius < 1 mm	366
rGO/Si hybrid paper	vacuum filtration	>2200 mA h g^{-1} at 50 mA g^{-1}	bendable	370
rGO/Si hybrid paper	vacuum filtration	3200 mAh g^{-1}at 1 A g^{-1}	bendable	372
rGO/TiO_2 hybrid paper	hydrothermal	175 mAh g^{-1} at 200 mA g^{-1}	bendable	191
V_2O_5/rGO paper	filtration and annealing	283 mAh g^{-1}	bendable	385
V_2O_5/rGO paper	filtration	806.6 mAh g^{-1}	bendable	309
FeF_3/rGO paper	vacuum filtration photothermal reduction	587 mA h g^{-1} at 20 mA g^{-1}	bendable	386
3D graphene foam	hydrothermal	170 mA h g^{-1} at 145 mA g^{-1}	bendable (r = 5 mm)	387
rGO paper	vacuum filtration	1393 mA h g^{-1}	bendable	399
graphene foam	electrochemical leavening and annealing	340 mA h g^{-1} at 100 mA g^{-1}		400

"breath figure" approach (Fig. 17a), which showed high conductivity, porosity, robust and mechanical stability.[364] This honeycomb graphene electrode exhibited a large reversible capacity (1600 mA h g^{-1}, and 1150 mA h g^{-1} after 50 cycles), highlighting the advantages of bioinspired hierarchical structures for high-performance LIBs. Porosity is important for improving the capacity and cycling performance of a disordered carbon anode material, because porous framework can significantly decrease the diffusion distance of the lithium ions into the disordered graphene layers; thus can enhance the charge/discharge rate performance of rechargeable LIBs (Fig. 17b-f). Furthermore, the flexible PET substrate contributed to the bendable use of these films.

CVD-graphene films were also used to fabricate flexible anodes because of their high electrical conductivity and few structural defects.[365, 366] A mechanically flexible all-solid-state battery was made by using monolayer graphene grown directly on Cu foil.[366] The total thickness of the resulting battery was around 50 μm. Such an ultrathin battery showed a high volumetric energy density of 10 W h L^{-1} and a high power density of 300 W L^{-1}. It also showed an excellent cycling stability, keeping a discharge current density of 100 μA cm^{-2} and an aerial capacity >0.02 mA h cm^{-2} in 100 cycles. The flexible graphene anode on Cu foil can be bendable (radius of less than 1 mm) and twisted with negligible change in its performance.

On the other hand, graphene paper/film anodes usually suffer from a large irreversible capacity, low initial efficiency and fast capacity fading. This is mainly due to the re-stacking of graphene sheets and side reactions between graphene and electrolytes arising from the functional groups and defects of graphene sheets. The discharge curves of graphene anodes also cannot give voltage plateaus for providing stable potential outputs. Thus, there is a large hysteresis (strong polarization) between the charge–discharge curves. To address this problem, an

electrochemically active component with high capacity and good cycling stability has to be introduced to graphene anode.[367]

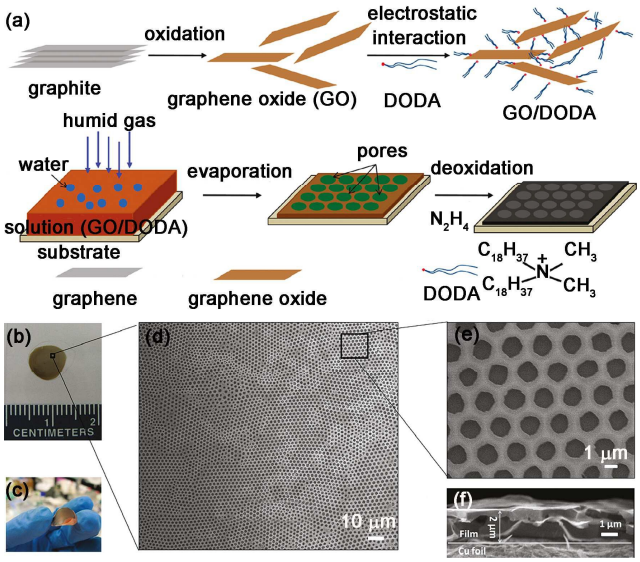

Fig. 17. (a) Schematic drawing of the preparation of the honeycomb structured film based on GO. (b) Photograph of the honeycomb film on the glass. (c) photograph of the honeycomb-patterned film on the copper foil. (d, e) SEM images of honeycomb-patterned film prepared from 1 mg mL^{-1} of the GO/DODA complex on the silicon wafer. (f) cross-sectional SEM image of the honeycomb-patterned film on the copper foil. Reprinted with permission from ref. 364.

This technique at least has two advantages: (1) the blended electroactive material can not only suppress the agglomeration and re-stacking of graphene sheets, but also increase the accessible surface area for electrochemical reactions, enhancing the electrochemical activity; (2) The second electroactive material can be uniformly immobilized on graphene surface, leading fast ion transport and consequently improve the electrochemical/mechanical performances.

Si is one of the most promising anode materials for LIBs because of its abundance in nature, low cost, low discharge potential and a high theoretical specific capacity of 4,200 mA h g^{-1}.[368, 369] Thus, Si nanoparticles loaded on graphene 3D network as anode of LIB showed a high Li storage capacity and cycling stability.[370] The assembled LIB exhibited a capacity of 2,200 mA h g^{-1} after 50 cycles and 1500 mA h g^{-1} after 200 cycles, decreasing by < 0.5% per cycle. In this case, graphene network functioned as a flexible mechanical support for strain release, offering electrically conducting channels. The nanosized silicon provided a higher stable capacity (708 mA h g^{-1}) than that of the cell with pure graphene (304 mA h g^{-1}).[371] Further treatment of graphene by acid-sonication can introduce more vacancies to immobilize more Si nanoparticles.[372] In this film anode, Si nanoparticles were encapsulated into graphene porous scaffold. The flexible graphene anode material showed an extremely high reversible capacity of 3,200 mA h g^{-1} at 1 A g^{-1} with a 99.9% retention for over 150 cycles. Particularly, this anode has a high rate capacity, it can be charged within 8 min, among the highest performance of graphene-based LIBs. Si nanowires (NWs) are able to accommodate large strain without pulverization, providing good electronic contacts with current collector, and displaying short lithium insertion distances because of their 1D nanostructures.[368] A self-supporting flexible anode paper was prepared by filtration and reduction of the mixed dispersion of GO sheets and Si NWs.[373] In this composite paper, overlapped graphene sheets coated on Si NWs as adaptable sealed sheaths, preventing the direct exposure of encapsulated Si NWs to the electrolyte and enabled the structural stabilization of this material. As-prepared flexible LIB based on this anode exhibited a high reversible specific capacity of 1,600 mA h g^{-1} at 2.1 A g^{-1}, and 80% capacity retention after 100 cycles.

Metal oxides particles that can store lithium through conversion reactions have also attracted a great deal of interest because of their high specific capacities.[374–376] Transition metal oxides such as Fe_2O_3 nanoparticles,[376] Fe_3O_4 spindles,[377] Co_3O_4 nanosheets[378] and MnO_2 nanotubes[379] were homogeneously incorporated with graphene sheets through vacuum filtration to prepare flexible hybrid films. These hybrid papers were used as anodes in flexible LIBs, and exhibited high specific capacity, good rate capability and promising cycling stability. This is mainly due to the tight interfacial adhesion of the additives with the graphene conductive network, providing porosity for both buffering volume expansion and rapid ion transport.

Another lithium storage mechanism of metal oxides is based on a lithium ion intercalation reaction, and TiO_2 is a typical example.[380, 381] Lithium intercalation and extraction with a small lattice change (less than 4%) ensured the structural stability and cycling life. Hu *et al.* reported a novel ex-situ approach to fabricate flexible graphene/TiO_2 hybrid paper with a high mass loading of oxide.[191] The intercalation of TiO_2 nanoparticles into a solvated graphene paper led to the formation of an open 3D porous structure with a well maintained paper geometry and flexibility. As-fabricated LIB using hybrid paper electrode showed a stable specific capacity of 122 mA h g^{-1} after 100 charge/discharge cycles at a current rate of 2 A g^{-1}.

4.2.2 Cathodes. One of the bottlenecks for the development of high-performance LIBs is the low capacities of their cathodes.[382, 383] Thus, a variety of oxides have been explored as the cathode materials; however the low conductivities of oxides strongly decreases their performances. V_2O_5 is a typical intercalation compound because of its layered structure. It is also cheap and abundant, and has a high energy density.[384] A free-standing, flexible V_2O_5/graphene composite film was prepared by simple filtration and annealing, and it has been used as the cathode material of LIB.[385] V_2O_5 nanowires were preferentially oriented along the plane of the film as they were sandwiched between stacked graphene sheets in the composite film. In a LIB cell, a composite film containing 75.8 wt% V_2O_5 delivered a discharge capacities of 283 and 252 mA h g^{-1} at a current density of 50 mA g^{-1} in the first and 50th cycles, respectively. This good performance is resulted from the integrated structure of the V_2O_5 network embedded in graphene materials. In this case, V_2O_5 acted as a Li^+ host and graphene acted a conductive component. Graphene materials can be used in both the cathode and the anode of a fully flexible LIB.[309] A graphene-based LIB was fabricated using flexible graphene and V_2O_5/graphene

composite papers as its anode and cathode, respectively. The composite was prepared by pulsed laser deposition.[309] The integration of graphene into the electrodes ensured not only the possibility of operating the LIB under deformation, but also provided it with electrochemical performance superior to that of the devices with conventional electrodes.

FeF_3 is also an attractive cathode material of LIB because of its high theoretical capacity (712 mA h g^{-1}) and redox potential. A facile photothermal reduction route was developed to synthesize free-standing, flexible FeF_3/graphene paper.[386] This paper contains well-dispersed FeF_3 nanoparticles and has a porous electrically conducting network of graphene sheets. It demonstrated promising applications as cathode in high-energy density Li-ion batteries with a stable capacity of 580 mA h g^{-1} after 10 cycles at 100 mA g^{-1}.

4.2.3 Current collectors. Flexible 3D graphene frameworks can be used as current collectors to load electroactive materials. In comparison with conventional metal current collectors, graphene collectors have larger specific surface areas, smaller volumes and lighter weights. For example, Li *et al.* fabricated a flexible LIB using $Li_4Ti_5O_{12}$ and $LiFePO_4$ loaded on flexible graphene foams as anode and cathode, respectively.[387] 3D flexible and conductive interconnected GF network acted as both a highly conductive pathway for electrons/ lithium ions and light current collector. The assembled flexible battery showed a high capacity (170 mA h g^{-1}), a good rate capability and long cycling life even under repeated bending to a radius of 5 mm. The fabrication of GF and subsequent loading of active materials can be easily scaled up, indicating the possibility for large-scale fabrication of high-performance flexible batteries.

4.3 Other batteries

LIBs have achieved a great success in the past three decades, especially for portable electronic devices. However, state-of-the-art LIBs still cannot meet the crucial demands of reducing sizes, weights and costs of batteries in emerging applications, such as electric vehicles and grid-level energy storage.[388] Recently, lithium–sulfur (Li–S) batteries are recognized as the next generation rechargeable battery because of their high theoretical specific capacity (1672 mA h g^{-1}) and energy density (2600 W h kg^{-1}).[389, 390] However, the practical application of Li-S battery has been plagued by several issues including the low electrical conductivity of S (5×10^{-30} S cm^{-1}), the dissolution of soluble polysulfides in the electrolyte and the large volume change (80%) of S, leading to a low sulfur utilization efficiency and poor cycling stability.[391, 392] To overcome these problems, carbon materials, such as carbon nanotubes/nanofibres,[393] porous carbon,[394, 395] hollow carbon spheres,[396] and graphene[397, 398] have been used to immobilize S for enhancing the electrical conductivity of S electrode and preventing the dissolution of polysulfides. Among all of these carbon materials, graphene has attracted special interest, due to its high electrical conductivity, strong mechanical property and good chemical stability.

Free-standing graphene–sulfur composite films have been prepared via a sulfur vapor treatment of mesoporous graphene papers. They can be directly applied as electrodes of Li–S batteries without using a binder, conductive additives or an extra current collector (Fig. 18a-b).[399] The porous graphene networks facilitated electron transfer and electrolyte diffusion. The Li–S battery with this sulfur–graphene paper as cathode delivered a high discharge capacity of 1393 mA h g^{-1} with an enhanced cycling stability and good rate performance (Fig. 18c).

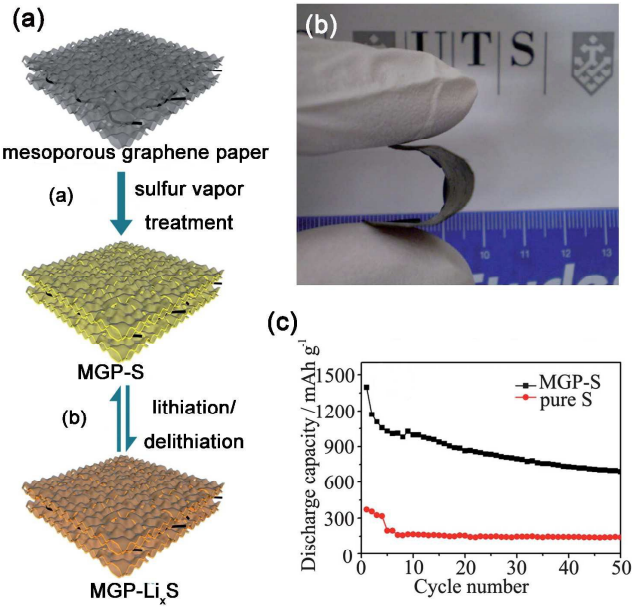

Fig. 18. (a) A schematic illustration for the preparation of mesoporous graphene paper–sulfur electrodes and application as cathode in lithium–sulfur batteries. (b) Digital photographs of the MGP paper, exhibiting an intact paper-like flexible property. (c) The cycling performance of the MGP-S and pure S electrodes. The cells were cycled at 0.1 C. Reprinted with permission from ref. 399.

Li–O_2 batteries are also one of the most promising candidates as the next generation energy storage system because of their high theoretical specific energy density (about 3500 W h kg^{-1}). This value is one order of magnitude higher than today's LIB batteries (around 380 W h kg^{-1}). Yan *et al.* developed an electrochemical leavening strategy to fabricate a 3D graphene foams, further treated by inert gas reduction.[400] The few structural defects in treated graphene foams are crucial to the structural stability of O_2 electrode and to acceleration of charge transfer. Thus treated graphene foam electrode annealed at 800 °C delivered a round-trip efficiency of up to 80% compared with untreated graphene foam with efficiency of 51 %. Such few defect graphene foams were bendable to use in a flexible Li–O_2 batteries.

Challenges: Single-component electrodes such as graphene papers have been extensively explored for the applications in flexible batteries. However, graphene composite electrodes are expected to have larger capacities and higher energy densities. To keep the performances of the composite electrodes with rigid inorganic components in their deformed state is still a topic requiring systematical studies. On the other hand, flexible graphene electrodes were often tested only in half-cells, and

many full LIB cells were examined by simply bending without quantitative analysis. Therefore, in-depth performance analyses combined with mechanical tests are needed for better understanding and evaluating flexible LIBs. The fabrication of batteries with high energy/power densities, operational safety and excellent cyclic stability is still a great challenge. Lightweight, thin, flexible, stable packaging materials with excellent barrier properties are also needed to protect battery materials, electrolytes and electrochemical reactions from being affected by the external environment.

5. Integrated flexible energy systems

Integrated flexible energy systems (IFESs) have attracted increasing attentions because of their diversified functions.[215, 401] The typical IFESs include a NG combined with a metal-ion-based wireless detector,[402, 403] an OPV with the capability of energy storage,[404] a LED integrated with a bendable LIB,[405] and a LIB powered by a piezoelectric NG.[406, 407] For example, Lee et al. prepared an all-in-one flexible LED system integrated with a bendable LIB wrapped with polymers.[405] Flexible photodetector based on a SnO_2 cloth powered by a flexible LIB has also been reported.[408] However, these devices are still too rigid and too bulky to construct lightweight and compact IFESs with satisfying flexibility. Thus, their performances need to be improved by using new flexible materials with excellent properties such as graphene. However, graphene-based integrated flexible energy systems have rarely been reported. One typical example is the integration of a SC and a photodetector on single fibre.[409] In this system, a fibre-shaped flexible SC was used as the energy storage device, using Ti/Co_3O_4 wires as the positive electrode, and graphene coated on carbon fibres as the negative electrode. Graphene on carbon fibres also acted as the photosensitive material. Upon the adsorption of light, the electron-hole pairs generated in graphene were separated under the external field applied by the graphene SC. Then, the electrons and holes were transported to the positive and negative electrodes correspondingly. Therefore, the integrated self-powered sensors can be operated without an external power source. Such IFESs are important for special applications, such as wireless environmental sensing and in-situ medical monitoring.

Challenges: The study on graphene-based IFESs is in its early stage and far from mature. For practical applications of these systems, at least, the following issues need to be addressed. (1) All the components in an IFES must be shape-conformable; thus, flexible graphene materials with good interfacial compatibility with other functional components are required. (2) The performances of these systems under large deformations still need improvements. (3) New packaging materials that can prevent the damage of the system integrity under deformation are expected.

6. Conclusions and perspective

Nowadays, energy devices, in particular portable, flexible and stretchable devices, is creating new services and products to change our daily life. Under the background of the quick development of lightweight, flexible, and wearable electronic devices in our society, flexible and highly efficient energy strategies are urgently needed. As the thinnest material ever known in the universe, graphene has been attracting tremendous attentions in multidisciplinary subjects because of its unique structure and excellent properties. An increasing market demand for versatile flexible and sustainable energy devices has stimulated huge opportunities for graphene materials and their assemblies or composites. In this critical review, we have covered recent researches on the synthesis of graphene-based materials and their applications in flexible devices related to energy conversion including OPVs, OLEDs, solar cells, photodetectors, fuel cells, actuators and NGs, and those for energy storage including SCs and LIBs. In the end, we also prospected the integrated energy devices for flexible use.

The progress in energy related flexible graphene devices is rapid and great achievements have been obtained in recent years. However, there are still many challenges to be addressed for realizing their practical applications. The problems in a special area have been summarized at the end of each section, thus only several common issues are listed as follows. First, large scale production of graphene materials with uniform structures and high qualities is still a challenging target. Although many devices work well in lab tests, it is difficult to scale up these devices to industrial levels because of the lacking of cheap and convenient techniques for the mass-production of high-quality graphene materials. Single layer graphene sheets can only be produced by expensive CVD technique. Furthermore, most of obtained graphene membranes have to be transferred onto other flexible substrates. The complicate transfer processes heavily limits the wide applications of single-layer of graphene. On the other hand, chemical method can produce a large amount of rGO at a relatively low cost; however, this technique suffers from complicate procedures of synthesis and purification, and have a heavy environmental duty. Furthermore, rGO sheets have relatively low electrical conductivities caused by their structural defects and residual oxygenated groups. Second, the large theoretical surface area of individual graphene sheets can hardly be completely transformed into corresponding macroscopic graphene materials because of their irreversible aggregation and stacking. Thus, porous graphene materials including graphene nanomesh, crumpled graphene and graphene foam have attracted tremendous interest. However, the fabrication of graphene frameworks with precisely controlled microstructures and compositions is a big technical challenge. Third, the performances of flexible graphene devices strongly depend on their structural configurations. Thus, the working mechanisms of the devices need to be revealed more clearly. The interfacial interactions between graphene component and other functional materials require systematical studies. Effective techniques that can assembling graphene devices with super-elasticity, small sizes and/or smart performances are expected. Nevertheless, accompanying with the technical breakthroughs in graphene production and device design, we believe flexible graphene devices and system will be seen in our daily lives.

Acknowledgements

This work was supported by the National Basic Research Program of China (2012CB933402, 2013CB933001), Natural Science Foundation of China (51161120361, 51433005).

Notes and references

*Department of Chemistry, Tsinghua University, Beijing 100084, People's Republic of China. Fax:+86-10-6277-1149; Tel:+86-10-62773743; E-mail: gshi@tsinghua.edu.cn.

1 G. Zhou, F. Li and H. -M. Cheng, *Energy Environ. Sci.*, 2014, **7**, 1307–1338.
2 S. Das, P. Sudhagar, Y. S. Kang and W. Choi, *J. Mater. Res.*, 2014, **29**, 299–319.
3 S.-W. Seo, E. Jung, S. J. Seo, H. Chae, H. K. Chung and S. M. Cho *J. Appl. Phys.*, 2013, **114**, 143505.
4 H. Gwon, J. Hong, H. Kim, D.-H. Seo, S. Jeon and K. Kang, *Energy Environ. Sci.*, 2014, **7**, 538–551.
5 Y. He, W. Chen, C. Gao, J. Zhou, X. Li and E. Xie, *Nanoscale*, 2013, **5**, 8799–8820.
6 S. Park, G. Wang, B. Cho, Y. Kim, S. Song, Y. Ji, M. -H. Yoon and T. Lee, *Nat. Nanotechnol.*, 2012, **7**, 438–442.
7 M. C. LeMieux and Z. N. Bao, *Nat. Nanotechnol.*, 2008, **3**, 585–586.
8 X. M. Lu and Y. N. Xia, *Nat. Nanotechnol.*, 2006, **1**, 163–164.
9 S. Park, M. Vosguerichian and Z. A. Bao, *Nanoscale*, 2013, **5**, 1727–1752.
10 A. Nathan, A. Ahnood, M. T. Cole, S. Lee, Y. Suzuki, P. Hiralal, F. Bonaccorso, T. Hasan, L. Garcia-Gancedo, A. Dyadyusha, S. Haque, P. Andrew, S. Hofmann, J. Moultrie, D. Chu, A. J. Flewitt, A. C. Ferrari, M. J. Kelly, J. Robertson, G. A. J. Amaratunga and W. I. Milne, *Proc. Ieee*, 2012, **100**, 1486–1517.
11 H. Ko, R. Kapadia, K. Takei, T. Takahashi, X. Zhang and A. Javey, *Nanotechnology*, 2012, **23**, 344001.
12 R. Li, B. Nie, P. Digiglio and T. Pan, *Adv. Funct. Mater.*, 2014, **24**, 6195-6203.
13 D. -H. Kim, J. Viventi, J. J. Amsden, J. Xiao, L. Vigeland, Y. -S. Kim, J. A. Blanco, B. Panilaitis, E. S. Frechette, D. Contreras, D. L. Kaplan, F. G. Omenetto, Y. Huang, K. -C. Hwang, M. R. Zakin, B. Litt and J. A. Rogers, *Nat. Mater.*, 2010, **9**, 511–517.
14 H. Nishide and K. Oyaizu, *Science*, 2008, **319**, 737–738.
15 G. H. Gelinck, H. E. A. Huitema, E. Van Veenendaal, E. Cantatore, L. Schrijnemakers, J. Van der Putten, T. C. T. Geuns, M. Beenhakkers, J. B. Giesbers, B. H. Huisman, E. J. Meijer, E. M. Benito, F. J. Touwslager, A. W. Marsman, B. J. E. Van Rens and D. M. De Leeuw, *Nat. Mater.*, 2004, **3**, 106–110.
16 C. Meng, C. Liu, L. Chen, C. Hu and S. Fan, *Nano Lett.*, 2010, 10, 4025–4031.
17 Z. Wang, N. Bramnik, S. Roy, G. Di Benedetto, J. L. Zunino III and S. Mitra, *J. Power Sources*, 2013, 237, 210–214.
18 L. Nyholm, G. Nyström, A. Mihranyan and M. Strømme, *Adv. Mater.*, 2011, 23, 3751–3769.
19 H. Wang, G. Wang, Y. Ling, F. Qian, Y. Song, X. Lu, S. Chen, Y. Tong and Y. Li, *Nanoscale*, 2013, **5**, 10283–10290.
20 W. Cai, T. Lai, W. Dai and J. Ye, *J. Power Sources*, 2014, **255**, 170–178.
21 Y. Q. Sun, Q. Wu and G. Q. Shi, *Energy Environ. Sci.*, 2011, **4**, 1113-1132.
22 C. C. Huang, C. Li and G. Q. Shi, *Energy Environ. Sci.*, 2012, **5**, 8848–8868.
23 Y. Xu, Z. Lin, X. Huang, Y. Liu, Y. Huang and X. Duan, *ACS Nano*, 2013, **7**, 4042–4049.
24 E. Kymakis, K. Savva, M. M. Stylianakis, C. Fotakis and E. Stratakis, *Adv. Funct. Mater.*, 2013, **23**, 2742–2749.
25 H. Tian, S. Ma, H. M. Zhao, C. Wu, J. Ge, D. Xie, Y. Yang and T. L. Ren, *Nanoscale*, 2013, **5**, 8951–8957.
26 Y. H. Wang, K. Bian, C. G. Hu, Z. P. Zhang, N. Chen, H. M. Zhang and L. T. Qu, *Electrochem. Commun.*, 2013, **35**, 49–52.
27 J. Liu, Z. He, J. W. Xue and T. T. Tan, *J. Mater. Chem. B*, 2014, **2**, 2478–2482.
28 C. Yan, J. H. Cho and J. -H. Ahn, *Nanoscale*, 2012, **4**, 4870–4882.
29 D. Spirito, D. Coquillat, S. L. De Bonis, A. Lombardo, M. Bruna, A. C. Ferrari, V. Pellegrini, A. Tredicucci, W. Knap and M. S. Vitiello, *Appl. Phys. Lett.* , 2014, **104**, 061111.
30 J. Zhang, F. Zhao, Z. P. Zhang, N. Chen and L. T. Qu, *Nanoscale*, 2013, **5**, 3112–3126.
31 C. Xu, B. Xu, Y. Gu, Z. Xiong, J. Sun and X. S. Zhao, *Energy Environ. Sci.*, 2013, **6**, 1388–1414.
32 J. Kwon, B. K. Sharma and J. -H. Ahn, *Jap. J. Appl. Phys.*, 2013, **52**. 06GA02.
33 K. Rana, J. Singh and J.-H. Ahn, *J. Mater. Chem. C*, 2014, **2**, 2646–2656.
34 H. J. Choi, S. M. Jung, J. M. Seo, D. W. Chang, L. Dai and J. B. Baek, *Nano Energy*, 2012, **1**, 534–551.
32 R. J. Seresht, M. Jahanshahi, A. Rashidi and A. A. Ghoreyshi, *Appl. Surf. Sci.*, 2013, **276**, 672–681.
36 R. R. Nair, P. Blake, A. N. Grigorenko, K. S. Novoselov, T. J. Booth, T. Stauber, N. M. Peres and A. K. Geim, *Science*, 2008, **320**, 1308.
37 K. I. Bolotin, K. J. Sikes, Z. Jiang, M. Klima, G. Fudenberg, J. Hone, P. Kim and H. L. Stormer, *Solid State Commun.*, 2008, **146**, 351–355.
38 S. V. Morozov, K. S. Novoselov, M. I. Katsnelson, F. Schedin, D. C. Elias, J. A. Jaszczak and A. K. Geim, *Phys. Rev. Lett.* , 2008, **100**, 016602.
39 C. Li and G. Q. Shi, *Adv. Mater.*, 2014, **26**, 3992–4012.
40 Y. X. Xu and G. Q. Shi, *J. Mater. Chem.,* 2011, **21**, 3311–3323.
41 Z. L. Dong, C. C. Jiang, H. H. Cheng, Y. Zhao, G. Q. Shi, L. Jiang and L. T. Qu, *Adv. Mater.*, 2012, **24**, 1856–1861.
42 S. Guo and S. Dong, *Chem. Soc. Rev.*, 2011, **40**, 2644–2672.
43 C. Lee, X. Wei; J. W. Kysar and J. Hone, *Science*, 2008, **321**, 385–388.
44 T. T. Quang, S. Ramasundaram, S. W. Hong and N.-E. Lee, *Adv. Funct. Mater.*, 2014, **24**, 3438–3445.
45 Y. H. Kahng, M. -L. Kim, J.-H. Lee, Y. J. Kim, N. Kim, D.-W. Park and K. Lee, *Sol. Energ. Mat. Sol. C.*, 2014, **124**, 86–91.
46 K. S. Novoselov, A. K. Geim, S. V. Morozov, D. Jiang, Y. Zhang, S. V. Dubonos, I. V. Grigorieva and A. A. Firsov, *Science*, 2004, **306**, 666-669.
47 Y. Zhang, L. Zhang and C. Zhou, *Acc. Chem. Res.*, 2013, **46**, 2329–2339.
48 H. Kim, S. -H. Bae, T. -H. Han, K.-G. Lim, J. -H. Ahn and T. -W. Lee, *Nanotechnology*, 2014, **25**, 014012.
49 L. G. De Arco, Y. Zhang, C. W. Schlenker, K. Ryu, M. E. Thompson and C. Zhou, *ACS Nano*, 2010, **4**, 2865–2873.
50 W. S. Hummers and R. E. Offeman, *J. Am. Chem. Soc.*, 1958, **80**, 1339–1339.
51 D. C. Marcano, D. V. Kosynkin, J. M. Berlin, A. Sinitskii, Z. Sun, A. Slesarev, L. B. Alemany, W. Lu and J. M. Tour, *ACS Nano*, 2010, **4**, 4806–4814.
52 D. A. Dikin, S. Stankovich, E. J. Zimney, R. D. Piner, G. H. B. Dommett, G. Evmenenko, S. T. Nguyen and R. S. Ruoff, *Nature*, 2007, **448**, 457-460.
53 S. Stankovich, D. A. Dikin, R. D. Piner, K. A. Kohlhaas, A. Kleinhammes, Y. Jia, Y. Wu, S. T. Nguyen and R. S. Ruoff, *Carbon*, 2007, **45**, 1558–1565.
54 X. L. Wang, L. Y. Jiao, K. X. Sheng, C. Li, L. M. Dai and G. Q. Shi, *Sci. Rep.*, 2013, **3,** 1996**.**
55 J. T. Robinson, F. K. Perkins, E. S. Snow, Z. Wei and P. E. Sheehan, *Nano Lett.*, 2008, **8**, 3137–3140.
56 H. -J. Shin, K. K. Kim, A. Benayad, S. -M. Yoon, H. K. Park, I. -S. Jung, M. H. Jin, H. -K. Jeong, J. M. Kim, J. -Y. Choi and Y. H. Lee, *Adv. Funct. Mater.* , 2009, **19**, 1987–1992.
57 W. Gao, L. B. Alemany, L. Ci and P. M. Ajayan, *Nat. Chem.*, 2009, **1**, 403–408.
58 Y. Si and E. T. Samulski, *Nano Lett.*, 2008, **8**, 1679–1682.
59 Z. J. Fan, W. Kai, J. Yan, T. Wei, L. J. Zhi, J. Feng, Y. Ren, L. P. Song and F. Wei, *ACS Nano*, 2010, **5**, 191–198.
60 X. Mei and J. Ouyang, *Carbon*, 2011, **49**, 5389–5397.
61 M. J. Fernandez-Merino, L. Guardia, J. I. Paredes, S. Villar-Rodil, P. Solis-Fernandez, A. Martinez-Alonso and J. M. Tascon, *J. Phys. Chem. C*, 2010, **114**, 6426–6432.
62 S. F. Pei, J. P. Zhao, J. H. Du, W. C. Ren and H. M. Cheng, *Carbon*, 2010, **48**, 4466–4474.
63 L. Zhang and G. Q. Shi, *J. Phys. Chem. C*, 2011, **115**, 17206–17212.
64 K. X. Sheng, H. Bai, Y. Q. Sun, C. Li and G. Q. Shi, *Polymer*, 2011, **52**, 5567–5572.
65 X. Wang, L. Zhi and K. Müllen, *Nano Lett.*, 2007, **8**, 323–327.

66 I. Jung, D. A. Dikin, R. D. Piner and R. S. Ruoff, *Nano Lett.*, 2008, **8**, 4283–4287.
67 Y. H. Ng, A. Iwase, A. Kudo and R. Amal, *J. Phys. Chem. Lett*, 2010, **1**, 2607–2612.
68 O. Akhavan and E. Ghaderi, *J. Phys. Chem. C*, 2009, **113**, 20214–20220.
69 G. Williams, B. Seger and P. V. Kamat, *ACS Nano*, 2008, **2**, 1487–1491.
70 H. L. Guo, X. F. Wang, Q. Y. Qian, F. B. Wang and X. H. Xia, *ACS Nano*, 2009, **3**, 2653–2659.
71 D. A. Sokolov, K. R. Shepperd and T. M. Orlando, *J. Phys. Chem. Lett*, 2010, **1**, 2633–2636.
72 Y. X. Xu, K. X. Sheng, C. Li and G. Q. Shi, *ACS Nano*, 2010, **4**, 4324–4330.
73 Y. Zhou, Q. Bao, L. A. L. Tang, Y. Zhong and K. P. Loh, *Chem. Mater.*, 2009, **21**, 2950–2956.
74 M. Choucair, P. Thordarson and J. A. Stride, *Nat. Nanotechnol.*, 2009, **4**, 30–33.
75 L. P. Biro, P. Nemes-Incze and P. Lambin, *Nanoscale*, 2012, **4**, 1824–1839.
76 W. J. Jie and J. H. Hao, *Nanoscale*, 2014, **6**, 6346–6362.
77 W. Li, C. Tan, M. A. Lowe, H. D. Abruna and D. C. Ralph, *ACS Nano*, 2011, **5**, 2264–2270.
78 Y. Si and E. T. Samulski, *Chem. Mater.*, 2008, **20**, 6792–6797.
79 K. A. Ritter and J. W. Lyding, *Nanotechnology*, 2008, **19**, 015704.
80 K. Yan, L. Fu, H. Peng and Z. Liu, *Acc. Chem. Res.*, 2013, **46**, 2263–2274.
81 Y. H. Kwak, D. S. Choi, Y. N. Kim, H. Kim, D. H. Yoon, S. -S. Ahn, J.-W. Yang, W. S. Yang and S. Seo, *Biosens. Bioelectron.* 2012, **37**, 82–87.
82 T. Kobayashi, M. Bando, N. Kimura, K. Shimizu, K. Kadono, N. Umezu, K. Miyahara, S. Hayazaki, S. Nagai, Y. Mizuguchi, Y. Murakami and D. Hobara, *Appl. Phys. Lett.*, 2013, **102**, 023112.
83 S. Bae, H. Kim, Y. Lee, X. Xu, J. -S. Park, Y. Zheng, J. Balakrishnan, T. Lei, H. R. Kim, Y. I. Song, Y. -J. Kim, K. S. Kim, B. Ozyilmaz, J. -H. Ahn, B. H. Hong and S. Iijima, *Nat. Nanotechnol.*, 2010, **5**, 574–578.
84 D. Y. Wang, I. S. Huang, P. H. Ho, S. S. Li, Y. C. Yeh, D. W. Wang, W. L. Chen, Y. Y. Lee, Y. M. Chang, C. C. Chen, C. T. Liang and C. W. Chen, *Adv. Mater.*, 2013, **25**, 4521–4526.
85 Q. B. Zheng, Z. G. Li, J. H. Yang and J. -K. Kim, *Prog. Mater. Sci.*, 2014, **64**, 200–247.
86 L. Huang, G. L. Guo, Y. Liu, Q. H. Chang and W. Z. Shi, *Mater. Res. Bul.*, 2013, **48**, 4163–4167.
87 Y. S. Yun, D. H. Kim, B. Kim, H. H. Park and H.-J. Jin, *Synth. Met.*, 2012, **162**, 1364–1368.
88 J. Hong, J. Y. Han, H. Yoon, P. Joo, T. Lee, E. Seo, K. Char and B. -S. Kim, *Nanoscale*, 2011, **3**, 4515–4531.
89 X. L. Wang, H. Bai and G. Q. Shi, *J. Am. Chem. Soc.*, 2011, **133**, 6338–6342.
90 D. W. Lee, T.-K. Hong, D. Kang, J. Lee, M. Heo, J. Y. Kim, B.-S. Kim and H. S. Shin, *J. Mater. Chem.*, 2011, **21**, 3438–3442.
91 J. Zhu and J. He, *Nanoscale*, 2012, **4**, 3558–3566.
92 Z. Niu, J. Du, X. Cao, Y. Sun, W. Zhou, H. H. Hng, J. Ma, X. Chen and S. Xie, *Small*, 2012, **8**, 3201–3208.
93 O. C. Compton, D. A. Dikin, K. W. Putz, L. C. Brinson and S. T. Nguyen, *Adv. Mater.*, 2010, **22**, 892–896.
94 S. Park, K. S. Lee, G. Bozoklu, W. Cai, S. T. Nguyen and R. S. Ruoff, *ACS Nano*, 2008, **2**, 572–578.
95 X. Brunetaud, L. Divet and D. Damidot, *Cement Concrete Res.*, 2008, **38**, 1343–1348.
96 X. L. Wang, H. Bai, Y. Y. Jia, L. J. Zhi, L. T. Qu, Y. X. Xu, C. Li and G. Q. Shi, *RSC Adv.*, 2012, **2**, 2154–2160.
97 S. Stankovich, R. D. Piner, X. Q. Chen, N. Q. Wu, S. T. Nguyen and R. S. Ruoff, *J. Mater. Chem.*, 2006, **16**, 155–158.
98 S. Z. Zu and B. H. Han, *J. Phys. Chem. C*, 2009, **113**, 13651–13657.
99 S. Stankovich, R. D. Piner, S. T. Nguyen and R. S. Ruoff, *Carbon*, 2006, **44**, 3342–3347.
100 Y. Y. Liang, D. Q. Wu, X. L. Feng and K. Müllen, *Adv. Mater.*, 2009, **21**, 1679–1683.
101 J. R. Lomeda, C. D. Doyle, D. V. Kosynkin, W. -F. Hwang and J. M. Tour, *J. Am. Chem. Soc.* , 2008, **130**, 16201–16206.
102 M. Lotya, P. J. King, U. Khan, S. De and J. N. Coleman, *ACS Nano*, 2010, **4**, 3155–3162.
103 H. F. Yang, C. S. Shan, F. H. Li, D. X. Han, Q. X. Zhang and L. Niu, *Chem. Commun.*, 2009, 3880–3882.
104 A. J. Patil, J. L. Vickery, T. B. Scott and S. Mann, *Adv. Mater.*, 2009, **21**, 3159–3164.
105 D. Li, M. B. Muller, S. Gilje, R. B. Kaner and G. G. Wallace, *Nat Nanotechnol*, 2008, **3**, 101–105.
106 C. Valles, J. D. Nunez, A. M. Benito and W. K. Maser, *Carbon*, 2012, **50**, 835–844.
107 Z. Xu, H. Sun, X. Zhao and C. Gao, *Adv. Mater.*, 2013, **25**, 188–193.
108 L. Kou and C. Gao, *Nanoscale*, 2013, **5**, 4370–4378.
109 R. Jalili, S. H. Aboutalebi, D. Esrafilzadeh, R. L. Shepherd, J. Chen, S. Aminorroaya-Yamini, K. Konstantinov, A. I. Minett, J. M. Razal and G. G. Wallace, *Adv. Funct. Mater.* , 2013, **23**, 5345–5354.
110 C. S. Xiang, C. C. Young, X. Wang, Z. Yan, C. -C. Hwang, G. Cerioti, J. Lin, J. Kono, M. Pasquali and J. M. Tour, *Adv. Mater.*, 2013, **25**, 4592–4597.
111 Y. N. Meng, Y. Zhao, C. G. Hu, H. H. Cheng, Y. Hu, Z. P. Zhang, G. Q. Shi and L. T. Qu, *Adv. Mater.*, 2013, **25**, 2326–2331.
112 Z. Xu and C. Gao, *Nat. Commun.*, 2011, **2**, 571.
113 B. Vigolo, A. Penicaud, C. Coulon, C. Sauder, R. Pailler, C. Journet, P. Bernier and P. Poulin, *Science*, 2000, **290**, 1331–1334.
114 M. Zhang, K. R. Atkinson and R. H. Baughman, *Science*, 2004, **306**, 1358–1361.
115 Y. Zhao, C. C. Jiang, C. G. Hu, Z. L. Dong, J. L. Xue, Y. N. Meng, N. Zheng, P. W. Chen and L. T. Qu, *ACS Nano*, 2013, **7**, 2406–2412.
116 L. Jiang and Z. Fan, *Nanoscale*, 2014, **6**, 1922–1945.
117 C. Li, G. Q. Shi, *Nanoscale*, 2012, **4**, 5549–5563.
118 M. A. Worsley, P. J. Pauzauskie, T. Y. Olson, J. Biener, J. H. Satcher, Jr. and T. F. Baumann, *J. Am. Chem. Soc.*, 2010, **132**, 14067–14069.
119 Z. Xu, Y. Zhang, P. Li and C. Gao, *ACS Nano*, 2012, **6**, 7103–7113.
120 Z. Niu, J. Chen, H. H. Hng, J. Ma and X. Chen, *Adv. Mater.*, 2012, **24**, 4144–4150.
121 G. Zhu, Z. He, J. Chen, J. Zhao, X. Feng, Y. Ma, Q. Fan, L. Wang and W. Huang, *Nanoscale*, 2014, **6**, 1079–1085.
122 J. Ge, H. B. Yao, W. Hu, X. F. Yu, Y. X. Yan, L. B. Mao, H. H. Li, S. S. Li and S. H. Yu, *Nano Energy*, 2013, **2**, 505–513.
123 W. Chen, Y. X. Huang, D. B. Li, H. Q. Yu and L. Yan, *RSC Adv.*, 2014, **4**, 21619–21624.
124 L. B. Zhang, G. Y. Chen, M. N. Hedhili, H. N. Zhang and P. Wang, *Nanoscale*, 2012, **4**, 7038–7045.
125 X. Zhang, Z. Sui, B. Xu, S. Yue, Y. Luo, W. Zhan and B. Liu, *J. Mater. Chem.*, 2011, **21**, 6494–6497.
126 H. Hu, Z. Zhao, W. Wan, Y. Gogotsi and J. Qiu, *Adv. Mater.*, 2013, **25**, 2219–2223.
127 L. Qiu, J. Z. Liu, S. L. Y. Chang, Y. Z. Wu and D. Li, *Nat. Commun.*, 2012, **3**, 1241.
128 Y. R. Li, J. Chen, L. Huang, C. Li, J. -D. Hong and G. Q. Shi, *Adv. Mater.*, 2014, **26**, 4789–4793.
129 X. F. Gao, J. Jang and S. Nagase, *J. Phys. Chem. C*, 2010, **114**, 832–842.
130 D. R. Dreyer, S. Park, C. W. Bielawski and R. S. Ruoff, *Chem. Soc. Rev.*, 2010, **39**, 228–240.
131 G. Widawski, M. Rawiso and B. Francois, *Nature*, 1994, **369**, 387–389.
132 A. Boker, Y. Lin, K. Chiapperini, R. Horowitz, M. Thompson, V. Carreon, T. Xu, C. Abetz, H. Skaff, A. D. Dinsmore, T. Emrick and T. P. Russell, *Nat. Mater.*, 2004, **3**, 302–306.
133 H. Yabu and M. Shimomura, *Chem. Mater.*, 2005, **17**, 5231–5234.
134 S. H. Lee, H. W. Kim, J. O. Hwang, W. J. Lee, J. Kwon, C. W. Bielawski, R. S. Ruoff and S. O. Kim, *Angew. Chem. Int. Edit.*, 2010, **49**, 10084–10088.
135 V. Strong, S. Dubin, M. F. El-Kady, A. Lech, Y. Wang, B. H. Weiller and R. B. Kaner, *ACS Nano*, 2012, **6**, 1395–1403.
136 J. Kim, J.-H. Jeon, H.-J. Kim, H. Lim and I.-K. Oh, *ACS Nano*, 2014, **8**, 2986–2997.
137 M. F. El-Kady and R. B. Kaner, *Nat. Commun.*, 2013, **4**, 1475.

138 F. Tristán-López, A. Morelos-Gómez, S. M. Vega-Díaz, M. L. García-Betancourt, N. Perea-López, A. L. Elías, H. Muramatsu, R. Cruz-Silva, S. Tsuruoka, Y. A. Kim, T. Hayahsi, K. Kaneko, M. Endo and M. Terrones, *ACS Nano*, 2013, **7**, 10788–10798.

139 X. Lin, P. Liu, Y. Wei, Q. Li, J. Wang, Y. Wu, C. Feng, L. Zhang, S. Fan and K. Jiang, *Nat. Commun.*, 2013, **4**, 2920.

140 Z. Yan, Z. Peng, G. Casillas, J. Lin, C. Xiang, H. Zhou, Y. Yang, G. Ruan, A. R. O. Raji, E. L. G. Samuel, R. H. Hauge, M. J. Yacaman and J. M. Tour, *ACS Nano*, 2014, **8**, 5061–5068.

141 S. Han, D. Q. Wu, S. Li, F. Zhang and X. L. Feng, *Adv. Mater.*, 2014, **26**, 849–864.

142 S. Yin, Z. Niu and X. Chen, *Small*, 2012, **8**, 2458–2463.

143 J. Lu, D. Yuan, J. Liu, W. Leng and T. E. Kopley, *Nano Lett.*, 2008, **8**, 3325–3329.

144 B. You, L. Wang, L. Yao and J. Yang, *Chem. Commun.*, 2013, **49**, 5016–5018.

145 J. H. Zou, J. H. Liu, A. S. Karakoti, A. Kumar, D. Joung, Q. A. Li, S. I. Khondaker, S. Seal and L. Zhai, *ACS Nano*, 2010, **4**, 7293–7302.

146 A. Y. Cao, P. L. Dickrell, W. G. Sawyer, M. N. Ghasemi-Nejhad and P. M. Ajayan, *Science*, 2005, **310**, 1307–1310.

147 M. Xu, D. N. Futaba, T. Yamada, M. Yumura and K. Hata, *Science*, 2010, **330**, 1364–1368.

148 D. P. Hashim, N. T. Narayanan, J. M. Romo-Herrera, D. A. Cullen, M. G. Hahm, P. Lezzi, J. R. Suttle, D. Kelkhoff, E. Munoz-Sandoval, S. Ganguli, A. K. Roy, D. J. Smith, R. Vajtai, B. G. Sumpter, V. Meunier, H. Terrones, M. Terrones and P. M. Ajayan, *Sci. Rep.*, 2012, **2**, 363.

149 K. H. Kim, Y. Oh and M. F. Islam, *Nat. Nanotechnol.*, 2012, **7**, 562–566.

150 H. Sun, Z. Xu and C. Gao, *Adv. Mater.*, 2013, **25**, 2554–2560.

151 Z. Y. Yang, Y. F. Zhao, Q. Q. Xiao, Y. X. Zhang, L. Jing, Y. M. Yan and K. N. Sun, *ACS Appl. Mater. Inter.*, 2014, **6**, 8497–8504.

152 X. Dong, Y. Ma, G. Zhu, Y. Huang, J. Wang, M. B. Chan-Park, L. Wang, W. Huang and P. Chen, *J. Mater. Chem.*, 2012, **22**, 17044–17048.

153 H. P. Cong, X. C. Ren, P. Wang and S. H. Yu, *Energy Environ. Sci.*, 2013, **6**, 1185–1191.

154 Z. D. Huang, R. Liang, B. Zhang, Y. B. He and J. K. Kim, *Compos. Sci. Technol.*, 2013, **88**, 126–133.

155 L. Li, K. Xia, L. Li, S. Shang, Q. Guo and G. Yan, *J. Nanopart. Res.*, 2012, **14**, 908.

156 Y. X. Xu, W. J. Hong, H. Bai, C. Li and G. Q. Shi, *Carbon*, 2009, **47**, 3538–3543.

157 X. L. Wang, H. Bai, Z. Y. Yao, A. R. Liu and G. Q. Shi, *J. Mater. Chem.*, 2010, **20**, 9032–9036.

158 Q. Wu, Y. Y. Xu, Z. Y. Yao, A. R. Liu and G. Q. Shi, *ACS Nano*, 2010, **4**, 1963–1970.

159 L. Huang, C. Li and G. Q. Shi, *J. Mater. Chem. A*, 2014, **2**, 968–974.

160 L. Huang, C. Li, W. J. Yuan and G. Q. Shi, *Nanoscale*, 2013, **5**, 3780–3786.

161 M. Zhang, L. Huang, J. Chen, C. Li and G. Q. Shi, *Adv. Mater.*, 2014, DOI: 10.1002/adma.201403322.

162 X. Huang, X. Y. Qi, F. Boey and H. Zhang, *Chem. Soc. Rev.*, 2012, **41**, 666–686.

163 Y. Q. Sun and G. Q. Shi, *J. Polym. Sci. Pol. Phys.*, 2013, **51**, 231–253.

164 X. S. Zhou, T. B. Wu, B. J. Hu, G. Y. Yang and B. X. Han, *Chem. Commun.*, 2010, **46**, 3663–3665.

165 K. Zhang, L. L. Zhang, X. S. Zhao and J. S. Wu, *Chem. Mater.*, 2010, **22**, 1392–1401.

166 J. Yan, T. Wei, B. Shao, Z. J. Fan, W. Z. Qian, M. L. Zhang and F. Wei, *Carbon*, 2010, **48**, 487–493.

167 H. L. Wang, Q. L. Hao, X. J. Yang, L. D. Lu and X. Wang, *ACS Appl. Mater. Inter.* , 2010, **2**, 821–828.

168 J. Xiang and L. T. Drzal, *Chem. Phys. Lett.*, 2014, **593**, 109–114.

169 J. W. Park, S. J. Park, O. S. Kwon, C. Lee, J. Jang, J. Jang, J. W. Park, S. J. Park, C. Lee and O. S. Kwon, *Chem. Mater.*, 2014, **26**, 2354–2360.

170 J. L. Lutkenhaus, K. D. Hrabak, K. McEnnis and P. T. Hammond, *J. Am. Chem. Soc.*, 2005, **127**, 17228–17234.

171 Z. Y. Tang, N. A. Kotov, S. Magonov and B. Ozturk, *Nat. Mater.*, 2003, **2**, 413–418.

172 E. Kharlampieva, V. Kozlovskaya, R. Gunawidjaja, V. V. Shevchenko, R. Vaia, R. R. Naik, D. L. Kaplan and V. V. Tsukruk, *Adv. Funct. Mater.*, 2010, **20**, 840–846.

173 R. Gunawidjaja, C. Y. Jiang, S. Peleshanko, M. Ornatska, S. Singamaneni and V. V. Tsukruk, *Adv. Funct. Mater.*, 2006, **16**, 2024–2034.

174 D. D. Kulkarni, I. Choi, S. Singamaneni and V. V. Tsukruk, *ACS Nano*, 2010, **4**, 4667–4676.

175 B. -H. Wee and J. -D. Hong, *Adv. Funct. Mater.*, 2013, **23**, 4657–4666.

176 S. S. Mahapatra, M. S. Ramasamy, H. J. Yoo and J. W. Cho, *RSC Adv.*, 2014, **4**, 15146–15153.

177 F. Li, Z. Lin, B. Zhang, Y. Zhang, C. Wu and T. Guo, *Org. Electron.*, 2013, **14**, 2139–2143.

178 H. Gao, Y. Wang, F. Xiao, C. B. Ching and H. Duan, *J. Phys. Chem. C*, 2012, **116**, 7719–7725.

179 Q. Chen, Y. N. Meng, C. G. Hu, Y. Zhao, H. B. Shao, N. Chen and L. T. Qu, *J. Power Sources*, 2014, **247**, 32–39.

180 B. Wang, X. Li, B. Luo, Y. Jia and L. Zhi, *Nanoscale*, 2013, **5**, 1470–1474.

181 L. Yan, Y. N. Chang, W. Yin, X. Liu, D. Xiao, G. Xing, L. Zhao, Z. Gu and Y. Zhao, *Phys. Chem. Chem. Phys.*, 2014, **16**, 1576–1582.

182 P. Zhai, Y. H. Chang, Y. T. Huang, T. C. Wei, H. Su and S. P. Feng, *Electrochimica Acta*, 2014, **132**, 186–192.

183 M. G. Chung, D. -H. Kim, D. K. Seo, T. Kim, H. U. Im, H. M. Lee, J.-B. Yoo, S.- H. Hong, T. J. Kang and Y. -H. Kim, *Sen. Actuat. B-Chem.*, 2012, **169**, 387–392.

184 J. Zhi, W. Zhao, X. Y. Liu, A. R. Chen, Z. Q. Liu and F. Q. Huang, *Adv. Funct. Mater.*, 2014, **24**, 2013–2019.

185 B. G. Choi, S. -J. Chang, H.-W. Kang, P. P. Chan, H. J. Kim, W. H. Hong, S. G. Lee and Y. S. Huh, *Nanoscale*, 2012, **4**, 4983–4988.

186 Z. Li, Y. Mi, X. Liu, S. Liu, S. Yang and J. Wang, *J. Mater. Chem.*, 2011, **21**, 14706–14711.

187 S. D. Perera, M. Rudolph, R. G. Mariano, N. Nijem, J. P. Ferraris, Y. J. Chabal and K. J. Balkus, Jr., *Nano Energy*, 2013, **2**, 966–975.

188 Y. Liu, W. Wang, Y. Wang, Y. Ying, L. Sun and X. Peng, *RSC Adv.*, 2014, **4**, 16374–16379.

189 C. Yuan, L. Yang, L. Hou, J. Li, Y. Sun, X. Zhang, L. Shen, X. Lu, S. Xiong and X. W. Lou, *Adv. Funct. Mater.*, 2012, **22**, 2560–2566.

190 J. Liang, Z. Cai, Y. Tian, L. Li, J. Geng and L. Guo, *ACS Appl. Mater. Inter.*, 2013, **5**, 12148–12155.

191 T. Hu, X. Sun, H. Sun, M. Yu, F. Lu, C. Liu and J. Lian, *Carbon*, 2013, **51**, 322–326.

192 C. Yuan, X. Zhang, L. Su, B. Gao and L. Shen, *J. Mater. Chem.*, 2009, **19**, 5772–5777.

193 J. Liang, Y. Huang, J. Oh, M. Kozlov, D. Sui, S. Fang, R. H. Baughman, Y. Ma and Y. Chen, *Adv. Funct. Mater.*, 2011, **21**, 3778–3784.

194 Z. L. Wang and J. H. Song, *Science*, 2006, **312**, 242–246.

195 K. I. Park, M. Lee, Y. Liu, S. Moon, G. T. Hwang, G. Zhu, J. E. Kim, S. O. Kim, D. K. Kim, Z. L. Wang and K. J. Lee, *Adv. Mater.*, 2012, **24**, 2999–3004.

196 C. T. Huang, J. H. Song, C. M. Tsai, W. F. Lee, D. H. Lien, Z. Y. Gao, Y. Hao, L. J. Chen and Z. L. Wang, *Adv. Mater.*, 2010, **22**, 4008–4013.

197 Y. F. Lin, J. Song, Y. Ding, S. Y. Lu and Z. L. Wang, *Adv. Mater.*, 2008, **20**, 3127–3130.

198 C. Jing, X. Feng, W. Jun, Q. Khan, Z. Yidan, L. Wei, S. Li and Z. Yan, *Nanoscale*, 2012, **4**, 441–443.

199 D. Zhang, F. Xie, P. Lin and W. C. H. Choy, *ACS Nano*, 2013, **7**, 1740–1747.

200 S. Liu, R. Wang, M. Liu, J. Luo, X. Jin, J. Sun and L. Gao, *J. Mater. Chem. A*, 2014, **2**, 4598–4604.

201 X. L. Zan, Z. Fang, J. Wu, F. Xiao, F. W. Huo and H. W. Duan, *Biosens. Bioelectron.*, 2013, **49**, 71–78.

202 L. Jiang, X. Lu and X. Zheng, *J. Mater. Sci.-Mater. El.*, 2014, **25**, 174–180.

203 S. T. Han, Y. Zhou, C. Wang, L. He, W. Zhang and V. A. L. Roy, *Adv. Mater.*, 2013, **25**, 872–877.

204 Z. Q. Niu, J. J. Du, X. B. Cao, Y. H. Sun, W. Y. Zhou, H. H. Hng, J. Ma, X. D. Chen and S. S. Xie, *Small*, 2012, **8**, 3201–3208.

205 F. Xiao, J. Song, H. Gao, X. Zan, R. Xu and H. Duan, *ACS Nano*, 2012, **6**, 100–110.

206 T. Georgiou, R. Jalil, B. D. Belle, L. Britnell, R. V. Gorbachev, S. V. Morozov, Y.-J. Kim, A. Gholinia, S. J. Haigh, O. Makarovsky, L. Eaves, L. A. Ponomarenko, A. K. Geim, K. S. Novoselov and A. Mishchenko, *Nat. Nanotechnol.*, 2013, **8**, 100–103.

207 M.-S. Lee, K. Lee, S.-Y. Kim, H. Lee, J. Park, K.-H. Choi, H.-K. Kim, D.-G. Kim, D.-Y. Lee, S. Nam and J.-U. Park, *Nano Lett.*, 2013, **13**, 2814–2821.

208 D. Kuang and W.-B. Hu, *J. Inorg. Mater.*, 2013, **28**, 235–246.

209 Y. Dai, S. Cai, W. Yang, L. Gao, W. Tang, J. Xie, J. Zhi and X. Ju, *Carbon*, 2012, **50**, 4648–4654.

210 G. Ferey, M. Haouas, T. Loiseau and F. Taulelle, *Chem. Mater.*, 2014, **26**, 299–309.

211 Y. M. He, W. J. Chen, X. D. Li, Z. X. Zhang, J. C. Fu, C. H. Zhao and E. Q. Xie, *ACS Nano*, 2013, **7**, 174–182.

212 Y. Sun, S. Gao and Y. Xie, *Chem. Soc. Rev.*, 2014, **43**, 530–546.

213 J. Zhu, D. Yang, Z. Yin, Q. Yan and H. Zhang, *Small*, 2014, **10**, 3480–3498.

214 H. Wang, H. Feng and J. Li, *Small*, 2014, **10**, 2165–2181.

215 L. Li, Z. Wu, S. Yuan and X.-B. Zhang, *Energy Environ. Sc.*, 2014, **7**, 2101–2122.

216 M. Tathavadekar, M. Biswal, S. Agarkar, L. Giribabu and S. Ogale, *Electrochim. Acta*, 2014, **123**, 248–253.

217 J. B. Wu, M. Agrawal, H. A. Becerril, Z. N. Bao, Z. F. Liu, Y. S. Chen and P. Peumans, *Acs Nano*, 2010, **4**, 43–48.

218 H. Meng, J. Luo, W. Wang, Z. Shi, Q. Niu, L. Dai and G. Qin, *Adv. Funct. Mater.*, 2013, **23**, 3324–3328.

219 N. Liu, H. Tian, G. Schwartz, J. B. H. Tok, T.-L. Ren and Z. Bao, *Nano Lett.*, 2014, **14**, 3702-3708.

220 B. Y. Zhang, T. Liu, B. Meng, X. Li, G. Liang, X. Hu and Q. J. Wang, *Nat. Commun.*, 2013, **4**, 1811.

221 L. Kong and W. Chen, *Adv. Mater.*, 2014, **26**, 1025−1043.

222 Y. Zhao, L. Song, Z. Zhang and L. Qu, *Energy Environ. Sci.*, 2013, **6**, 3520−3536.

223 S. Kim, M. K. Gupta, K. Y. Lee, A. Sohn, T. Y. Kim, K.-S. Shin, D. Kim, S. K. Kim, K. H. Lee, H.-J. Shin, D.-W. Kim and S.-W. Kim, *Adv. Mater.*, 2014, **26**, 3918–3925.

224 M. Layani, A. Kamyshny and S. Magdassi, *Nanoscale*, 2014, **6**, 5581–5591.

225 J. Du, S. Pei, L. Ma and H. M. Cheng, *Adv. Mater.*, 2014, **26**, 1958–1991.

226 H. Ma, D. Wu, Z. Cui, Y. Li, Y. Zhang, B. Du and Q. Wei, *Anal. Lett.* 2013, **46**, 1–17.

227 Z. Liu, J. Li and F. Yan, *Adv. Mater.*, 2013, **25**, 4296–4301.

228 D. Jariwala, V. K. Sangwan, L. J. Lauhon, T. J. Marks and M. C. Hersam, *Chem. Soc. Rev.*, 2013, **42**, 2824–2860.

229 Q. Zhang, X. J. Wang, F. Xing, L. Huang, G. K. Long, N. B. Yi, W. Ni, Z. B. Liu, J. G. Tian and Y. S. Chen, *Nano Res.*, 2013, **6**, 478–484.

230 S. -I. Na, Y. -J. Noh, S. -Y. Son, T. -W. Kim, S. -S. Kim, S. Lee and H. -I. Joh, *Appl. Phys. Lett.* , 2013, **102**, 043304.

231 J. Wu, H. A. Becerril, Z. Bao, Z. Liu, Y. Chen and P. Peumans, *Appl. Phys. Lett.* , 2008, **92**, 263302.

232 Y. Wang, S. W. Tong, X. F. Xu, B. Özyilmaz and K. P. Loh, *Adv. Mater.*, 2011, **23**, 1514–1518.

233 Y. Xu, G. Long, L. Huang, Y. Huang, X. Wan, Y. Ma and Y. Chen, *Carbon*, 2010, **48**, 3308–3311.

234 Z. Y. Yin, S. Y. Sun, T. Salim, S. X. Wu, X. A. Huang, Q. Y. He, Y. M. Lam and H. Zhang, *ACS Nano*, 2010, **4**, 5263–5268.

235 J. H. Huang, J. H. Fang, C. C. Liu and C. W. Chu, *ACS Nano*, 2011, **5**, 6262–6271.

236 Y. Zhu, Z. Sun, Z. Yan, Z. Jin and J. M. Tour, *ACS Nano*, 2011, **5**, 6472–6479.

237 Z. Liu, J. Li, Z.-H. Sun, G. Tai, S.-P. Lau and F. Yan, *ACS Nano*, 2011, **6**, 810–818.

238 T. H. Seo, T. S. Oh, S. J. Chae, A. H. Park, K. J. Lee, Y. H. Lee and E.-K. Suh, *Jpn. J. Appl. Phys.*, 2011, **50**, 125103.

239 Y. Q. Sun and G. Q. Shi, *J. Polym. Sci. Pol. Phys.*, 2013, **51**, 231–253.

240 D. W. Zhang, X. D. Li, H. B. Li, S. Chen, Z. Sun, X. J. Yin and S. M. Huang, *Carbon*, 2011, **49**, 5382−5388.

241 Y. X. Xu, H. Bai, G. W. Lu, C. Li and G. Q. Shi, *J. Am. Chem. Soc.*, 2008, **130**, 5856–5858..

242 W. J. Hong, Y. X. Xu, G. W. Lu, C. Li and G. Q. Shi, *Electrochem. Commun.*, 2008, **10**, 1555–1558.

243 K. S. Lee, Y. Lee, J. Y. Lee, J. -H. Ahn and J. H. Park, *ChemSusChem*, 2012, **5**, 379–382.

244 N. Yeh and P. Yeh, *Renew. Sust. Energ. Rev.*, 2013, **21**, 421–431.

245 S. C. Lo and P. L. Burn, *Chem. Rev.*, 2007, **107**, 1097–1116.

246 S. Reineke, F. Lindner, G. Schwartz, N. Seidler, K. Walzer, B. Lussem, K. Leo, *Nature*, 2009, **459**, 234–238.

247 J. Wu, M. Agrawal, H. A. Becerril, Z. Bao, Z. Liu, Y. Chen and P. Peumans, *ACS Nano*, 2009, **4**, 43–48.

248 T. Sun, Z. L. Wang, Z. J. Shi, G. Z. Ran, W. J. Xu, Z. Y. Wang, Y. Z. Li, L. Dai and G. G. Qin, *Appl. Phys. Lett.* , 2010, **96**, 133301.

249 T. -H. Han, Y. Lee, M. -R. Choi, S. -H. Woo, S. -H. Bae, B. H. Hong, J. -H. Ahn and T. -W. Lee, *Nat. Photon.*, 2012, **6**, 105–110.

250 Y. Liu, E. Jung, Y. Wang, Y. Zheng, E. J. Park, S. M. Cho and K. P. Loh, *Small*, 2014, **10**, 944–949.

251 Y. Han, L. Zhang, X. Zhang, K. Ruan, L. Cui, Y. Wang, L. Liao, Z. Wang and J. Jie, *J. Mater. Chem. C*, 2014, **2**, 201–207.

252 N. Li; S. Oida, G. S. Tulevski, S. Han; J. B. Hannon, D. K. Sadana, T. Chen, *Nat. Commun.*, 2013, **4**, 2294.

253 Q. Wang, M. Safdar, K. Xu, M. Mirza, Z. Wang and J. He, *ACS Nano*, 2014, **8**, 7497–7505.

254 S. R. Tamalampudi, Y. Y. Lu, R. U. Kumar, R. Sankar, C. D. Liao, K. B. Moorthy, C. H. Cheng, F. C. Chou and Y. T. Chen, *Nano Lett.*, 2014, **14**, 2800–2806.

255 L. Peng, L. Hu and X. Fang, *Adv. Funct. Mater.*, 2014, **24**, 2591–2610.

256 R. R. Nair, P. Blake, A. N. Grigorenko, K. S. Novoselov, T. J. Booth, T. Stauber, N. M. R. Peres and A. K. Geim, *Science*, 2008, **320**, 1308–1308.

257 T. Mueller, F. N. A. Xia and P. Avouris, *Nat. Photon.*, 2010, **4**, 297–301.

258 F. N. Xia, T. Mueller, Y. M. Lin, A. Valdes-Garcia and P. Avouris, *Nat. Nanotechnol.*, 2009, **4**, 839–843.

259 T. Mueller, F. Xia and P. Avouris, *Nat. Photon.*, 2010, **4**, 297–301.

260 Z. Gao, W. Jin, Y. Zhou, Y. Dai, B. Yu, C. Liu, W. Xu, Y. Li, H. Peng, Z. Liu and L. Dai, *Nanoscale*, 2013, **5**, 5576–5581.

261 K. K. Manga, S. Wang, M. Jaiswal, Q. L. Bao and K. P. Loh, *Adv. Mater.*, 2010, **22**, 5265–5270.

262 G. Konstantatos, M. Badioli, L. Gaudreau, J. Osmond, M. Bernechea, F. P. G. de Arquer, F. Gatti and F. H. L. Koppens, *Nat. Nano*, 2012, **7**, 363–368.

263 Z. Sun, Z. Liu, J. Li, G. Tai, S.-P. Lau and F. Yan, *Adv. Mater.*, 2012, **24**, 5878–5883.

264 H. X. Chang, Z. H. Sun, M. Saito, Q. H. Yuan, H. Zhang, J. H. Li, Z. C. Wang, T. Fujita, F. Ding, Z. J. Zheng, F. Yan, H. K. Wu, M. W. Chen and Y. Ikuhara, *ACS Nano*, 2013, **7**, 6310–6320.

265 H. X. Wang, Q. Wang, K. G. Zhou and H. L. Zhang, *Small*, 2013, **9**, 1266–1283.

266 B. H. Lee, J. H. Lee, Y. H. Kahng, N. Kim, Y. J. Kim, J. Lee, T. Lee and K. Lee, *Adv. Funct. Mater.*, 2014, **24**, 1847–1856.

267 M. F. El-Kady, V. Strong, S. Dubin and R. B. Kaner, *Science*, 2012, **335**, 1326–1330.

268 C. L. Hsu, C. T. Lin, J. H. Huang, C. W. Chu, K. H. Wei and L. J. Li, *ACS Nano*, 2012, **6**, 5031–5039.

269 N. G. Sahoo, Y. Pan, L. Li and S. H. Chan, *Adv. Mater.*, 2012, **24**, 4203–4210.

270 X. L. Wang, C. Li and G. Q. Shi, *Phys. Chem. Chem. Phys.*, 2014, **16**, 10142–10148.

271 Y. Q. Sun, C. Li, Y. X. Xu, H. Bai, Z. Y. Yao and G. Q. Shi, *Chem. Commun.*, 2010, 46, 4740–4742.

272 M. Sawangphruk, A. Krittayavathananon and N. Chinwipas, *J. Mater. Chem. A*, 2013, **1**, 1030–1034.

273 S. S. Li, H. P. Cong, P. Wang and S. H. Yu, *Nanoscale*, 2014, **6**, 7534–7541.

274 J. E. Mink, R. M. Qaisi and M. M. Hussain, *Energy Technol.*, 2013, **1**, 648–652.
275 Y. J. Heo, T. Kan, E. Iwase, K. Matsumoto and I. Shimoyama, *Micro & Nano Lett.*, 2013, **8**, 865–868.
276 Q. Wang, Y. Hou and C. Dong, *Int. J. Robust Nonlin.*, 2012, **22**, 1019–1035.
277 M. Karpelson, G. Y. Wei and R. J. Wood, *Sensor. Actuat. A-Phys.*, 2012, **176**, 78–89.
278 J. Li, Z. Ji, X. Shi, F. You, F. Fu, R. Liu, J. Xia, N. Wang, J. Bai, Z. Wang, X. Qin and X. Dong, *Bio.-Med. Mater. Eng.*, 2013, **23**, S569–575.
279 B. K. S. Woods, M. F. Gentry, C. S. Kothera and N. M. Wereley, *J. Intel. Mat. Syst. Str.*, 2012, **23**, 327–343.
280 E. Pagounis, R. Chulist, M. J. Szczerba and M. Laufenberg, *Scripta Mater.* 2014, **83**, 29–32.
281 K. Min, J. Y. Jung, T. H. Han, Y. Park, C. Jung, S. M. Hong and C. M. Koo, *Mol. Cryst. Liq. Cryst.*, 2011, **539**, 260–265.
282 G. W. Rogers and J. Z. Liu, *J. Am. Chem. Soc.*, 2012, **134**, 1250–1255.
283 G. W. Rogers and J. Z. Liu, *J. Am. Chem. Soc.*, 2011, **133**, 10858–10863.
284 K. Y. Shin, J. Y. Hong and J. Jang, *Chem. Commun.*, 2011, **47**, 8527–8529.
285 J. Park, G. Gu; Z. Wang, D. Kwon and K. L. DeVries, *Thin Solid Films*, 2013, **539**, 350–355.
286 S. Park, J. An, J. W. Suk and R. S. Ruoff, *Small*, 2010, **6**, 210–212.
287 N. Zhang, R. Li, L. Zhang, H. Chen, W. Wang, Y. Liu, T. Wu, X. Wang, W. Wang, Y. Li, Y. Zhao and J. Gao, *Soft Matter*, 2011, **7**, 7231–7239.
288 G. Sun, Y. Pan, Z. Zhan, L. Zheng, J. Lu, J. H. L. Pang, L. Li and W. Huang, *J. Phys. Chem. C*, 2011, **115**, 23741–23744.
289 C. Wu, J. Feng, L. Peng, Y. Ni, H. Liang, L. He and Y. Xie, *J. Mater. Chem.*, 2011, **21**, 18584–18591.
290 S. Ansari, M. M. Neelanchery and D. Ushus, *J. Appl. Polym. Sci.*, 2013, **130**, 3902–3908.
291 J. Zang, R. S. Ryu, P. Nicola, Q. Wang, T. Q. Tu, M. J. Buehler and X. Zhao, *Nat. Mater.*, 2013, **12**, 321–325.
292 A. R. Liu, W. J. Yuan and G. Q. Shi, *Thin Solid Films*, 2012, **520**, 6307–6312.
293 T. Hwang, H.-Y. Kwon, J.-S. Oh, J.-P. Hong, S.-C. Hong, Y. Lee, H. R. Choi, K. J. Kim, M. H. Bhuiya and J.-D. Nam, *Appl. Phys. Lett.* , 2013, **103**, 023106.
294 J. Loomis, B. King, T. Burkhead, P. Xu, N. Bessler, E. Terentjev and B. Panchapakesan, *Nanotechnology*, 2012, **23**, 045501.
295 J. J. Liang, Y. F. Xu, Y. Huang, L. Zhang, Y. Wang, Y. F. Ma, F. F. Li, T. Y. Guo and Y. S. Chen, *J. Phys. Chem. C*, 2009, **113**, 9921–9927.
296 K. Y. Lee, B. Kumar, J. S. Seo, K.-H. Kim, J. I. Sohn, S. N. Cha, D. Choi, Z. L. Wang and S. W. Kim, *Nano Lett.*, 2012, **12**, 1959–1964.
297 Y. Yang, H. Tian, H. Sun, R. J. Xu, Y. Shua and T. L. Ren, *RSC Adv.*, 2014, **4**, 2115–2118.
298 M. P. Lu, J. Song, M.-Y. Lu, M. T. Chen, Y. Gao, L. J. Chen and Z. L. Wang, *Nano Lett.*, 2009, **9**, 1223–1227.
299 L. Lin, C. -H. Lai, Y. Hu, Y. Zhang, X. Wang, C. Xu, R. L. Snyder, L. -J. Chen and Z. L. Wang, *Nanotechnology*, 2011, **22**, 475401.
300 L. Valentini, S. B. Bon and J. Kenny, *J. Polym. Sci. Pol. Phys.*, 2013, **51**, 1028–1032.
301 M. K. Gupta, J.-H. Lee, K. Y. Lee and S.-W. Kim, *ACS Nano*, 2013, **7**, 8932–8939.
302 M. Zelisko, Y. Hanlumyuang, S. Yang, Y. Liu, C. Lei, J. Li, P. M. Ajayan and P. Sharma, *Nat. Commun.*, 2014, **5**, 4284.
303 M. A. Rahman, B. -C. Lee, D. -T. Phan and G. -S. Chung, *Smart Mater. Struct.* 2013, **22**, 085017.
304 J. -H. Lee, K. Y. Lee, B. Kumar, T. Nguyen Thanh, N. -E. Lee and S. -W. Kim, *Energy Environ. Sci.*, 2013, **6**, 169–175.
305 J. -H. Lee, K. Y. Lee, M. K. Gupta, T. Y. Kim, D. -Y. Lee, J. Oh, C. Ryu, W. J. Yoo, C. -Y. Kang, S. -J. Yoon, J. -B. Yoo and S. -W. Kim, *Adv. Mater.*, 2014, **26**, 765–769.
306 M. Hussain, M. A. Abbasi, Z. H. Ibupoto, O. Nur and M. Willander, *Phys. Status. Solidi. A*, 2014, **211**, 455–459.
307 B. Kumar, K. Y. Lee, H.-K. Park, S. J. Chae, Y. H. Lee and S.-W. Kim, *ACS Nano*, 2011, **5**, 4197–4204.
308 J. Kwon, W. Seung, B. K. Sharma, S.-W. Kim and J.-H. Ahn, *Energy Environ. Sci.*, 2012, **5**, 8970–8975.
309 H. Gwon, H. S. Kim, K. U. Lee, D. H. Seo, Y. C. Park, Y. S. Lee, B. T. Ahn and K. Kang, *Energy Environ. Sci.*, 2011, **4**, 1277–1283.
310 L. Li, Z. Wu, S. Yuan and X. B. Zhang, *Energy Environ. Sci.*, 2014, **7**, 2101–2122.
311 J. M. MacLeod and F. Rosei, *Small*, 2014, **10**, 1038–1049.
312 X. Peng, L. L. Peng, C. Z. Wu and Y. Xie, *Chem. Soc. Rev.*, 2014, **43**, 3303–3323.
313 X. Zhao, B. M. Sanchez, P. J. Dobson and P. S. Grant, *Nanoscale*, 2011, **3**, 839–855.
314 Y. Cheng, H. Zhang, S. Lu, C. V. Varanasi and J. Liu, *Nanoscale*, 2013, **5**, 1067–1073.
315 L. L. Zhang and X. S. Zhao, *Chem. Soc. Rev.*, 2009, **38**, 2520–2531.
316 J. Chen, C. Li and G. Q. Shi, *J. Phys. Chem. Lett.,* 2013, **4**, 1244–1253.
317 W. Liu, X. Yan, J. Lang, C. Peng and Q. Xue, *J. Mater. Chem.*, 2012, **22**, 17245–17253.
318 Z. Weng, Y. Su, D. W. Wang, F. Li, J. Du and H. M. Cheng, *Adv. Energy Mater.*, 2011, **1**, 917–922.
319 S. Wang and R. A. W. Dryfe, *J. Mater. Chem. A*, 2013, **1**, 5279–5283.
320 A. L. M. Reddy and S. Ramaprabhu, *J. Phys. Chem. C*, 2007, **111**, 7727–7734.
321 J. Yan, Z. J. Fan, T. Wei, W. Z. Qian, M. L. Zhang and F. Wei, *Carbon*, 2010, **48**, 3825–3833.
322 B. G. Choi, Y. S. Huh, W. H. Hong, D. Erickson and H. S. Park, *Nanoscale*, 2013, **5**, 3976–3981.
323 M. Sawangphruk, P. Srimuk, P. Chiochan, A. Krittayavathananon, S. Luanwuthi and J. Limtrakul, *Carbon*, 2013, **60**, 109–116.
324 Y. Li, K. Sheng, W. Yuan and G. Shi, *Chem. Commun.*, 2013, **49**, 291–293.
325 D. Zhang, M. Miao, H. Niu and Z. Wei, *ACS Nano*, 2014, **8**, 4571–4579.
326 Y. Hu, H. Cheng, F. Zhao, N. Chen, L. Jiang, Z. Feng and L. Qu, *Nanoscale*, 2014, **6**, 6448–6451.
327 J. Smithyman and R. Liang, *Mater. Sci. Eng. B-Adv.*, 2014, **184**, 34–43.
328 Z. Xu, H. Sun, X. Zhao and C. Gao, *Adv. Mater.* 2013, **25**, 188–193.
329 S. H. Aboutalebi, R. Jalili, D. Esrafilzadeh, M. Salari, Z. Gholamvand, S. A. Yamini, K. Konstantinov, R. L. Shepherd, J. Chen, S. E. Moulton, P. C. Innis, A. I. Minett, J. M. Razal and G. G. Wallace, *ACS Nano*, 2014, **8**, 2456–2466.
330L. Bao and X. Li, *Adv. Mater.*, 2012, **24**, 3246–3252.
331 L. Kou, T. Huang, B. Zheng, Y. Han, X. Zhao, K. Gopalsamy, H. Sun and C. Gao, *Nat. Commun.*, 2014, **5**, 3754.
332 C. Chen, Q. Zhang, C. Huang, X. Zhao, B. Zhang, Q. Kong, M. Wang, Y. Yang, R. Cai and D. Su, *Chem. Commun.*, 2012, **48**, 7149–7151.
333 B. G. Choi, M. Yang, W. H. Hong, J. W. Choi and Y. S. Huh, *ACS Nano*, 2012, **6**, 4020–4028.
334 X. Yang, J. Zhu, L. Qiu and D. Li, *Adv. Mater.*, 2011, **23**, 2833–2838.
335 Y. M. Wang, J. C. Chen, J. Y. Cao, Y. Liu, Y. Zhou, J. H. Ouyang and D. C. Jia, *J.Power Sources*, 2014, 271, 269–277.
336 K. Gao, Z. Shao, J. Li, X. Wang, X. Peng, W. Wang and F. Wang, *J. Mater. Chem. A*, 2013, **1**, 63–67.
337 K. Gao, Z. Shao, X. Wu, X. Wang, Y. Zhang, W. Wang, F. Wang, *Nanoscale*, 2013, **5**, 5307–5311.
338 Q. Su, Y. Liang, X. Feng and K. Müllen, *Chem. Commun.*, 2010, **46**, 8279–8281.
339 X. Lu, H. Dou, B. Gao, C. Yuan, S. Yang, L. Hao, L. Shen and X. Zhang, *Electrochim. Acta*, 2011, **56**, 5115–5121.
340 D. Wang, F. Li, J. Zhao, W. Ren, Z. Chen, J. Tan, Z. Wu, I. Gentle, G. Lu and H. Cheng, *ACS Nano*, 2009, **3**, 1745–1752.
341 X. Yan, J. Chen, J. Yang, Q. Xue and P. Miele, *ACS Appl. Mater. Inter.* , 2010, **2**, 2521–2529.
342 J. Zhang, Y. Yu, L. Liu and Y. Wu, *Nanoscale*, 2013, **5**, 3052–3057.

343 A. Sumboja, C. Y. Foo, X. Wang and P. S. Lee, *Adv. Mater.*, 2013, **25**, 2809–2815.
344 Y. Jin, H. Chen, M. Chen, N. Liu and Q. Li, *ACS Appl. Mater. Inter.* , 2013, **5**, 3408–3416.
345.G. Yu, L. Hu, N. Liu, H. Wang, M. Vosgueritchian, Y. Yang, Y. Cui and Z. Bao, *Nano Lett.*, 2011, **11**, 4438–4442.
346 Y. Shao, H. Wang, Q. Zhang and Y. Li, *J. Mater. Chem. C*, 2013, **1**, 1245–1251.
347 D. A. C. Brownson, L. C. S. Figueiredo-Filho, X. Ji, M. Gomez-Mingot, J. Iniesta, O. Fatibello-Filho, D. K. Kampouris and C. E. Banks, *J. Mater. Chem. A*, 2013, **1**, 5962–5972.
348 J. Chen, K. X. Sheng, P. H. Luo, C. Li, G. Q. Shi, *Adv. Mater.*, 2012, 24, 4569–4573.
349 W. Chen, S. Li, C. Chen and L. Yan, *Adv. Mater.*, 2011, **23**, 5679–5683.
350 K. X. Sheng, Y. Q. Sun, C. Li, W. J. Yuan and G. Q. Shi, *Sci. Rep.*, 2012, **2**, 247.
351 Y. He, W. Chen, J. Zhou, X. Li, P. Tang, Z. Zhang, J. Fu and E. Xie, *ACS Appl. Mater. Inter.* , 2014, **6**, 210–218.
352 X. Peng, L. Peng, C. Wu and Y. Xie, *Chem. Soc. Rev.*, 2014, **43**, 3303–3323.
353 J. P. Alper, S. Wang, F. Rossi, G. Salviati, N. Yiu, C. Carraro and R. Maboudian, *Nano Lett.*, 2014, **14**, 1843–1847.
354 J. J. Yoo, K. Balakrishnan, J. Huang, V. Meunier, B. G. Sumpter, A. Srivastava, M. Conway, A. L. M. Reddy, J. Yu, R. Vajtai and P. M. Ajayan, *Nano Lett.*, 2011, **11**, 1423–1427.
355 Z. Niu, L. Zhang, L. Liu, B. Zhu, H. Dong and X. Chen, *Adv. Mater.*, 2013, **25**, 4035–4042.
356 L. Peng, X. Peng, B. Liu, C. Wu, Y. Xie and G. Yu, *Nano Lett.*, 2013, **13**, 2151–2157.
357 H. Chen, M. B. Müller, K. J. Gilmore, G. G. Wallace and D. Li, *Adv. Mater.*, 2008, **20**, 3557–3561.
358 C. Wang, D. Li, C. O. Too and G. G. Wallace, *Chem. Mater.*, 2009, **21**, 2604–2606.
359 A. Abouimrane, O. C. Compton, K. Amine and S. T. Nguyen, *J. Phys. Chem. C*, 2010, **114**, 12800–12804.
360 Y. Hu, X. Li, J. Wang, R. Li and X. Sun, *J. Power Sources*, 2013, **237**, 41–46.
361 X. Zhao, C. M. Hayner, M. C. Kung and H. H. Kung, *ACS Nano*, 2011, **5**, 8739–8749.
362 R. Mukherjee, A. V. Thomas, A. Krishnamurthy and N. Koratkar, *ACS Nano*, 2012, **6**, 7867–7878.
363 F. Liu, S. Song, D. Xue and H. Zhang, *Adv. Mater.*, 2012, **24**, 1089–1094.
364 S. Yin, Y. Zhang, J. Kong, C. Zou, C. M. Li, X. Lu, J. Ma, F. Y. C. Boey and X. Chen, *ACS Nano*, 2011, **5**, 3831–3838.
365 G. Q. Ning, C. G. Xu, Y. M. Cao, X. Zhu, Z. M. Jiang, Z. J. Fan, W. Z. Qian, F. Wei and J. S. Gao, *J. Mater. Chem. A*, 2013, **1**, 408–414.
366 D. Wei, S. Haque, P. Andrew, J. Kivioja, T. Ryhanen, A. Pesquera, A. Centeno, B. Alonso, A. Chuvilin and A. Zurutuza, *J. Mater. Chem. A*, 2013, **1**, 3177–3181.
367 N. Mahmood, C. Zhang, F. Liu, J. Zhu and Y. Hou, *ACS Nano*, 2013, **7**, 10307–10318.
368 C. K. Chan, H. L. Peng, G. Liu, G, K. Mcilwrath, X. F. Zhang, R. A. Huggins, and Y. Cui, *Nat. Nanotechnol.*, 2008, **3**, 31–35.
369 A. Magasinski, P. Dixon, B. Hertzberg, A. Kvit, J. Ayala, G. Yushin, *Nat. Mater.*, 2010, **9**, 353–358.
370 J. K. Lee, K. B. Smith, C. M. Hayner and H. H. Kung, *Chem. Commun.*, 2010, **46**, 2025–2027.
371 J. Z. Wang, C. Zhong, S. L. Chou and H. K. Liu, *Electrochem. Commun.* , 2010, **12**, 1467–1470.
372 X. Zhao, C. M. Hayner, M. C. Kung and H. H. Kung, *Adv. Energy Mater.*, 2011, **1**, 1079–1084.
373 B. Wang, X. Li, X. Zhang, B. Luo, M. Jin, M. Liang, S. A. Dayeh, S. T. Picraux and L. Zhi, *ACS Nano*, 2013, **7**, 1437–1445.
374 P. Poizot, S. Laruelle, S. Grugeon, L. Dupont and J. M. Tarascon, *Nature*, 2000, **407**, 496–499.
375 J. Cabana, L. Monconduit, D. Larcher and M. R. Palacín, *Adv. Mater.*, 2010, **22**, E170–E192.
376 L. Li, G. Zhou, Z. Weng, X. Y. Shan, F. Li and H. M. Cheng, *Carbon*, 2014, **67**, 500–507.
377 R. Wang, C. H. Xu, J. Sun, L. Gao and C. Lin, *J. Mater. Chem. A*, 2013, **1**, 1794–1800.
378 R. Wang, C. Xu, J. Sun, Y. Liu, L. Gao and C. Lin, *Nanoscale*, 2013, **5**, 6960–6967.
379 A. Yu, H. W. Park, A. Davies, D. C. Higgins, Z. Chen and X. Xiao, *J. Phys. Chem. Lett*, 2011, **2**, 1855–1860.
380 A. R. Armstrong, G. Armstrong, J. Canales, R. García and P. G. Bruce, *Adv. Mater.*, 2005, **17**, 862–865.
381 D. Deng, M. G. Kim, J. Y. Lee and J. Cho, *Energy Environ. Sci.*, 2009, **2**, 818–837.
382 D. Wei, P. Andrew, H. Yang, Y. Jiang, F. Li, C. Shan, W. Ruan, D. Han, L. Niu; C. Bower, T. Ryhanen, M. Rouvala, G. A. J. Amaratunga, and A. Ivaska, *J. Mater. Chem.*, 2011, **21**, 9762–9767.
383 G. Jeong, Y. -U. Kim, H. Kim, Y. -J. Kim and H. -J. Sohn, *Energy Environ. Sci.*, 2011, **4**, 1986–2002.
384 Y. Wang and G. Cao, *Adv. Mater.*, 2008, **20**, 2251–2269.
385 Y. Qian, A. Vu, W. Smyrl and A. Stein, *J. Electrochem. Soc.*, 2012, **159**, A1135–A1140.
386 X. Zhao, C. M. Hayner, M. C. Kung and H. H. Kung, *Chem. Commun.*, 2012, **48**, 9909–9911.
387 N. Li, Z. P. Chen, W. C. R. Ren, F. Li and H. M. Chen, *Proc. Natl. Acad. Sci. U. S. A.*, 2012, **109**, 17360–17365.
388 K. Xi, P. R. Kidambi, R. Chen, C. Gao, X. Peng, C. Ducati, S. Hofmann and R. V. Kumar, *Nanoscale*, 2014, **6**, 5746–5753.
389 Y. Yang, G. Zheng and Y. Cui, *Chem. Soc. Rev.*, 2013, **42**, 3018–3032.
390 S. S. Zhang, *J. Power Sources*, 2013, **231**, 153–162.
391 Z. Seh, W. Li, J. Cha, G. Zheng, Y. Yang, M. McDowell, P. Hsu and Y. Cui, *Nat Commun*, 2013, **4**, 1331.
392 K. Li, B. Wang, D. Su, J. Park, H. Ahn and G. Wang, *J. Power Sources*, 2012, **202**, 389–393.
393 J. Guo, Y. Xu and C. Wang, *Nano Lett.*, 2011, **11**, 4288–4294.
394 H. S. Ryu, J. W. Park, J. Park, J. -P. Ahn, K. -W. Kim, J. -H. Ahn, T. -H. Nam, G. Wang and H. -J. Ahn, *J. Mater. Chem. A*, 2013, **1**, 1573–1578.
395 H. Ye, Y. X. Yin, S. Xin and Y. G. Guo, *J. Mater. Chem. A*, 2013, **1**, 6602–6608.
396 X. Ji, K. T. Lee and L. F. Nazar, *Nat. Mater.*, 2009, **8**, 500–506.
397 H. Wang, Y. Yang, Y. Liang, J. T. Robinson, Y. Li, A. Jackson, Y. Cui and H. Dai, *Nano Lett.*, 2011, **11**, 2644–2647.
398 L. Ji, M. Rao, H. Zheng, L. Zhang, Y. Li, W. Duan, J. Guo, E. J. Cairns and Y. Zhang, *J. Am. Chem. Soc.,* 2011, **133**, 18522–18525.
399 X. Huang, B. Sun, K. Li, S. Chen and G. Wang, *J. Mater. Chem. A*, 2013, **1**, 13484–13489.
400 W. Zhang, J. Zhu, H. Ang, Y. Zeng, N. Xiao, Y. Gao, W. Liu, H. H. Hng and Q. Yan, *Nanoscale*, 2013, **5**, 9651–9658.
401 X. Wang, X. Lu, B. Liu, D. Chen, Y. Tong and G. Shen, *Adv. Mater.*, 2014, **26**, 4763–4782.
402 Z. H. Lin, G. Zhu, Y. S. Zhou, Y. Yang, P. Bai, J. Chen and Z. L. Wang, *Angew. Chem. Int. Edit.*, 2013, **52**, 5065–5069.
403 Y. Yang, S. Wang, Y. Zhang and Z. L. Wang, *Nano Lett.*, 2012, **12**, 6408–6413.
404 W. X. Guo, X. Y. Xue, S. H. Wang, C. J. Lin and Z. L. Wang, *Nano Lett.*, 2012, **12**, 2520–2523.
405 M. Koo, K.-I. Park, S. H. Lee, M. Suh, D. Y. Jeon, J. W. Choi, K. Kang and K. J. Lee, *Nano Lett.*, 2012, **12**, 4810–4816.
406 X. Xue, S. Wang, W. Guo, Y. Zhang and Z. L. Wang, *Nano Lett.*, 2012, **12**, 5048–5054.
407.X. Xue, P. Deng, S. Yuan, Y. Nie, B. He, L. Xing and Y. Zhang, *Energy Environ. Sci.*, 2013, **6**, 2615–2620.
408 X. J. Hou, B. Liu, X. F. Wang, Z. R. Wang, Q. F. Wang, D. Chen and G. Z. Shen, *Nanoscale*, 2013, **5**, 7831–7837.
409 X. F. Wang, B. Liu, R. Liu, Q. F. Wang, X. J. Hou, D. Chen, R. M. Wang and G. Z. Shen, *Angew. Chem. Int. Edit.*, 2014, **53**, 1849–1853.

Broader Context

Flexible devices related to energy conversion and storage have potential applications in wearable and portable electronics such as roll-up displays, electronic papers, touch screens, active radio-frequency identification tags, wearable sensors and implantable medical devices. Thus, they have attract a great deal of attentions in recent years from both academic and industrial aspects. Graphene is a unique and attractive material for this purpose because of its atom-thick two-dimensional structure and excellent properties. Particularly, the atom-thick structure makes graphene sheet easily deforms in the direction normal to its surface, providing it with good flexibility. This critical review will summarize the methods of synthesizing flexible graphene materials and their applications in energy related flexible devices including photovoltaic devices, organic light-emission diodes, photodetectors, fuel cells, nanogenerators, supercapacitors and batteries. The challenges facing the design and construction of the devices will also be discussed.

Biographical Notes

Xiluan Wang received her B. Eng. from the Department of Polymer Science and Engineering at Beijing University of Chemical Technology in 2010. She is currently a Ph. D. candidate in Prof. Gaoquan Shi's Laboratory at the Department of Chemistry, Tsinghua University. Her research interests focus on the synthesis and applications of chemically modified graphene.

Prof. Gaoquan Shi received his BS degree (1985) and PhD degree (1992) at the Department of Chemistry, Nanjing University. Then he joined Nanjing University and was promoted to full professor in 1995. In 2000, he moved to Tsinghua University as a Professor of Chemistry. His research interests are focused on synthesis and applications of graphene materials and conducting polymers. He received the 2nd Grade Award of Natural Science of China and the Youth Knowledge Innovation Prize of the Chinese Chemical Society and BASF Company in 2004, and the 1st Grade Award of Natural Science of Chinese Education Ministry in 2013.

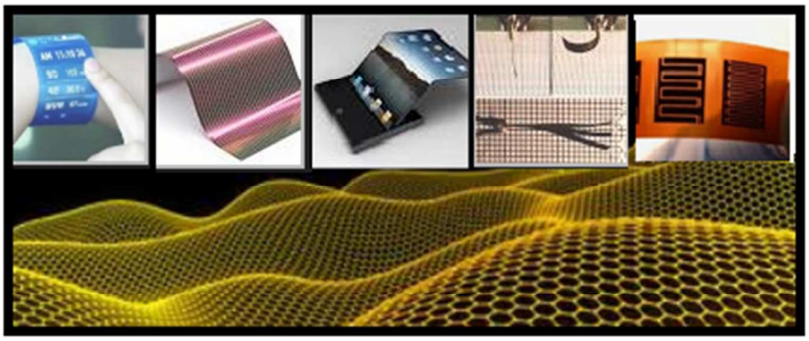

This review summarizes the recent advancements in the synthesis and applications of graphene materials for flexible graphene devices related to energy conversion and storage.